ATP11A causes autosomal-dominant progressive, non-syndromic auditory synaptopathy / auditory neuropathy

Department of Biology
University of Hamburg

Institute of Human Genetics
University Medical Center Hamburg-Eppendorf

This dissertation is submitted to the University of Hamburg
for the degree of Doctor rerum naturalium.

Sarah Maria von Loh
2021

Data page

Thesis title:	ATP11A causes autosomal-dominant progressive, non-syndromic auditory synaptopathy / auditory neuropathy
Department:	Department of Biology University of Hamburg
Laboratory workplace:	Institute of Human Genetics University Medical Center Hamburg-Eppendorf
Matriculation number:	6752679
Last name, first name:	von Loh, Sarah Maria
Primary reviewer:	Prof. Dr. med. Christian Kubisch
Contact data:	Institute of Human Genetics Martinistraße 52 D-20246 Hamburg
Secondary reviewer:	Prof. Dr. Julia Kehr
Contact data:	Biocenter Klein Flottbek Ohnhorststr. 18 D-22609 Hamburg
Date of submission:	May 2021
Date of disputation:	24.09.2021

Contents

Abstract (english)

This thesis studies the phospholipid translocating P4-ATPase *ATP11A*, a novel deafness gene causing autosomal-dominant inherited isolated auditory synaptopathy / auditory neuropathy (AS/AN). The causative mutation is a 5,500 bp deletion covering the last coding exon. This results in aberrant splicing with the use of an alternative last exon, without induction of nonsense-mediated mRNA decay. Immunohistochemistry of the transfected variant into HEK293T cells reveals correct CDC50A-dependent subcellular localisation to the plasma membrane. A flippase activity assay with the NBD-labelled fluorescent phospholipids phosphatidylserine (PS) displays a hypoactivity of PS translocating function from the exoplasmic to the cytoplasmic leaflet of the plasma membrane in the presence of the mutation.

An artificially constructed variant of human ATP11A having neither the physiological nor the alternative last exon, presented overly active. This suggests that the deleted sequence of *hATP11A* codes for a regulatory domain, acting (i) through simple length-dependent sterical hindrance of the catalytic core or (ii) with a similar mechanism to the yeast ortholog Drs2p, where a cofactor activates a conformational change of the inhibitory peptide. In the overly active variant the autoinhibitory interaction with the deleted C-terminal domain is completely missing. In the mutant protein the altered C-terminal region is thought to be (i) either longer and therefore results in stronger deactivation or (ii) inhibits to a similar level compared to wild type peptide, but the deletion prevents the conformational change and thus the activation of flippase function.

Studies on the role of PS tanslocation, distribution across the plasma membrane and the outcome of ATPase deficiency in mice demonstrate an importance of ATPases in a multitude of cellular functions. Disturbance in cell stability and shape, endo- and exocytosis, apoptosis, neurite degeneration and regeneration as well as impaired Ca^{2+} levels and interaction of proteins with the plasma membrane can be caused by changes in the asymmetry of PS in the plasma membrane and lead to subsequent degeneration of inner ear cells.

Finding diminished hATP11A function to be the cause of a novel hereditary form of AS/AN broadens the knowledge of inner ear physiology and contributes to more personalised treatment of hearing loss in the future.

Abstract (deutsch)

Diese Arbeit untersucht die Phospholipid transportierende P4-ATPase *ATP11A* - ein neues Taubheitsgen, welches autosomal-dominant vererbte Auditorische Synaptopathie und Neuropathie (AS/AN) auslöst. Die krankheitsauslösende Mutation ist eine 5.500 bp große Deletion, die das letzte kodierende Exon beinhaltet. Bei dem dadurch ausgelösten abnormalen Spleißen wird ein alternatives letztes Exon verwendet, wodurch jedoch kein Stopcodon-vermittelter Abbau der mRNA ausgelöst wird. Immunfärbungen von HEK293 Zellen, die mit verschiedenen Varianten von ATP11A transfiziert wurden, belegen außerdem eine korrekte CDC50A-abhängige subzelluläre Lokalisation an der Plasmamembran. Ein Flippase Aktivitäts Assay mit dem NBD-markierten fluoreszierenden Phospholipid Phosphatidylserin (PS) zeigt, dass bei Vorhandensein der Mutation die Fähigkeit, PS von der exoplasmatischen zur cytoplasmatischen Seite der Membran zu transportieren, stark eingeschränkt ist.

Eine künstlich erzeugte Variante des humanen ATP11A, die weder das physiologische, noch das alternative letzte Exon verwendet, ist im Experiment überaktiv. Dies legt nahe, dass die deletierte Sequenz des hATP11A für eine regulatorische Domäne kodiert. Die Regulation könnte entweder (i) aus einer einfachen längenabhängigen sterischen Hinderung des katalytischen Kerns bestehen oder aber (ii) auf einem Mechanismus basieren, der Ähnlichkeiten zu der Regulation des Hefeorthologs Drs2p aufweist, bei dem die Bindung eines Cofaktors Konformationsänderungen des inhibitorischen Peptids hervorruft. In der überaktiven Variante fehlt die autoinhibitorische Interaktion mit der deletierten C-terminalen Domäne vollständig. Die C-terminale Region des mutierten Proteins ist (i) zum einen länger als im Wildtyp und könnte daher zu stärkerer Deaktivierung führen, oder (ii) inhibiert die Aktivität auf einem ähnlichen Niveau wie im Wildtyp, durch die Deletion wird jedoch die Konformationsänderung und somit auch die Aktivierung der Flippasefunktion verhindert.

Studien der Rolle von PS Translokation und der Verteilung innerhalb der Plasmamembran, sowie die Folgen von ATPase-Verlust in Mäusen, demonstrieren die Wichtigkeit der ATPasen in einer Vielzahl von zellulären Funktionen. Durch Veränderungen der asymmetrischen Verteilung von PS in der Plasmamembran könnten Störungen der Zellstabilität und -form, Endo- und

Exozytose, Apoptose, Neuritdegeneration und -regeneration, ebenso wie Beeinträchtigungen des Ca^{2+} Spiegels und der Interaktion von Proteinen mit der Plasmamembran ausgelöst werden. Dies wiederum kann in der Konsequenz potentiell zu Degeneration von Zellen des Innenohrs führen.

hATP11A-Funktionsreduktion als Ursache für eine neuartige Form von AS/AN zu identifizieren erweitert das Wissen über die Physiologie des Innenohrs und kann dazu beitragen, in Zukunft eine personalisiertere Medizin für Hörverlust zu entwickeln.

1. Introduction

Hearing is a finely tuned process in which a sound input is processed to the brain. Knowing the mechanics behind this enables to distinguish between different categories of hearing loss and is necessary to understand what underlying causes can lead to them.

AS/AN is an autosomal-dominant form of sensorineural hearing loss and was found to coincide with a 5,500 bp deletion in *hATP11A* in an affected family. The medical history of this family, as well as the cellular function of ATP11A as a phospholipid flippase and its mechanism are important for the interpretation of the characterisation of the pathogenesis performed in this thesis.

1.1. Anatomy and functioning of the auditory system

When we notice a noise, already a vibration of the air was translated into a signal understandable for the brain (see fig. 1.1). At first the sound is collected by the pinna and enters the ear through the external auditory canal. From here it comes to the tympanic membrane, which starts vibrating in concordance with the sound waves. The tympanic membrane is connected to the ossicles. The ossicles are three small bones of the middle ear called malleus, incus and stapes that conduct the vibration to the inner ear. For this the stapes is pushed against a flexible membrane named oval window, which separates the middle ear from the fluid filled cochlea [90, 154].

The cochlea is a spiral shaped tube, which is split lengthwise into three chambers (see fig. 1.2). The vestibular membrane and the basilar membrane separate the scala vestibuli, the scala media and the scala tympani. The scala vestibuli and the scala tympani are connected at the apex of the cochlea and are filled with perilymph. The perilymph is composed similarly to the cerebrospinal fluid. The scala media, in contrast, is filled with potassium rich endolymph, similar to intracellular fluid [90, 154].

When the stapes pushes against the oval window, the perilymph in the scala vestibuli is set in motion and the wave is conducted through the whole spiral and back through the scala tympani. This perilymph displacement is possible due to another flexible membrane in the medial wall, the round window. At the organ

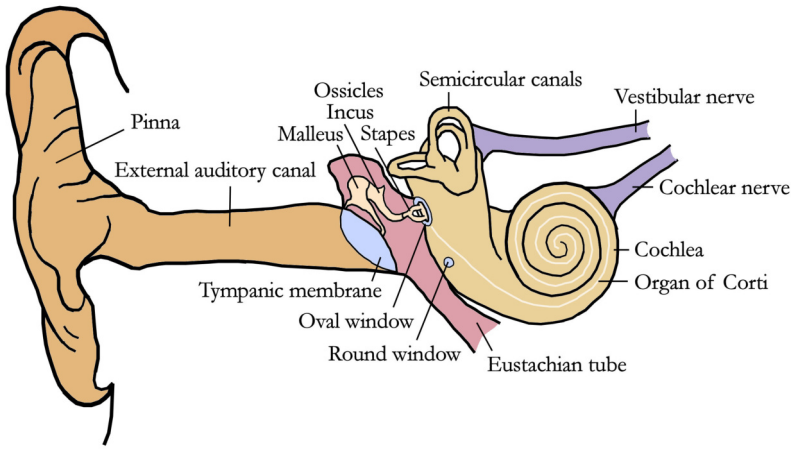

Figure 1.1.: Anatomical overview of the ear

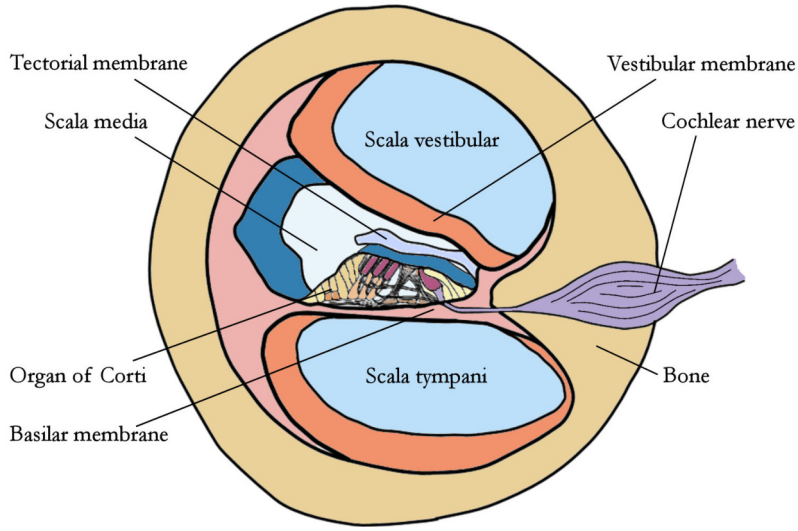

Figure 1.2.: Anatomical cross section of the cochlea

of Corti this mechanical wave gets translated into an electrochemical signal. The organ of Corti is placed in the scala media, where the basilar membrane takes up the vibration from the perilymph and is connected to mechanosensory hair cells by supporting cells, like the pillar cells (see fig. 1.3) [90, 154].

In the human ear in total about 15,500 hair cells are divided in one row of inner hair cells and three to five rows of outer hair cells lenghtwise along the spiral. Each hair cell has a mechanically sensitive hair bundle out of stereocilia on the apical surface touching the tectorial membrane [90, 154]. The cochlea is organised in a tonotopic manner. The responsiveness depends on gradual differences in height of stereocilia and width and thickness of the basilar membrane. High frequencies are registered at the basal entrance, while the resonance for low frequencies is located at the apex [133, 159, 160]. When the motion from the perilymph is conducted to the resonating part of the basilar membrane, the stereocilia of the hair cells are bent against the tectorial membrane. This causes the depolarisation of the hair cells by opening motion gated ion channels that result in fast K^+ influx from the endolymph [154]. As response to the depolarisation, voltage gated Ca^{2+} and K^+ channels at the hair cell soma membrane are opened. The Ca^{2+} influx leads to further depolarisation and, in the case of inner hair cells, to neurotransmitter release at the ribbon synapse at the base of the cell. The outflow of cations at the basal part of the cell into the perilymph along the electrochemical gradient through the opened channels allows for repolarisation [209, 315].

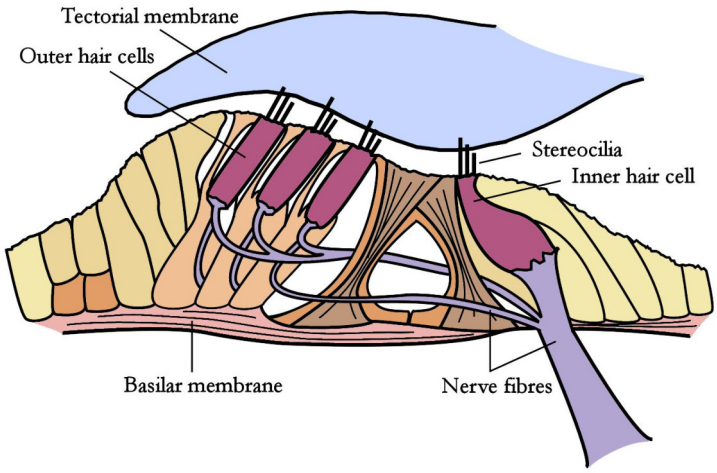

Figure 1.3.: Anatomical cross section of the organ of Corti

Many dendrites of spiral ganglion cells contact to the ribbon synapses of an inner hair cells. These are called type I cells, which are myelinated, bipolar and have a large cell body. They represent 95% of auditory nerve fibers. The rest are smaller, unmyelinated and unipolar type II spiral ganglion cells. One type II cell contacts several outer hair cells [154].

The axons of the spiral ganglion cells bundle together and form the auditory nerve. This branches when it enters the brain stem and sends the evoked action potentials onwards to the dorsal and ventral cochlear nuclei of the respective side of the head. To preserve the tonotopic information received from the cochlea organisation, axons from spiral ganglion cells activated by different frequencies project to different portions of the cochlear nuclei. Each axon corresponding to a certain frequency of sound is connected to only a few certain dendrites, making sure frequencies can still be distinguished. Higher up the auditory information transmission pathways' binaural information is merged and analysed on specific characteristics like frequency, intensity, binaural localisation and temporal modulation. Subsequently, the auditory information is connected to visual and sensory input from non-auditory pathways. Not until finally processed at the auditory cortex the sound bears a meaning, can be distinguished in background noise and important sound, consciously connected with other information and interpreted as speech or music [324, 90].

1.2. Hearing loss

Hearing loss is a heterogeneous condition that can develop at every age, due to environmental or genetic reasons and may affect different parts of the auditory system.

Regarding the age, hearing impairment is subclassified into postlingual and prelingual hearing loss. Late onset, postlingual hearing loss is most often non-genetic or multigenic. Also a combination is possible, as some mutations are thought to be associated with increased risk of noise induced hearing loss [116]. The rare forms of monogenic postlingual hearing loss are often, but not always, inherited in an autosomal-dominant pattern [323]. In adults the prevalence of hearing impairment strongly correlates with age. A study with 2837 adult American participants published in 2011 [166] shows incidence rates as listed:

- Ages 21 to 34: 2.9%
- Ages 35 to 44: 6.4%
- Ages 45 to 54: 10.9%
- Ages 55 to 64: 25.1%
- Ages 65 to 84: 42.7%

Men are affected more frequently compared to women. Less educated participants who had worked in noisy jobs have a higher chance of developing hearing loss compared to participants with a higher socioeconomic status [166]. Also ototoxic medication, penetration or sudden pressure changes causing trauma to the middle or inner ear, lead to hearing impairment, as well as acoustic neurinoma or autoimmune diseases. Furthermore, infections of the middle ear can induce hearing loss, but children are much more prone to this compared to adults. Consistent with the rising incidence in elderly people, the normal aging process often come with a progressive loss of hearing ability called presbycusis [125].

Prelingual hearing loss can be congenital or develops in early infancy and has a great impact on speech and language development of the affected children. Impaired hearing is one of the most common congenital disorders and caused by either nongenetic factors or by mutations in genes involved in ear development, structure or function [49]. Newborn screenings for congenital hearing loss find comparable prevalences of 1 to 3 in 1,000 live birth [169, 111]. While nongenetic risk factors such as in utero infections, maternal diabetes or drug use, limited prenatal care, multiple births or neonatal exposure to specific antibiotics or diuretics, meconium aspiration, assisted ventilation after birth or hyperbilirubinemia also contribute much to this prevalence [125], about half of the cases are caused monogenic [323]. In genetic hearing loss non-syndromic variants are as common as syndromic variants, where the hearing impairment is accompanied by other clinical abnormalities. For both forms there are known deafness loci with autosomal recessive inheritance ($\sim 80\%$), as well as autosomal dominant ($\sim 20\%$), X-linked ($\sim 1\%$) or mitochondrial patterns ($< 1\%$) [49, 76, 261]. This will be discussed further in section 1.3.2.

Irrespective of syndromic or non-syndromic and the way of inheritance, hearing loss can also be divided into conductive and sensorineural forms. Conductive hearing loss arises from defects in the outer or middle ear, which disturbs the conduction of sound waves, whereas sensorineural hearing loss stems from defects in the cochlea or the auditory nerve and inhibits the correct processing of auditory information [90]. Most genetically caused cases of hearing loss affect the inner ear and are defined as sensorineural for this reason. A special variant of sensorineural hearing loss is auditory synaptopathy / auditory neuropathy (AS/AN).

1.3. AS/AN

As mentioned, AS/AN is a subvariant of sensorineural hearing loss [158, 157]. While the definition of sensorineural hearing loss comprises all inner ear deficits that cause interruption of auditory processing, AS/AN only includes the inner hair cell, synaptic or neuronal deficits [232].

1.3.1. Pathologies of AS/AN

Depending on the underlying defects, AS/AN is divided into presynaptic synaptopathy, where the malfunction is related to the inner hair cells or their synapses, and postsynaptic neuropathy, where the auditory nerves or ganglion cells are affected [266]. On the presynaptic side, the isolated dysfunction or loss of inner hair cells in the presence of functioning outer hair cells influences the auditory nerve activity by reduction of the receptor potential [214]. Also abnormal neurotransmitter release at the ribbon synapses causes reduction and asynchronism of the auditory nerve activation [234]. In the case of postsynaptic neuropathy interference with the neural synchrony can be induced by the demyelination of the nerve fibres [220]. Another postsynaptic cause for hearing loss is the degeneration of auditory ganglion cells. This can happen directly or as a consequence of axonal loss. Also dendritic nerve terminals can alter their size or withdraw from the ribbon synapse and degenerate with aging [33] or after noise trauma [120]. In addition to this progressive loss of auditory nerve cells there are also cases of congenital hypoplasia of the auditory nerve [24].

1.3.2. Genetic causes of AS/AN

Non-syndromic deafness loci are named with the prefix DFN and consecutively numbered after their date of discovery. The letter A is added between prefix and number for autosomal dominant, the letter B for autosomal recessive and the letter X for X-linked inheritance. For AS/AN the prefix AUN is used. Through combination of genetic, histological and physiological studies in human and mouse, several genes involved in hearing loss could be identified. They are involved in protein transport, the building and maintenance of the cytoskeleton, cell-cell junctions or extracellular matrix, synapse transduction or ion homeostasis or work as regulatory elements [reviewed in 49, 268, 55, 323]. A frequently updated overview is given by the Hereditary Hearing loss Homepage [302].

Gene mutations resulting in AS/AN are often associated with peripheral neuropathies. These non-isolated, syndromic AS/AN can be inherited in a dominant way (*PMP22, MPZ, NF-L, GJB3, OPA1*), as well as recessive (*FXN,*

TMEM126A, WFS1, NDRG1), mitochondrial (*mtND4*) and X-linked (*TIMM8A, AUNX1, GJB1*) [232]. For isolated AS/AN four genes are described.

Of these, mutations in *OTOF* and *PJVK* are inherited in an autosomal-recessive manner. *OTOF* encodes for otoferlin, which is a transmembrane protein involved in glutamate vesicle release at the inner hair cell ribbon synapse. It is part of the ferlin family that generally takes part in membrane-membrane fusion. It contains several C2 domains for Ca^{2+} and phospholipid binding and a coiled-coil domain presumably interacting with α-helices of partners like SNARE proteins [192]. Recent research provides evidence for a model in which otoferlin, bound to synaptic vesicles, connects the presynaptic membrane with Ca^{2+} channels and SNARE as a scaffolding protein. The close proximity is thought to elevate Ca^{2+} influx induced exocytosis fidelity [87]. It was also shown that mutations in the C2C domain that lower its Ca^{2+} binding affinity don't effect synapse structure, Ca^{2+} currents and otoferlin distribution, but disturb a likely function as a Ca^{2+} sensor for synaptic vesicle fusion regulation and vesicle pool replenishment [150]. Interestingly there are not only *OTOF* based cases of profound prelingual AS/AN, but some missense mutations and in-frame deletions that lead to a temperature-sensitive hearing loss, probably due to loss of function through heat-dependent protein destabilisation and degradation [192].

Mutations in *PJVK* are reported to cause severe congenital hearing loss with possible dysfunctions of the cochlea and AS/AN. It encodes for pejvakin, which is a member of the gasdermin protein family, localized in spiral ganglion cells, hair cells and supporting cells and involved in stereocilia maintenance [109]. While it is established that truncating mutations are associated with progressive cochlear hearing loss [51], it is currently under debate if *PJVK* mutations really cause AS/AN. Missing otoacoustic emissions (OAE) in patients [38] and histological findings only suggest a cochlear dysfunction. Nevertheless, a remaining theory is that AS/AN is linked to more benign mutations with mainly inner hair cell interference and only slow outer hair cell degeneration [109].

The mitochondrial gene *MT-RNR1*, coding for 12S ribosomal RNA, participating in mitochondrial protein synthesis, is the cause of moderate, adult onset AS/AN in a Chinese patient. Before, mutations in the *MT-RNR1* gene were only associated with aminoglycoside-induced non-syndromic senorineural hearing loss [319]. In the patient with AS/AN the mutation T1095C in a highly conserved region has been identified as the underlying genetic cause and two other variants in conserved regions of the same gene are suspected to alter the phenotypic expression of symptoms [319]. The occurrence of the T1095C mutation in two unrelated families argues for its involvement in hearing loss. Neverthe-

less, it is questionable whether this variant causes especially isolated AS/AN, because one Italian family presented with aminoglycoside-induced hearing loss, Parkinson's disease and neuropathy [289] and another Italian family with actually isolated, but cochlear hearing loss [286].

DIAPH3 is to date the only identified and published gene known to cause dominantly inherited isolated AS/AN. A mutation in the highly conserved 5'UTR (c.-172G>A) was found in a family with moderate hearing loss beginning in the second decade of life, leading to profound deafness after 40 - 50 years. Over the time sound perception threshold increases more at high frequencies than at low frequencies. OAE exclude cochlear involvement, as loss of OAEs only occurs in older and severely affected family members. Here a cochlear component adds to the AS/AN, probably as a secondary consequence to the previous dysfunctions [267]. The mutation interrupts a GC box element for transcription factor binding, which results in gain of function through a 2 to 3 fold overexpression of DIAPH3 mRNA [238]. *DIAPH3* encodes for one of three human orthologs of *Drosophila Diaphanous*. It is a member of the *diaphanous*-related formin family that acts as actin-nucleation factors [341] in the regulation of actin and microtubule networks [96]. DIAPH3 interacts with actin and microtubules in inner hair cells and is expected to regulate the actin polymerization in stereocilia. The pathologic consequences could be shown in mouse models of DIAPH3 overexpression, where parallel development of hearing loss and stereocilia defects in inner hair cells, followed by significant degradation of ribbon synpases were observed [239].

1.3.3. Clinical symptoms and social consequences

Loss of inner hair cell, synaptic or neuronal function in AS/AN causes a certain spectrum of psychophysical and neurophysiological symptoms. Frequency resolution, sound intensity discrimination and adaptation and reduced signal audibility in patients with sensory hearing impairment are usually not present in AS/AN patients [335, 216]. Instead they experience severe impairment caused by disturbed signal synchronisation and lower temporal resolution. Through this, their ability for binaural localisation of low frequency sounds is reduced [335, 219], as is the identification of rapid signal changes like 'gap detection' and 'amplitude modulation detection' [216, 335] that occur for example in speech for the discrimination of voiced and unvoiced stop-consonants [217, 218]. These effects of temporal processing disruption interfere with speech perception even more in combination with high levels of background noise that additionally complicate the identification of gaps [314]. In some forms of AS/AN, especially

reported for ribbon synapse dysfunctions, also possible background noise adaptation happens with alteration of the activation threshold for sound perception [326, 233]. In combination the ability to prioritise certain sound signals due to their location and discrimination from background noise, called 'cocktail party' effect [73], is disturbed. This again reduces the speech perception threshold in noise situations by about 5 dB in AS/AN patients compared to control [219].

As imaginable, this has not only an impairing effect on language learning in cases of congenital hearing loss [291], but is also difficult in social interaction when adult persons already integrated in a hearing society develop AS/AN and have problems with understanding other people and maintaining clear speech patterns themselves [6]. Difficulties in speech perception can also have influence on the education and employment of patients, since the school system and work places are dominated by verbal instructions and interaction [21, 287]. To best sustain quality of life for the patients, it is important to diagnose their hearing impairment early. This way, assistance can be offered directly based on the underlying mechanism causing the dysfunction [291, 204].

1.3.4. Audiological assessment of patients

To identify if a person with hearing loss is suffering from AS/AN a hearing screening is performed that especially pays attention to the auditory brainstem response (ABR) and otoacoustic emissions (OAE) or cochlear microphonics (CM). Those non-invasive methods are objective and can be applied for newborns in contrast to behavioural hearing tests [65, 85, 13].

During the testing an audio stimulus provokes a synchronised impulse of electrical activity at the auditory nerve and up to the brain pathways. The electrical response activity, resulting from the transformation of the mechanical acoustic energy from a sound into electrical energy at the auditory hair cells, can be measured as cortical auditory evoked potentials (CAEP) with a set of scalp surface electrodes [259, 118]. The measurement consists of several peaks and spreads out several milliseconds after the stimulus. Depending on latency there are many CAEP that can be differentiated. Important features of the resulting data are latency, amplitude and morphology [61]. The most commonly used for auditory screenings is the mentioned ABR [118]. The ABR represents the electrical energy that is evoked in neurons at the auditory nerve and the brain stem in in 5 to 7 waves [84]. The waves originate from different components of the auditory brainstem, so analysing the wave form of each region gives hints to the exact location of the hearing impairment [61].

The latency between waves is linked to the speed of auditory nerve conduction

and can display deleterious deceleration [27, 56, 266]. By comparing the wave V latency of both ears synchronism of binaural processing can be tested [61]. Also the amplitude ratio of wave V/I is used as a tool [237, 83, 95], as well as the ABR threshold, meaning the lowest possible stimulus level to still get an ABR wave V response [148].

The cochlea is not only a receptor for sound stimuli, but also emits sounds through motion of outer hair cells, the so-called OAE. This sounds can be spontaneous or triggered by external stimulation and are recorded at the external auditory canal. With recording the OAE as a function of the stimulus frequency the functionality of the outer hair cells can be measured [110]. Screenings usually use evoked OAE that can be done in two ways, differing in the applied stimulus and the excited area of the cochlea. For transient evoked OAE (TEOAE), where almost all outer hair cells are excited, a click sound is used. For a distortion product evoked OAE (DPOAE) two pure tones are played and only the outer hair cells corresponding to the frequencies react [110, 104]. Without problems in sound conduction or at the cochlea normal evoked OAE can be observed. In contrast, if there is a dysfunction, the amplitude of the evoked OAE decreases, the response threshold rises or the OAE is completely lost [20, 104]. This way evoked OAE measurement can be used in differential diagnosis as an objective tool to further discriminate cochlear from synaptic and neural causes in patients with sensorineural hearing impairment indicated by the absence of ABR responses [110, 104].

Likewise, the measurement of the CM is a tool that can be used similar to the OAE. It also represents the outer hair cell response to an acoustic stimulus which is given as a click using an inserted microphone and loudspeaker. Normal appearance of the CM are a proof for outer hair cell functionality. While the amplitude of the CM of patients with AS/AN does not differ from that of healthy controls, the duration of the signal is longer [reviewed in 262].

1.3.5. Management and treatment

Although, given that the further development of a child with absent ABR and present OAE can not be predicted, an early diagnosed AS/AN has several impacts on the following management and intervention [65]. First, the assessment is repeated over the next year to exclude a delayed maturation of the infant [208, 7]. Also age-appropriate behavioural hearing tests need to be performed as soon as possible to get knowledge about the child's actual hearing ability, even if there are correlations between the ABR and behavioural hearing thresholds [148]. In combination with monitoring the child's language development

and speech reception, it is important to find a method of visual aided communication suitable for the child and the rest of the family [177]. The benefit of conventional hearing aids is currently in discussion. There are evidence for and against aiding children early on [213]. However, it is recommended in the Guidelines of the British National Heath Service and the Children's Hospital in Colorado, USA to only aid patients with elevated behavioural hearing thresholds, independent of their ABR results [65, 93]. Since the disturbed temporal processing that is the underlying cause for impaired speech recognition and speech-in-noise filtering in AS/AN can not be fixed by conventional hearing aids, but only the loudness is elevated, communication skills will most likely not be improved if there is no additional problem with behavioural hearing thresholds [266, 213]. Even if in some patients, probably those with little temporal processing problems, rising the overall sound intensity with conventional hearing aids helps with speech perception [34, 227, 215], in most patients there is no benefit noticed [213, 15]. In cases where a complete auditory nerve deficiency is ruled out [24], but no progress in speech perception is made, it is possible to consider cochlear implantation. In contrast to conventional hearing aids, cochlear implants are capable of correcting temporal processing, presumably if the dysfunction at the inner hair cell or synapse is bypassed by it. The dysfunction can be overcome by stimulating a synchronous discharge of the auditory nerve in a way that it is possible to evoke ABR signals [203]. Oftentimes speech perception can be improved this way [137, 143, 217]. In order to better estimate the benefit of cochlear implants compared to conventional hearing aids and other forms of assistance for a patient, genetic characterisation can provide additional information on the exact location and impairment causing the hearing loss.

1.4. A family with autosomal-dominant AS/AN

In this thesis' case a family with a new variant of hereditary autosomal-dominant AS/AN is presented. In total 11 individuals spanning four generations are affected. The pedigree is shown in figure 1.4.

1.4.1. Clinical history

The family was diagnosed with an non-syndromic AS/AN after hearing tests were performed on all affected living family members (see table 1.1).

A detailed description of the family's clinical history, hearing assessment and genetic localisation of AUNA2 can be found in a report by Lang-Roth *et al.* [124].

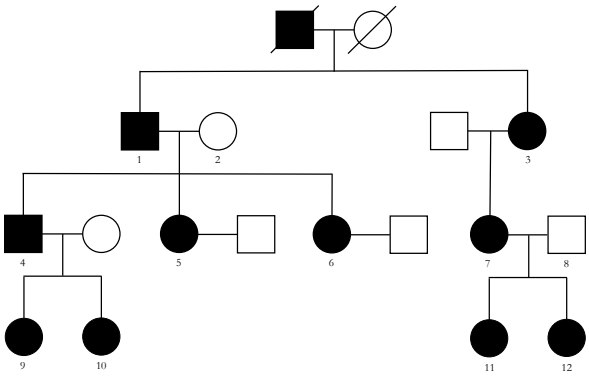

Figure 1.4.: Pedigree of a family with autosomal-dominant AS/AN. Filled symbols represent clinically affected individuals. Circles symbolise females, squares symbolise males.

The clinical features of the family differed from those described for AUNA1 patients, as listed in table 1.2. Hearing thresholds were tested with air and bone conduction pure tone audiometry and quantified according to the classifications of the European Thematic Network on Genetic Deafness (GENDEAF) [146]. TEOAE were detectable for patients with normal hearing or only mild to moderate hearing loss. Severe and profound levels of hearing loss came with an additional loss of TEOAE, probably as a late consequence of the AS/AN, as it is reported to happen for some people [151, 43].

Click evoked ABR were absent (patients 3, 4, 6 and 9) or pathologically changed in most family members. Changes included poor synchrony and only minimal amplitudes of wave V with absent waves I and III (patients 7 and 10). For patient 5 TEOAE were poor and ABR thresholds were elevated, but the wave pattern was normal. Her speech discrimination is better compared to the rest of her generation. Late CAEP were tested for most family members and could be generally detected with normal amplitudes and synchrony in patients with mild to moderate hearing loss. Patient 6 only showed CAEP at low repetition rates in the left ear. Older individuals with profound hearing loss had higher CAEP thresholds, resulting in sometimes poorly synchronised (patient 4) signals only after louder stimulation.

Taken together from the test results and the patients' descriptions the AUNA2 progress describes as follows: In the first decade of the patients' life hearing appears to be normal, but at least the results of the 7 year old indicates an already pathologically altered ABR in the presence of normal TEOAE. During the next ten years mild hearing loss in the middle and high frequencies and

Table 1.1.: Hearing test results of a family with progressive AS/AN.
Hearing loss was measured with pure tone audiometry and quantified according to the GENDEAF classification; Speech recognition: Mean of both ears was tested at 65 dB by age-appropriate monosyllabic word tests. If bilateral hearing aids are used the improved speech recognition is noted in brackets; TEOAE: Transient-evoked otoacustic emission; CM: cochlear microphonics; ABR: auditory brainstem response was click evoked; CAEP: cortical auditory evoked potentials; n.d: not detected; n.t.: not tested. Adapted from Lang-Roth *et al.* [124].

ID (Age)	Hearing loss	Speech rec. (aided)	TEOAE	CM	ABR	CAEP
11 (7 y)	normal	95%	present	CM right	pathological	n.t.
12 (10 y)	mild	90% (95%)	present	CM both	absent (85 dB)	normal
9 (11 y)	abnormal	95%	present	poor	absent (75 dB)	normal
10 (16 y)	mild	60% (80%)	present	CM both	pathological	normal
7 (38 y)	moderate	15% (n.t.)	present	CM both	pathological	normal
5 (40 y)	moderate	42% (70%)	poor	not tested	normal > 70 dB	n.t.
6 (41 y)	moderate	0% (n.t.)	present	poor	absent	only left at low repetition rate
4 (46 y)	profound	0% (10%)	n.d.	poor	absent	100 dB only (poorly synchronised)
3 (67 y)	severe	0%	n.d.	absent	absent	n.t.
1 (73 y)	profound	0% (10%)	n.d.	absent	absent	100 dB only

problems with speech discrimination start and progress to moderate levels in the third and forth decade, when also the low frequencies are affected. With further ageing conditions worsen to severe or profound hearing loss in combination with complete absence of ABR. Also the normal TEOAE get lost in later stages and CM worsens with age. Speech perception abilities and hearing threshold levels correlated for the tested individuals.

Table 1.2.: Comparison of the clinical presentation of AUNA1 and AUNA2. Adapted from Lang-Roth *et al.* [124]. ABR: auditory brainstem response; OAE: otoacoustic emission

	AUNA1	AUNA2
Age of onset	7 - 45 years	10 - 20 years
Progress	deafness at 20 years	deafness at 40 - 50 years
Type of hearing loss	symmetric, with high frequencies more affected	symmetric, mid and high frequencies more affected, progression to all frequencies
Speech recognition	poorer than expected for cochlear sensory hearing loss	almost according to expectations for cochlear sensory hearing loss
ABR	abnormal / absent	abnormal / absent before noticeable hearing loss
OAE	lost with moderate hearing loss, starting with higher frequencies	lost with severe hearing loss
Locus	13q21-q24	12q24 or 13q34

Family members with hearing aids reported only little benefit from it, as it is typical for most people affected with AS/AN [213, 15]. Although, three members fulfil cochlear implantation criteria, to the time of examination none had received an implant.

No neurological symptoms were described for all but two family members. Patients 1 (73 years old) and 3 (67 years old) had neurological complaints as a consequence of a carpal tunnel syndrome for both patients and a severe cervical and lumbar polyradiculopathy for patient 1. However, neurological examinations showed no indication for a generalized hereditary peripheral neuropathy in both family members.

Patient 9 (11 years old) had frequently relapsing nephrotic syndrome, medicated with immunosuppression using ciclosporin A, and chronic renal failure with hypertension. At the age of five she had an episode of posterior reversible encephalopathy syndrome with generalized epilepsy in consequence of the hypertension or as a side effect of the immunosuppression [59, 338]. No abnormalities connected to other diseases were found in MRI scanning.

1.4.2. AUNA2 locus

For the dominantly inherited form of AS/AN that the patients were affected by, only the AUNA1 locus [114], later identified as the gene DIAPH3 [238], was known to the time the family presented for genetic evaluation of their hearing loss. Preliminary to my work this locus was checked with genotyping of short tandem repeat markers from the AUNA1 flanking chromosomal region 13q14-21 (see fig. 1.5). When no common haplotype for that region could be found for all affected members of the family, linkage was excluded and with this also AUNA1 as a reason for the hearing loss [124].

To narrow down the chromosomal regions in which the cause of the hereditary AS/AN can be present, next a whole-genome linkage analysis was performed. Shared haplotypes for all affected family members were identified on loci 12q24 and 13q34 (see fig. 1.6). Together both regions contain 34 known or predicted genes, but no mutations could be found by the subsequent Sanger sequencing.

1.4.3. Deletion in *hATP11A*

When whole-genome sequencing became widely available it was used to further screen the patients' DNA for alterations not noticeable by Sanger sequencing. Genomic DNA of two family members was sequenced. Although, some of the genes listed in the hereditary hearing loss homepage [301] are not yet fully proven to be the direct cause of hearing loss or are called in question

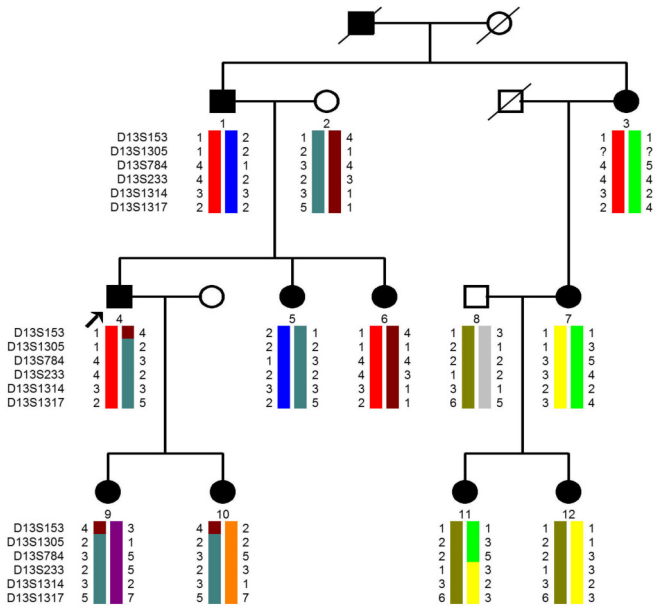

Figure 1.5.: Haplotype analysis with short tandem repeat markers flanking AUNA1. There is no shared haplotype for the locus. The figure was taken with kind permission from PD. Dr. med. Alexander Volk.

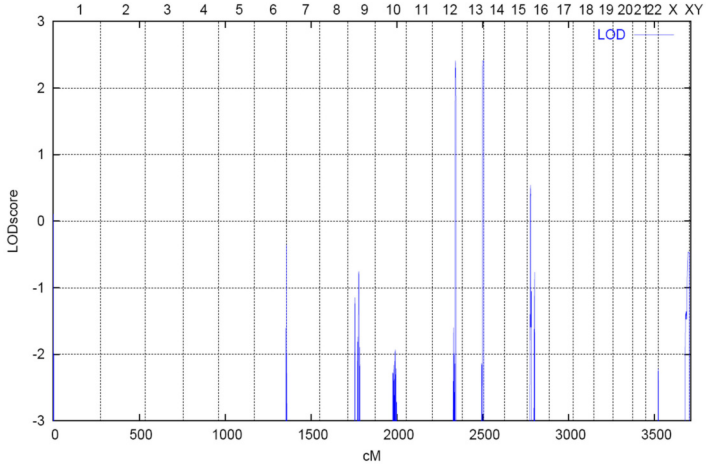

Figure 1.6.: Whole genome linkage analysis was performed using the 250k SNP array from Affymetrix. A shared haplotype for all 10 affected family members was found on loci 12q24 and 13q34. The figure was taken with kind permission from PD. Dr. med. Alexander Volk.

after being taken for a deafness gene for some time, this database is the closest to being a complete collection. Thus, the homepage's complete lists from 2011 was used to exclude an already known cause for hearing loss in the examined family. When comparing the linked regions common SNPs were also excluded. Further filtering revealed the most promising alteration, a heterozygous 5,500 bp deletion in the 3′-end of the gene *ATP11A*. This deletion includes the last coding exon of both *hATP11A* isoforms. It spans from position 13: 112877723 – 112883222 according to the Reference Genome GRCh38/hg38, which corresponds to c.3327+1782del5500. The excerpt in figure 1.7 of the genomic structure of *hATP11A* beginning at exon 28 shows the deletion and the exon usage of *hATP11A* isoform 1 and isoform 2.

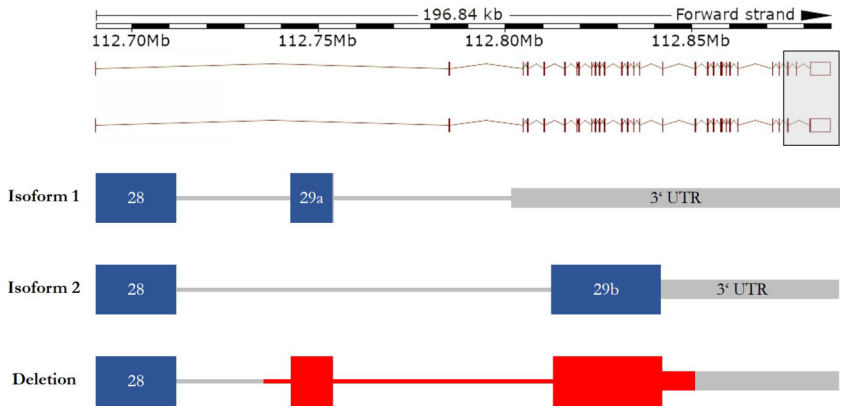

Figure 1.7.: Genomic structure of the 3' region of *hATP11A* with focus on the deletion site. The last coding exons 29a and 29b of both *hATP11A* isoforms are deleted. Coding exons of the different isoforms are marked as blue boxes, whereas introns are shown as thin grey lines. The deletion at the mutated allele is illustrated in red and the beginning of the 3'UTR as a thinner grey box. The complete overview of *hATP11A* isoform 1 and 2 at the top is taken from the Ensembl Genome Browser [336]. The section of the blow up is placed in the light grey box.

1.4.4. Stable mRNA expression of the mutated *hATP11A* allele

A possible consequence of the deletion of *hATP11A* exon 29a and 29b could be a truncated protein due to the use of an alternative stop codon. To prevent possible gain-of-function or dominant-negative effects of truncated variants, shortened mRNA is recognised in the cell during translation and degraded in a process called nonsense-mediated mRNA decay. The mutant allele harbours a

heterozygous SNP rs11616795 in exon 28 of *ATP11A*, which was found during earlier diagnostic sequencing. This was taken advantage of, to investigate if the deletion gives rise to a stable mRNA transcript or if it underlies nonsense-mediated mRNA decay. The presence of a heterozygous signal for guanine and adenine during amplification of *ATP11A* exon 28 proves the existence of stable mRNA of both alleles.

1.5. The phospholipid translocating P4-ATPase hATP11A

ATPases are protein pumps that transport ions and other molecules through biomembranes in ATP dependent manner. They are divided into several classes based on their function.

1.5.1. Transport through biomembranes

Biomembranes represent important boundaries inside cells. Without help these membranes are impermeable for a lot of molecules. Those molecules need to be transported in and out of the cell or from one organelle compartment to another by transmembrane proteins.

For active transport against a concentration gradient energy dependent, membrane spanning pumps are necessary. The needed energy is obtained trough ATP hydrolysation or co-transport of a second substrate, mainly Na^+ or H^+ ions [308].

1.5.2. ATP generating and consuming transport

There are four types of transporting ATPases, which are types F, V, P and ABC transporters. Not all of them consume ATP for their transport.

F-type ATPases, also called ATP synthases, are located in the inner membrane of mitochondria and chloroplasts. They are the main producer of ATP. F-type ATPases consist of two functional domains. The transmembrane spanning F0 domain builds the pore and the catalytic and hydrophilic F1 part synthesises ATP. The energy necessary for this is acquired by proton transport along the concentration gradient [197].

ATP consuming transport through biomembranes against a concentration gradient can be performed by the remaining three transporter types.

ABC-transporter are divided into import and export transporters. Import transporters are only present in prokaryotes to import nutrients, while export

transporters are also found in eukaryotes [64]. Human ABC transporters contain two transmembrane domains and two ATP binding domains. Upon ATP binding and hydrolysis in the presence of a divalent cation, the transmembrane domains perform conformational changes in order to transport the bound molecule trough the membrane. A general mechanism for this class can not be described, because the structure of those transmembrane domains differs critically between each transporter [197].

The ATP consuming V-type ATPase resembles the described F-type ATPases in such a way that they consist of a membrane bound V0 pore part and a catalytic V1 part, but act inversely. The V1 part of V-type ATPases is hydrolysing ATP to gain energy for the transport of protons. Through pumping cellular protons out of the cell, they regulate the pH in acidic organelles like endosomes, lysosomes and Golgi membranes [142, 236].

The other class of the ATPase family actively transporting molecules through biomembranes are the P-type ATPases. The different subclasses of P-type ATPases pump mainly different ions and phospholipids. Their structure, mechanism and function will be described in detail in the next sections [197, 280].

1.5.3. Structure of P-type ATPases

P-type ATPases can be found in all cellular membranes, across which they maintain important gradients by translocating cations, heavy metals and lipids. They contain the catalytically active α-subunit that can be accompanied by β- and γ-subunits or have additional helices and extensions, depending on the specific subclass [23].

The first known P-type ATPase structure was the Ca^{2+}-ATPase of rabbit muscle cells, analysed with x-ray crystallography [294]. It followed other P-type pumps, like the Na^+/K^+-ATPase [156, 254] and the H^+-ATPase. The structural homology between the P-type ATPases is high, so the knowledge gained this way can be adapted for other P-type transporters [198, 188].

Ion transporting P-type ATPases consist of five domains (see fig 1.8). They have an even number of transmembrane segments, thus both ends of the protein are on the cytoplasmic side of the membrane. They separate into a T-domain (transport) and a S-domain (class specific support). The six membrane spanning segments of the T-domain are flexible and move during the transport cycle. Each three segments form a half-channel through which the substrate enters and binds to a varying number of binding sites. A conserved proline residue indicates a common binding mechanism for ions or water. The S-domain is more rigid and can be placed at the N-terminal or C-terminal end [188]. Oftentimes

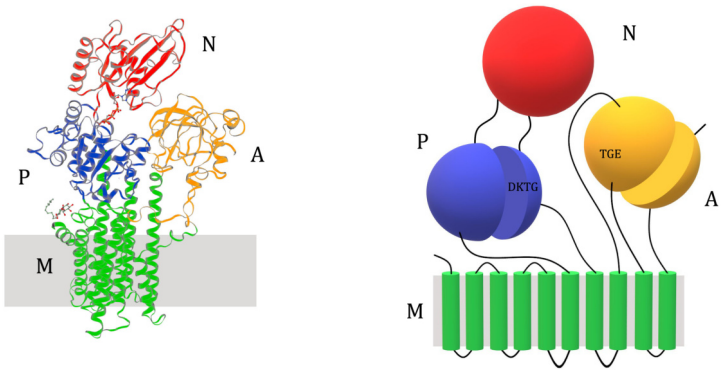

(a) 3D structure of AHA2, modified from SWISS Model (swiss-model.expasy.org)

(b) Simplified 3D structure of AHA2 that can be adapted to other P-ATPases

Figure 1.8.: 3D structure of the *Arabidopsis thaliana* H^+-ATPase 2 (AHA2). The membrane spanning M-domain is connected to the A-domain and the catalytic active P-domain, whose DKTG motive sequence is phosphorylated during ATP hydrolysis. A β-sheet structure in between the P-domain builds the nucleotide binding N-domain. The TGE motive of the A-domain interacts with the P-domain during transport.

both T- and S-domain are together labelled as M-domain [23].

All other domains are cytoplasmic. The evolutionary conserved catalytic center is the P-domain for phosphorylation. During ATP hydrolysis the aspartic acid (D) in the DKTG motive is phosphorylated. In between the amino acid stretches that form the P-domain is a sequence folded as a β-sheet, which forms the N-domain for nucleotide binding. The third cytoplasmic domain is a conserved A-Domain, short for actuator domain. It is connected to the transmembrane domains by a flexible linker and contains the signature TGE motive which interacts with the P-domain during the transport. At the N- or C-terminus an additional regulatory R-domain can be present, which for example acts through autoinhibition, as cation sensor or affinity regulator [188].

1.5.4. Subclassification of P-type ATPases

P-type ATPases transport mainly ions, but also some other molecules. They are for example involved in maintaining membrane potentials and composition or Ca^{2+} homeostasis. P-type ATPases are divided into five different groups according to their sequence homology. Inside those groups the subclassification is performed with regard to the transported substrate. Group I is devided into

Ia, pumping K^+ ions in bacteria, and Ib, transporting heavy metals. Group II is devided from A to D, where group A and B contain Ca^{2+} pumps, group C Na^+/K^+ and H^+/K^+ pumps of animals and group D fungal Na^+ pumps. Subgroup IIIa subsumes all proton pumps, while there are known only a few bacterial ATPases transporting Mg^{2+} ions classified as subtype IIIb. For P-type ATPases of group V the specific substrate is not identified yet [187, 188, 9].

1.5.5. P4-ATPases

Eukaryotic biological membranes consist of a phospholipid bilayer. The different phospholipids contained in it are often distributed asymmetrically across the bilayer. For example in the plasma membrane the exoplasmic leaflet is enriched with phosphatidylcholine (PC), sphingomyelin (SM) and glycosphingolipids, while the cytoplasmic leaflet contains mostly phosphatidylserine (PS) and phosphatidylethanolamine (PE) [333]. A schematic overview can be found in figure 1.9. This asymmetric distribution plays an important role in many vital cellular processes, like shape determination, membrane stability, cell signaling, apoptosis regulation, cell migration, membrane trafficking and many more. Section 1.5.7 gives a more detailed overview on the role of the membrane asymmetry in cell physiology.

To counteract spontaneous lipid flip-flop between the leaflets and scramblase action dissipating the asymmetry, phospholipids are actively transported by floppases or flippases depending on the orientation of transport [252, 2]. ATPases of group IV, also called P4-ATPases or phospholipid flippases, are part of the latter and facilitate unidirectional transport of specific phospholipids from the exoplasmic leaflet to the cytosolic leaflet. The exoplasmic leaflet can be either the extracellular leaflet of the plasma membrane or the luminal leaflet of the Golgi apparatus or endosome membranes [245, 334].

The P4-ATPases can be further divided in three evolutionary subgroups that appear to have separated early in eukaryotic development, based on specific signature sequences. P4a-ATPases are present in all eukaryotic groups, whereas P4b-ATPases can not be found in plants. P4c shares signature sequences with P4a and P4b-ATPases and thus represents an intermediate group between the other two. However, none of the grouping correlates to substrate specificity or membrane localisation. [185]. Another nomenclature of subclassification is also based on sequence similarities in the catalytic subunit within the P4-ATPase group [193]. Here subclasses seem to match with interaction specificity with CDC50 proteins [280].

Most P4-ATPases form a heterodimer with itself as the catalytic active α-unit

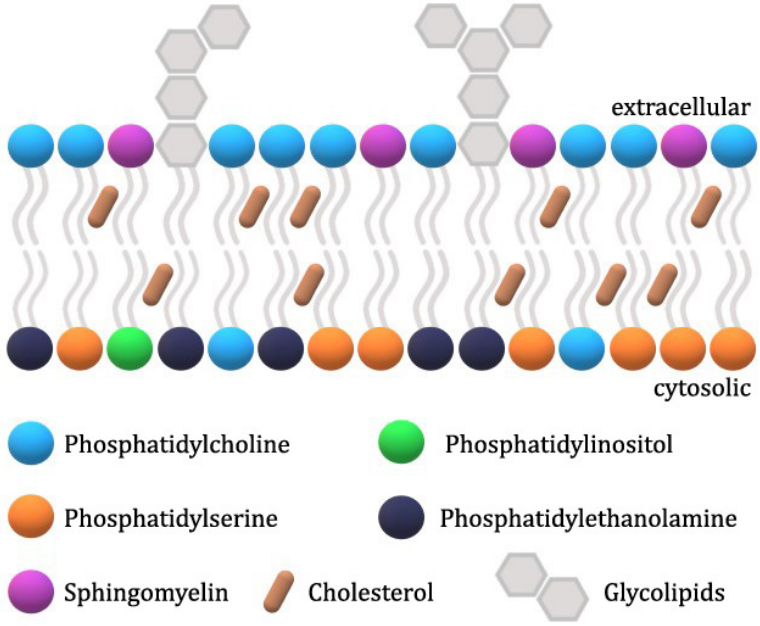

Figure 1.9.: Schematic overview of the asymmetric distribution of phospholipids in the plasma membrane. The extracellular leaflet contains phosphatidylcholine (PC), sphingomyelin (SM) and glycolipids. Phosphatidylserine (PS) and phosphatidylethanolamine (PE) are mainly present on the cytosolic leaflet, as well as some phosphatidylinositol and also phosphatidylcholine.

and a CDC50 β-unit for transport from the endoplasmatic reticulum to their destined location [16, 252]. There are three human CDC50 proteins, CDC50A, CDC50B and CDC50C. The majority of the P4-ATPases forms heterdimers with CDC50A, but some also use CDC50B solely or in addition. CDC50C is expressed exclusively in testis and is not known for dimerisation with any P4-ATPase [305, 181].

Dependence on a β-subunit from the CDC50 protein family, subcellular localisation and substrate specificity of the different mammalian P4-ATPases can be found in table 1.3 adapted from Shin and Takatsu [252].

CDC50 proteins are small membrane located glycoproteins, consisting of two transmembrane segments and a large exoplasmic domain. Both, the P4-ATPases and CDC50 only exit the endoplasmic reticulum (ER) as a heterodimer. Monomeric CDC50 accumulates in the ER. On its own, CDC50 dependent P4-ATPases are incapable of leaving the ER and no phosphorylation through ATP

Table 1.3.: Dependence on a CDC50A subunit, subcellular localisation and substrate specificity of mammalian P4-ATPases. ND = not determined, LE = late endosome, RE = recycling endosome, EE = early endosome, TGN = trans-Golgi network, PM = plasma membrane. Adapted from [252].

P4 ATPase	**CDC50 subunit**	**Localisation**	**Substrate**
ATP8A1	CDC50A	LE, RE, TGN, PM	PS, PE
ATP8A2	CDC50A	TGN, RE, PM	PS, PE
ATP8B1	CDC50A, CDC50B	PM	PC, PS
ATP8B2	CDC50A, CDC50B	PM	PC
ATP8B3		ND	(PS?)
ATP8B4	CDC50A, CDC50B	PM	ND
ATP9A	-	EE, RE, TGN	ND
ATP9B	-	Golgi	ND
ATP10A	CDC50A	PM	PC
ATP10B	CDC50A	LE	ND
ATP10D	CDC50A	PM	ND
ATP11A	CDC50A	PM	PS, PE
ATP11B	CDC50A	EE, RE	PS, PE
ATP11C	CDC50A	PM	PS, PE

hydrolysis is possible. The CDC50 subunit is necessary for correct folding, ER exit and catalytic activity [35]. While some similarities with the β-subunit from Na^+/K^+-ATPase can be drawn, there are many differences and the exact molecular function remains unkown. [210]. Though, in 2019 Hiraizumi *et al.* [97] were able to identify the way hCDC50A and P4-ATPases, in their case hATP8A1, build heterodimers. They could show that hCDC50A interacts with the extracellular transmembrane loops and some intracellular regions. The positive charged hCDC50A interacts through salt bridges and hydrophobic bonding with the negative charged extracellular loops of hATP8A1. Only the loop spanning from the M1 to the M2 domain remains uncovered. The two transmembrane domains of hCDC50A sit next to the M10 domain of hATP8A1 and the N-terminal tail stretches parallel to the plasma membrane to interact with the intracellular loops between M6 and M7, as well as M8 and M9 and the connection between M4 and the P-domain. Tone *et al.* [292] were able to show for hATP10A, hATP11A, B and C that for this interaction the ATPase needs to be in the E2P state of its catalytic cycle.

1.5.6. Mechanism of P4-ATPase transport

Since the structure of P4-ATPases resembles the general description given on P-type ATPases to a great extend, also the transport mechanism was believed to share similarities to the Post-Albers-Cycle, which is the general simplified model of transport for ion pumping P-type ATPases [4]. It describes a two conformation changing process with conformation states E1 and E2 based on the cycle of the Na^+/K^+ ATPase [106, 105]. Until recently, details on how a phospholipid, that is much larger than the usual ion substrate, is transported by P4-ATPases, remained elusive [312]. In the same study in which Hiraizumi *et al.* identified the interaction sites between p4-ATPases and hCDC50A, they were able to capture the transport cycle of P4-ATPases by cryo electron microscopy exemplified by the hATP8A1-CDC50A complex [97]. They found six intermediate states of the transport cycle corresponding to the proposed Post-Albers-Cycle without the need of a countertransported substrate (see fig. 1.10).

Essentially, E1 describes the starting state of the molecule. After binding an ATP in the so-called E1-ATP state, the N-domain and P-domain get in proximity to each other by conformational changes. The adenine ring interacts with Phe534 of the N-domain and the phosphate group is used for the phosphorylation of the nearby aspartic acid (D) of the DKTG motif of the P-domain. This way the two domains get linked in the E1P-ADP state and the A-domain is slightly shifted outwards. The remaining ADP is then released from the N-domain which induces further conformational changes that lead to the E2P state. In this the A-domain and N-domain interact through the conserved DGET motif of the A-domain, which is the corresponding region to the TGE motif in ion transporting P-ATPases. This is where the C-terminal regulatory domain found for hATP8A1 intervenes in the translocation process. It penetrates between the N-domain and the P-domain and stabilises the E2P state. It is thought that this way also the A-domain and the P-domain are kept apart, which facilitates the rotation of the A-domain to the E2Pi-PL state at least for hATP8A1. The exact state and mechanism in which the C-terminal regulatory domain modulates the flippase activity differs greatly between P4-ATPases. The rotation of the A-domain gives the first two transmembrane domains M1 and M2 flexibility for lateral movement. This way the hydrophilic cleft with the phospholipid binding site is opened between M1-M2 and the bulk of the other transmembrane domains. The phospholipid enters the hydrophilic cleft from the exoplasmic leaflet and is blocked by the Ile357 side chain in the PISL motif. The phospholipid is now occluded in the cleft because the loop between transmembrane domain M1 and M2 closes the exoplasmic exit. The

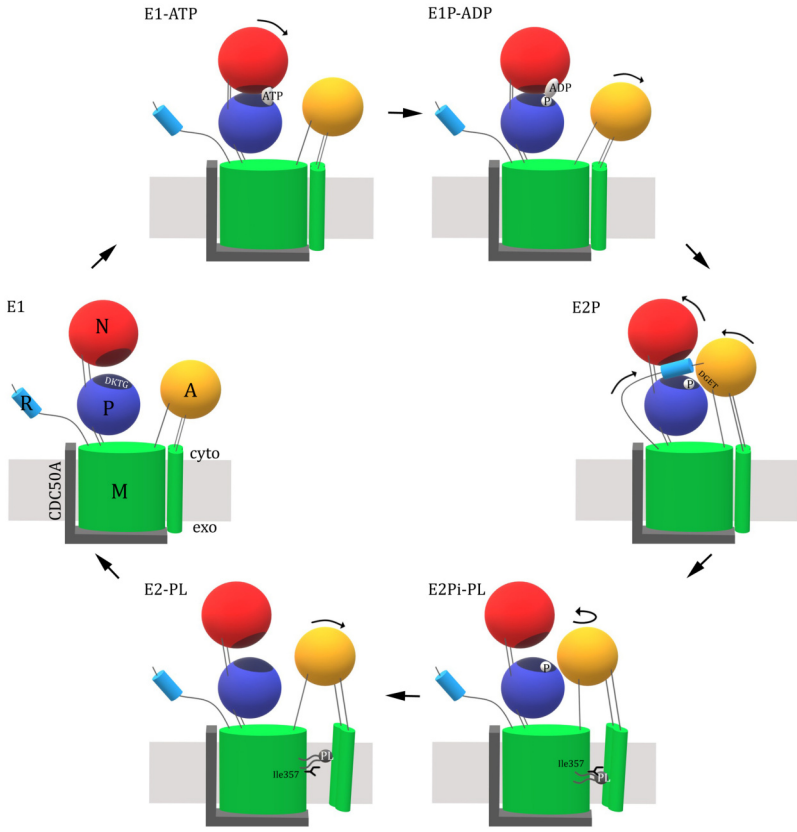

Figure 1.10.: Schematic model of the catalytic cycle of P4-ATPase transport based on the Post-Albers-Cycle exemplified by the hATP8A1-CDC50A complex. The color scheme is inherited from that of figure 1.6. The six states were found by Hiraizumi *et al.* [97] with cryo electron microscopy on the complex hATP8A1-hCDC50A.
E1: Starting state. E1-ATP: ATP is bound, P- and N-domain (blue and red) get in proximity. E1P-ADP: The DKTG motif gets phosphorylated. The A-domain (yellow) is shifted outward, so ADP can be released. E2P: The N- and A-domain interact after further conformational changes. The C-terminal R-domain (light blue) is now able to penetrate between the N- and P-domain and facilitates the conformational changes to E2Pi-PL (this might probably differ in detail for ATP11A and other P4-ATPases). E2Pi-PL: The A-domain rotates and the hydrophobic cleft between M1, M2 (green tubes) and the rest of the M-domain (green cylinder) opens. The phospholipid (PL) enters the cleft and is blocked by Ile357. E2-PL: Probably enabled by the dephosphorylation of the DKTG motif, M1, M2 and the A-domain are further shifted outwards, the cleft opens even more and the phospholipid can be translocated to the cytosolic leaflet. Afterwards the flippase shifts back to the E1 starting state.

phospholipid acyl chain sticks towards the lipid environment and is in part protected by a hydrophobic pocket between transmembrane domain M2 and M4. The head group is located in a hydrophilic cleft of the ATPase, whose residues are thought to define the phospholipid selectivity for PS and PE. Subsequently phospholipid binding induces further movement of the A-domain, so that the DKTG phosphorylation site gets targetable for hydrolysis. The release of the phosphate is believed to be coupled to the phospholipid translocation to the cytoplasmic leaflet, by enabling M1 and M2 to shift even further away from the bulk transmembrane domains. The phospholipid is released through the cleft, gets incorporated and laterally released in the cytoplasmic leaflet by diffusion. The P4-ATPase shifts back from the so-called E2-PL state to the E1 state to start the translocation of another phospholipid.

This model is further supported by the recently captured protein crystal structure of an isolated E2P state of human ATP11C [164]. The structure of hATP11C conforms with the described model mechanism, but exhibits some differences regarding the creation of the tunnel for the phospholipid. It was found that the helices of M2, M4 and M6 of hATP11C form a longitudinal crevice from the exoplasmic surface to the middle of the membrane. The crevice is blocked by a valine at position 357 instead of the isoleucine in hATP8A1 and hATP8A2. The PISL motif is changed to PVSL. Those crevice is not present in the hATP8A1 E2P state, because it is blocked by the longer C-terminal regulatory domain. In contrast to the hydrophilic cleft built by hATP8A1 in the E2-Pi-PL state, this crevice seems to be open earlier in the transport process, if not all the time, and is not blocked at the exoplasmic end. In fact, at this end an additional hydrophilic and electro-positive cavity connected to the crevice was found. It consists of the loop between transmembran domain M3 and M4 and the exoplasmic domain of CDC50A. Modelling showed that this cavity is most likely a second phospholipid binding site at which the hydrophilic head group of the lipid is bound in the cavity while the acyl chain sticks outwards to the lipid phase. Those changes were interpreted as an adaption to the position of hATP11C at the plasma membrane. It is proposed that the second phospholipid binding site might enable the energy-consuming step of getting the hydrophilic head of the phospholipid from the outer leaflet inside of the flippase at all. By providing an entrance to the protein that mimics the environment of the membrane the needed energy for the phospholipid acquisition might be decreased. This way the second binding site at the cavity indicates a slightly modified model mechanism for hATP11C. The model proposed by Nakanishi *et al.* [164] interprets the binding of the phospholipid to the cavity

as the initiation point of the translocation. After binding there, it is thought to diffuse through the crevice until it is blocked by the gating Val357 of the PVSL motif. Binding to that phospholipid binding and occlusion site is hypothesised to induce the conformational changes to the E2Pi-PL state. From there on the cycle would proceed with opening of the crevice towards the cytoplasmic leaflet through movement of the M1, M2 and A-domain, as described in the generally proposed catalytic cycle based on the hATP8A1 model.

1.5.7. Pathophysiology associated with P4-ATPases and phospholipid distribution across membranes

As mentioned before, the main function of P-type ATPases is to maintain a phospholipid gradient across bilayer membranes. The asymmetric phospholipid distribution is vital for several cellular functions. Based on this important role, it is no surprise that altered flippase activity can have clinical consequences. So far, mutations in the genes for *ATP8B1* and *ATP8A2* have been directly linked to human disorders.

Homozygous and compound heterozygous mutations in the *ATP8B1* gene have been found to cause a spectrum of liver disease in humans, divided into progressive familial intrahepatic cholestasis type 1 (PFIC1 or Byler's disease) on one end and a milder form called benign recurrent intrahepatic cholestasis type 1 (BRIC1) on the other end [25]. The severity of the liver disease seems to be dependent on the severity of the changes to the ATP8B1 protein structure. While misssense mutations often lead to BRIC1, large deletions, frameshift and nonsense mutations that have larger impact on protein structure tend to cause the severe PFIC1 [115, 307]. In PFIC1 patients the hepatic phenotype is more severe and often extrahepatic features like diarrhoea [136, 54], pancreatitis [296], pneumonia [221] and sensorineural hearing loss [265] occur. Testing the effects of missense mutations of BRIC1 and PFIC1 patients on the ATP8B1 protein showed that stability and interaction with CDC50A has been decreased or lost in several cases. In the liver ATP8B1 is expressed in canalicular membranes of hepatocytes. While there was still residual mutant protein at the canalicular membrane of WIF-B cells with BRIC1 mutations, mutant protein from PFIC1 patients was not to be found [69]. ATP8B1 is also expressed in the bladder, stomach, intestine and pancreas, where a loss of function might cause the extrahepatic symptoms [25].

ATP8B1 localises to the apical membrane of epithelial cells and translocates PS to the cytplasmic leaflet. The asymmetric membrane character of the canalicular membrane of rat hepatocytes was lost with knockdown of ATP8B1

function [60] which is thought to be the cause of cholestasis. With PS usually transported to the cytoplasmic leaflet, sphingomyelin accumulates in the outer leaflet of the plasma membrane and forms together with cholesterol a stiff membrane that is resistant to bile salts [304]. When ATP8B1 fails to flip PS, the membrane is destabilised and the detergent effects of hydrophobic bile salts in humans are thought to extract PS and cholesterol from the destabilised membrane into the canalicular lumen. This might consequently reduce the cholesterol content of the cytosolic leaflet and thus induce cholestasis by impairing ABCB11 bile transporter acitivity [194, 195]. Another hypothesis, suggesting direct involvement of ATP8B1 in a signalling cascade for bile excretion, remains controversial [29, 303, 32].

However, all the hypotheses have to be reassessed, considering the latest findings that ATP8B1 transports rather phosphatidylcholine (PC) than PS [281]. In accordance to the earlier hypothesis, the lack of PC at the inner leaflet of the canalicular membrane could also lead to diminished membrane stability. Nevertheless, the role of ATP8B1 in cholestasis is not fully understood and has to be further investigated.

For *ATP8A2* two cases of genetic defects leading to disorders have been reported. In one of them a de novo balanced translocation of chromosomes 10 and 13 disrupts the *ATP8A2* coding sequence, which leads to mental retardation and hypotonia [313]. The other case describes a consanguineous family with four individuals affected by cerebellar ataxia and mental retardation. A homozygous mutation in a conserved region coding for the M4 transmembrane segment causes loss of PS flippase activity through reduced PS affinity while maintaining a wild type (WT) like expression level [58, 312]. Similar neurological symptoms could be reproduced in two mouse models with *Atp8a2* deficiency. Here loss of ATP8A2 activity led to distal axonal degeneration of spinal motor neurons [340] and in addition also to loss of visual and auditory function through degeneration of photoreceptor and spiral ganglion cells [37]. One well studied function of P-type ATPases is the regulation of apoptosis together with scramblases [reviewed in 242, 89]. ATPases translocating PS and PE are important for the depletion of the extracellular leaflet of the plasma membrane from PS, since exposed PS represent a stimulus for phagocytic cells. Thus, changes in phospholipid flippase activity could lead to disturbed apoptosis. However, in both studies on *Atp8a2* deficiency no exposure of PS on the plasma membrane that could lead to phagocytosis has been detected. Accordingly, it is more likely that the underlying reason for the degeneration is abnormal vesicle trafficking.

Although there are no other reported cases of human disorders based on loss

of flippase activity, several studies and other mouse models further show the severe effects of P4-ATPase dysfunction.

Mice deficient in the ATP8A2 homolog ATP8A1 accumulated PS on the outer leaflet of the plasma membrane of hippocampal cells and showed reduced hippocamus-dependent learning [131]. Loss of both ATP8A1 and ATP8A2 in double mutants led to neonatal lethality [340]. ATP8A2 might also play a role in human tumorigenesis [272], while ATP8B3 has been associated with sperm capacitation in mice [318] and a single nucleotide polymorphism (SNP) near the *ATP8B4* gene sequence has been significantly overrepresented in patients with Alzheimer's disease [132]. ATP10A andATP10D are suggested to play a role in the controle of insulin-mediated glucose uptake in mice and associated with a elevated risk for Type 2 diabetes [46, 67].

Two mouse models with ATP11C deficiency exist that showed comparable phenotypes. In one of them hemizygous males and homozygous females developed hypercholanamia and hyperbilirubinemia and showed an arrest of adult B lymphopoesis in the bone marrow [256, 255]. In the other model also abnormalities in B lymphocyte differentiation and hyperbilirubinemia could be found in addition to anemia and hepatocellular carcinoma. The PS flippase activity of ATP11C was reduced, but once again no accumulation of PS in the exoplasmic leaflet of the plasma membrane could be detected [329]. Other studies showed that ATP11C deficiency in mice resulted in disturbed erythropoiesis, with short living and abnormal shaped erythrocytes displaying PS on their cell surface. The shortened lifespan probably relates to the activation of apoptosis, while the abnormal shape might come from disturbed interaction of the cytoskeleton with the plasma membrane, due to missing PS and PE in the cytoplasmic leaflet [330].

Another mouse model, which emulates a typical *ATP8B1* missense mutation causing the above mentioned liver disease PFIC1 in humans, was used to investigate the auditory symptoms that sporadically accompanies cholestasis. The study by Stapelbroek *et al.* [265] found that a majority of BRIC patients develops hearing difficulties around the age of 20 years, featured by abnormal TEOAE and ambilateral hearing loss more elevated at higher frequencies compared to lower ones. Although ATP8B1 expression was reduced, the mice only developed a mild hepatic phenotype due to different physiological reactions on bile salt accumulation in mice and men. Cholestasis could only be induced by feeding a bile salt enriched diet [196]. Nontheless, even on normal diet mice displayed progressing hearing loss associated with degeneration of cochlear hair cells and spiral ganglion cells. Stapelbroek *et al.* propose that a possible expla-

nation for this could again be a destabilised stereociliar membrane because of the lost phospholipid asymmetry, similar to findings for the red cell membrane [140] or the loss of ATP8B1 function at the canalicular membrane [304]. The phospholipid distribution could also indirectly influence the ATP-dependent Ca^{2+} transporter (PMCA) activity [285], needed for normalising Ca^{2+} after hair cell activation [315]. Another hypothesis is that the loss of the membrane asymmetry impairs the generation of phosphoinosides and thus disturbs maintenance of the hair bundle structure and inhibits correct mechanotransduction [91, 98].

Besides the composition of the cell membrane, the phospholipid asymmetry of intracellular membranes is important, too. It comes into play at vesicle trafficking. After being synthesised at the ER, most membrane phospholipids are distributed symmetrically across the ER membrane by scramblases. With vesicles the lipids are moved from the ER to the Golgi complex, where flippases and floppases establish an asymmetrical distribution of lipids in the trans-Golgi network (TGN) [2]. This asymmetry seems to be crucial for membrane curvature and accordingly also for organelle shape determination. Studies in yeast show that upon inactivation of the yeast P4-ATPase Drs2 the Golgi cisternae lose their tubular form and become large cup-shaped structures [31]. Curvature and the negative charge of PS on the cytoplasmic leaflet are suggested to be sensed by the +ALPS motif of the Gcs1 protein. This starts a cascade that leads to the recruitment of clathrin, which moulds vesicles from the curved Golgi membrane [327]. While most studies on P4-ATPases regarding vesicle trafficking are performed on yeast [241], a similar function is proposed for the retrograde transport from recycling endosomes to the Golgi in eukaryotic cells [297, 127]. The outcome of P4-ATPase deficiency experiments in other studies further strengthens the association of flippase based membrane asymmetry as a requirement for vesicle trafficking in eukaryotic cells, even though the mechanism is not determined [2, 37, 328].

Taken together, defects of P4-ATPase activity result in a variety of symptoms with an emphasis on hepatic and neurological phenotypes, including sensorineural hearing loss for ATP8A2 and ATP8B1. The underlying mechanisms still need to be determined in detail, but often seem to be linked to membrane stability, vesicle trafficking, indirect and protein activation or phagocytosis.

1.5.8. ATP11A

ATP11A is a human P4-ATPase. Evolutionary ATP11A can be sorted into the P4a-ATPases that exist in all eukaryotic groups [185] and further into P4-subclass 6 together with ATP11B and ATP11C, based on the sequence similarity of the catalytic subunit [193]. Its genomic sequence is located on chromosome 13:112,690,329 - 112,887,168 aligned to the Reference Genome GRCh38/hg38 with the UCSC genome browser [113, 112]. The size of the coding region is 187,878 bp and it spans 30 coding exons that can be translated into two isoforms of *ATP11A*. The first one uses exon 29 as the last coding exon. The mRNA of this isoform 1 (RefSeq: NM_015205.2) is 3405 bp long and encoding a protein with 1134 aa. Isoform 2 (RefSeq: NM_032189.3) skips exon 29 and uses exon 30 as its last coding exon. The mRNA contains 3576 bp and encodes a protein of 1191 aa [176]. The genetic intron-exon structure of human *ATP11A* is shown in figure 1.11.

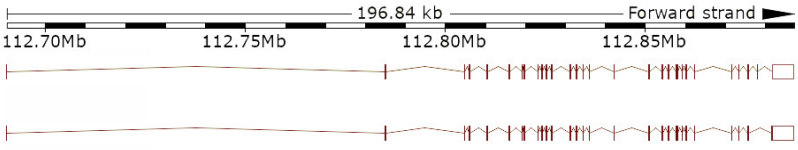

Figure 1.11.: Gene structure of *hATP11A*, adapted from the Ensembl Genome Browser, version 93 (www.ensembl.org) [336]. The upper intron-exon structure represents *hATP11A* isoform 1, while the lower structure shows isoform 2.

Human ATP11A is highly expressed in tubules of the kidney. In the brain ATP11A is found to be expressed in endothelial cells, neuronal cells and neurophils of the cerebral cortex and purkinje cells of the cerebellum. Medium level expression also takes places in the pancreas, in lung pneumocytes and in glandular cells of the gastrointestinal tract, appendix, gallbladder and placenta. Other brain areas, liver hepatocytes, urothelial cells, skin melanocytes and glandular cells in the female reproductive system express ATP11A at lower rates. An overview of the expression in the human body is shown in figure 1.12. [298, 299].

On the intracellular level ATP11A is synthesised in the ER. There it is translocated to the plasma membrane, but it can be also found in early endosomes and recycling endosomes. It depends on CDC50A for ER exit and has a flippase activity for PS and PE, but not for PC or SM [280, 281].

ATP11A has 10 transmembrane domains and both, the C-terminus and the N-terminus of the protein reach into the cytoplasm. A high resolution 3D pro-

tein structure of hATP11A is not yet examined. However, the protein crystal structure of an isolated E2P state of human ATP11C [164] has an amino acid sequence similarity of 67.01% compared to human ATP11A, which allows for a model, shown in figure 1.13.

Figure 1.12.: Expression of ATP11A in the human body, taken from the Human Protein Atlas, version 19.3 (https://www.proteinatlas.org/ENSG00000068650-ATP11A/tissue). Higher expression intensity is depicted by darker red tones. Expression in the female body is shown on the left and the male body on the right.

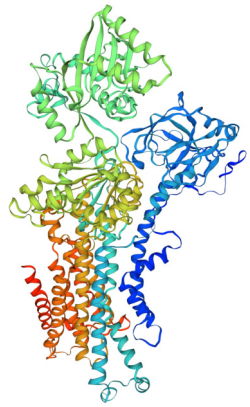

Figure 1.13.: 3D model of hATP11A, generated with SWISS Model (swiss-model.expasy.org)

To date, mutations in *ATP11A* have only been proposed as a predictive marker for colorectal cancer [153], but never been associated with sensorineural hearing loss until now.

Mutation studies based on known disease causing mutations in *hATP8B1* were performed to gain further inside in the molecular mechanism of *hATP11A* [271]. The hATP11A mutations Y308F and D913K, corresponding to L308 and E897 in hATP8B1, resulted in retention in the ER and consequential reduced PS intake, while Y308F also showed a reduced expression level, probably due to misfolding. The mutated residues are located within M3 and M5 and prevent the correct connection from of those to the M3-M4 loop and the M5-M6 loop. Since hCDC50A interacts with hATP11A through electrostatic binding to the loop region, the proper binding seems to be inhibited, which causes the protein to be dislocated.

Takatsu *et al.* [281] describes two *hATP11A* missense mutations with known effects on protein activity. hATP11A isoform 1 E186Q has a missense mutation at a conserved glutamate residue, that is necessary for the dephosphorylation process. The mutation is reported to result in loss of function, despite correct localisation at the membrane. The other mutant variant is hATP11A isoform 1 D414N. The mutation disables the interaction with hCDC50A and this inhibits translocation from the ER to the membrane [281, 130].

Using the prediction of hATP11A's two caspase cleavage sites, Segawa *et al.* [243] were able to modify both and use them for the analysis of flippase regulation by caspase and Ca^{2+} in HEK293T cells. They found WT hATP11A to be inactivated by caspase cleavage during apoptosis to expose PS on the cell surface. It was also shown that PS exposure during apoptosis is inhibited in the caspase resistant hATP11A mutant. Another way of regulation enables the transient downregulation of hATP11A flippase activity through high concentrations of Ca^{2+}. The high Ca^{2+} concentration also activates scramblase function, so that as an effect PS is reversibly exposed on the cell surface or on vesicles for certain biological processes when needed.

2. Aim of this study

After narrowing down two possible loci for the causative mutation in the family affected with AS/AN, a 5,500 bp deletion in a gene coding for the P4-ATPase ATP11A was detected. The deletion spans the last exon of both ATP11A splice variants.

The aim of this thesis is to characterise the influence of the deletion on gene expression and sequence changes, as well as to study the further implications following from those.

Expression of mRNA of both *ATP11A* splice variants in the presence of the deletion had been shown before through the presence of a heterozygous SNP in exon 28 of the patient in RNA analyses. This will be replicated. Afterwards, the first subject to be investigated is the mRNA sequence transcribed from the mutated *ATP11A* DNA allele. Possible outcomes for this are sequences encoding for a truncated protein or the elongation via additional exons. Therefore, a set of PCRs on patient cDNA, using a forward primer in an exon upstream of the deletion and different reverse primers located in the 3'UTR downstream of the deletion, should be used to identify and amplify the product of the mutant allele. Subsequent sequencing could provide the detailed sequence information, which needs to be examined for the used stop codon and potential alternative splice sites.

For further research on the mutant protein in human cell culture, construction of an expression vector encoding the found variant is necessary. Using the same cloning vector for both physiologic isoforms of *ATP11A* as well as the mutant variant ensures comparability. Also, the presence of a protein tag is beneficial for protein detection in immunocytochemistry (ICC) and Western blotting. As additional control an empty mock vector and the two reported missense variants E186Q and D414N should be used. Both protein variants encode for known loss of function and loss of transport proteins, respectively. Depending on the structure of the mutant protein, artificial mutant variants might be constructed and compared for supplementary information on the functional mechanism.

Like decribed for the D414N mutantion, one presumable way a protein loses its function is not being transported to its subcellular localisation. Since the P4-ATPase translocates phospholipids at the plasma membrane, the localisation of

the putative mutant variant of the protein in presence of CDC50A has to be investigated.

Another hypothesis that needs to be tested, is the possibility of changed flippase activity through the consequences of the deletion on protein level. In order to get comparable results, all ATP11A variants are going to be expressed in the same single cell derived cell line, stably expressing CDC50A. An assay using fluorescent labelled phospholipids would be appropriate to determine changes in flippase activity of the mutant ATP11A compared to wild type protein and controls. Therefore, an adapted flippase activity assay, based on experiments from Takatsu *et al.* [281], will be established. The cultivated cells, expressing the different ATP11A variants and CDC50A, are incubated with fluorescent labelled PS and PE for increasing time intervals, during which the phospholipids are transported into the cell by ATP11A on the cell surface. Afterwards, FACS analysis of the fluorescence level can be used to compare the uptake of phospholipids over time and thus also the flippase activity of the different ATP11A variants.

The results of this assay should be used to confirm or reject the hypothesis of altered activity and discuss possible mechanisms for the potential gain or loss of function with the help of literature research. Finally, a hypothesis on the molecular pathomechanism will be generated. For this, a detailed look into ATP11A-dependent cellular processes and evidence from ATPase deficient mouse models will help to interpret the results of the flippase assay. Thus, the genetic, molecular and cellular influence of the deletion of *ATP11A* and its impact on the hearing process can be discussed.

The insights gained this way will not only expand the knowledge of inner physiology and help to further understand the molecular details of auditory processing, but can be used to optimise the clinical assessment and assistance for patients with AS/AN.

3. Material

All material used in this thesis is listed in this chapter with its type specification or order number and the manufacturer. It is split in different categories like devices, consumable items, chemicals and reagents, enzymes, antibodies, commercial kit systems, bioinformatic tools and databases. Bacteria strains and cell lines are given with full name and description. All commercial and self made DNA primers and plasmids are listed with name and sequence, if not universally available through the manufacturer. In the section for buffers and solutions the recipes are given in detail.

3.1. Primary antibodies

Table 3.1.: List of primary antibodies

Antigen	Host	Dilution	Art. No.	Manufacturer
C-Myc	mouse	1:500 (ICC)	M5546	Sigma-Aldrich Corp. (USA)
Flag	mouse	1:500 (ICC)	F3165	Sigma-Aldrich Corp. (USA)
HA	rabbit	1:666 (ICC)	H6908	Sigma-Aldrich Corp. (USA)
V5	mouse	1:500 (ICC)	R960-25	Thermo Scientific Inc. (USA)
HA	rabbit	1:1000 (WB)	H6908	Sigma-Aldrich Corp. (USA)
Flag	mouse	1:500 (WB)	F3165	Sigma-Aldrich Corp. (USA)
V5	mouse	1:5000 (WB)	R961-25	Thermo Scientific Inc. (USA)

3.2. Secondary antibodies

Table 3.2.: List of secondary antibodies

Antigen	Host	Dilution	Label	Art. No.	Manufacturer
rabbit	goat	1:2500 (WB)	HRP	32460	Thermo Scientific Inc. (USA)
mouse	goat	1:2500 (WB)	HRP	32430	Thermo Scientific Inc. (USA)
rabbit	goat	1:1000 (ICC)	AF 488	A11008	Thermo Scientific Inc. (USA)
mouse	goat	1:1000 (ICC)	AF 633	A21052	Thermo Scientific Inc. (USA)
mouse	goat	1:1000 (ICC)	Cy3	115165003	Jackson Im. Research Inc. (USA)

3.3. Primers

Table 3.3.: List of primers

Name	Sequence	Size (b)	GC (%)	T_m (^oC)
ATP11A_Ex20f	CGACGGAGCTGCACTGTCTCTG	22	63.6	61.9
ATP11A_Ex24_25f	CTGTACAGGGACGTCGCCAAG	21	61.9	60,0
ATP11A_Ex27f	GCTGCTGTTCTACGTTGTCTTTTC	24	45.8	56.5
ATP11A_Ex28_f	CTACGTGTTCATCCAGATGCTGTCC	25	52,0	59.2
A[...]_Ex28End_pCAGhom_r	GTAGTCTGGTACATCGTATGGATACTCGAGTTCGAACCGCGGCTGGAC TCTCTCTGTTGC	60	53.3	70.3
ATP11A_Ex28r	TGTTGGCCACAGCTGC	16	62.5	56.5
ATP11A_Mut_Ex28-29mutr	GTGGTGCTTTCCTGGACTCTCTC	23	56.5	59.3
ATP11A_Mut_r	CTGTCGAGCACCTCGGAAACACCC	24	62.5	63.6
ATP11A_UTR_f	CTGGGGGTCGCTGCTGTTCTAC	22	63.6	62,0
ATP11A_UTR_r1	CCAGTTGCTCGCTACCCTCATCTT	24	54.2	60.7
ATP11A_UTR_r2	CTGGGACCCAACTTACTAAACCTTCAC	27	48.1	58.9
ATP11A_UTR_r3	CATGGCTATGAGTGAGCGTGGAG	23	56.5	59.6
ATP11A_UTR_r5	GGCCAAGGCTCAACTCAGGG	20	65,0	60.9
ATP11A_v1_1_F	GACAATGCCATGAACCAGTG	20	50,0	54.3
ATP11A_v1_1_R	GATCAAGTCGCAGGGAAAGG	20	55,0	55.8
ATP11A_v1_2_F	GCGTTCCTCATTGTGTATCTC	21	47.6	53.4
ATP11A_v1_2_R	CAGGGATGATGTAGTTAAAGAGGAC	25	44,0	54.7
ATP11A_v1_3_F	CGACATGATTGACTCGTCC	19	52.6	53,0
ATP11A_v1_3_R	CCTTTCGATGTGGTTCTCCCTG	22	54.5	57.7
ATP11A_v1_4_F	GCATTTGTAAGCTGCTGCAG	20	50,0	55.1
ATP11A_v1_4_R	GCCGTCTCCATCTTGTCTCC	20	60,0	57.6
ATP11A_v1_5_F	CTGGAAATCTGCCGGAG	17	58.8	52.9
ATP11A_v1_5_R	GCCCGTGAACAAGCAGCATC	20	60,0	59.6
ATP11A_v1_6_F	GTCGCCAAGAATGCCCTG	18	61.1	56.8
ATP11A_v1_6_R	CCTCCCCAGAGAAGCGAAAAG	21	57.1	57.8
ATP11A_v1_EndwoStop	GAAACTCAGGCTGCTGGAAGTCTGAG	26	53.8	61,0
ATP11A_v1_Ex29ar	CTCGACAGAAAGGCACTGGC	20	60,0	58.5
ATP11A_v1_Start	ATGGACTGCAGCCTCGTGCG	20	65,0	62.9
ATP11A_v2_Ex28-29br	AGAGTCCAGAATGGGTGC	18	55.6	54.4
ATP11A_v2_Ex29br	CCCTCTTGCCTCTCTGCA	18	61.1	57,0
ATP11A_v2_r	TCACACGAGCATTCCCACAC	20	55,0	57.7
ATP11A_v2_rnew	CACGAGCATTCCCACACGGGAC	22	63.6	62.6
CDC50A_attb_f	GACAAGTTTGTACAAAAAAGCAGGCTTCGAAGGAGATAGAACCATGGC GATGAACTATAACGCG	67	46.3	69.7
CDC50A_attb_r-	GGGGACCACTTTGTACAAGAAAGCTGGGTGAATGGTAATGTCAGCTGT ATTACTACTG	58	44.8	67.8
CDC50A_f	ATGGCGATGAACTATAACGCG	21	47.6	55.3
CDC50A_inner_f	GAAGACAAACCAATTGCTCCTTGTG	25	44,0	56.9
CDC50A_inner_r	GTTCTTCCAGGTTGTCTCCTCC	22	54.5	57.2
CDC50A_r	TTAAATGGTAATGTCAGCTGTATTACTACTG	31	32.3	55,0
CMV_f	CGCAAATGGGCGGTAGGCGTG	21	66.7	63.9
GPDH_f	AGGCTCCCACCTTTCTCATC	20	55,0	56.7
GPDH_r	AACTGGTTGAGCACAGGGTAC	21	52.4	57.2
HA_forw	TATCCATACGATGTACCAGACTACGCT	27	44.4	58.4
HA_rev	GGAGTGAATTAAGCGTAGTCTGGTACATCGTATGGATA	38	42.1	62,0
M13_R	GGAAACAGCTATGACCATG	19	47.4	50.8
M13f	GTAAAACGACGGCCAGT	17	52.9	52.6
pCAG_Assembly_Myc_F	GGTTCGAACTCGAGGTACCGGAACAAAAACTCATCTCAGAAGAG	44	47.7	66,0
pCAG_Assembly_Myc_R	TGGGACGTCGTATGGGTACGGGGGCAAACAACAGATGG	38	57.9	70,0
pCAG_f	GCAACGTGCTGGTTATTGTG	20	50,0	55,0
pCAG-Test_AmpPr_r	CAAATATGTATCCGCTCATGAGACAA	26	38.5	55.1
pCAG-Test_f1	CCGCCCAGCGTCTTGTC	17	70.6	59.5
pCAG-Test_f2	GACGCTCAAGTCAGAGGTGGC	21	61.9	60.3

Name	Sequence	Size (b)	GC (%)	T_m (°C)
pCAG-Test_f3	CATGGCTGATGCAATGCGGC	20	60,0	60.3
pCAG-Test_f4	GAGGTGAGCCCCACGTTC	18	66.7	58.4
pCAG-Test_f5	GAGTTCTTCTGAGGGGATCGGCA	23	56.5	60.5
pCAG-Test_f6	GCCTTAAAGGGCTCCGGGA	19	63.2	59.9
pCAG-Test_r1	ATTTCGGCTCCGCACAGATTTGG	23	52.2	60.3
pCAG-Test_r2	GCCTCCTCACTACTTCTGGAATAGCTC	27	51.9	59.8
pcDNA3_rev	GGCTGGCAACTAGAAGGC	18	61.1	56.2
pDest_TagControl	CTAGTTGCCAGCCATCTGTTG	21	52.4	56.1
pMxs-Test_f1	CCCAGTTCCGCCCATTCTCC	20	65,0	60.7
T7	TAATACGACTCACTATAGGG	20	40,0	47,5

3.4. Plasmids

Table 3.4.: List of plasmids. Tag specifications: CT = C-terminal tag, NT = N-terminal tag, KDEL = KDEL localisation tag. Manufacturer specifications: Dr. Shin (Kyoto University, Faculty of Pharmaceutical Sciences, Japan), Michael Davidson (Addgene plasmid # 58097), TFS = Thermo Fisher Scientific Inc. (MA, USA)

Vector	Resistance	Size	Tag	Design
HFN-hCDC50A pcDNA3	Amp / Kan	6530 bp	Flag / His (NT)	Dr. Shin
hATP11A-HA Iso. 1 WT pCAG	Amp	9556 bp	HA (CT)	Dr. Shin
hATP11A-HA Iso. 1 E186Q pCAG	Amp	9556 bp	HA (CT)	Dr. Shin
hATP11A-HA Iso. 1 D414N pCAG	Amp	9556 bp	HA (CT)	Dr. Shin
tdTomato-ER-3	Kan	4814 bp	KDEL	M. Davidson
pcDNA3.1(-) Myc/His	Amp	5522 bp	Myc / His (CT)	TFS
pDonr211	Kan	4761 bp		TFS
pEF5/FRT/V5-DEST	Amp / Hyg	7528 bp	V5 (CT)	TFS
pOG44	Amp	5785 bp		TFS
hATP11A-HA Iso. 2 pCAG	Amp	9661 bp	HA (CT)	S. von Loh
hATP11A-HA Patient pCAG	Amp	9529 bp	HA (CT)	S. von Loh
hATP11A-Myc/His Iso. 1 WT pCAG	Amp	9706 bp	Myc / His (CT)	S. von Loh
hATP11A-HA until ex28 pCAG	Amp	9415 bp	HA (CT)	S. von Loh
MCS-HA pCAG	Amp	6224 bp	HA (CT)	S. von Loh
pDonr211 hCDC50A	Kan	3647 bp		S. von Loh
pEF5/FRT hCDC50A-V5	Amp	6974 bp	V5	S. von Loh

3.5. Bacteria strains

Table 3.5.: List of bacteria strains

Abbr.	Specification	Manufacturer	Genotype
E. coli	*Escherichia coli*	Top10F' (Invitrogen)	F'{*lac* I^q Tn*10* (Tet^R)} *mcr*A Δ (*mrr-hsd*RMS-*mcr*BC) Φ80*lac*ZΔ M15 Δ*lac*X74 *rec*A1 *ara*D139Δ (*ara-leu*)7697 *gal*U *gal*K *rps*L *end*A1 *nup*G

3.6. Cell lines

Table 3.6.: List of cell lines

Abbreviation	Name
HEK293T	Human embryonic kidney cell line 293T (epithelial)
Flp-In 293	Human embryonic kidney cell line 293 with integrated FRT site for Flp-In transfection (epithelial) (Thermo Scientific Inc., MA, USA)

3.7. Chemicals and reagents

Table 3.7.: List of chemicals and reagents

Reagent	Article No.	Manufacturer
10× FastDigest buffer	B64	Thermo Scientific Inc. (USA)
18:1-06:0 NBD PE	810155	Avanti Polar Lipids Inc. (USA)
18:1-06:0 NBD PS	810194	Avanti Polar Lipids Inc. (USA)
2-Log DNA Ladder	N3200S	New England Biolabs Inc. (USA)
4× Bolt LDS Sample buffer	B0007	Thermo Scientific Inc. (USA)
5× Phusion HF buffer	B0518S	New England Biolabs Inc. (USA)
5× Phusion GC buffer	B0519S	New England Biolabs Inc. (USA)
7deaza dNTP	D8783-.5UMO	Sigma-Aldrich Corp. (USA)
Agar	A0949,0500	AppliChem GmbH (GER)
Agarose	16500-500	Thermo Scientific Inc. (USA)
Amphotericin B solution	A2942-100ML	Sigma-Aldrich Corp. (USA)
Ampicillin	A9393-5G	Sigma-Aldrich Corp. (USA)
Bacto-Tryptone	211705	Becton, Dickinson & Co. (USA)
Bacto-Yeast extract	288620	Becton, Dickinson & Co. (USA)
Biotin	21335	Thermo Scientific Inc. (USA)
Bromphenol blue	B5525-5G	Sigma-Aldrich Corp. (USA)
Boric acid	1.00165.5000	Merck KGaA (GER)
BSA	A4503-100g	Sigma-Aldrich Corp. (USA)
BSA, fatty acid free	A7030	Sigma-Aldrich Corp. (USA)
$CaCl_2$	1.2378.0500	Merck KGaA (GER)
$CaCl_2$ dihydrate	C7902-500G	Sigma-Aldrich Corp. (USA)
dATP	D4788-.1MMO	Sigma-Aldrich Corp. (USA)
DAPI mounting medium	P36962	Thermo Scientific Inc. (USA)
dCTP	D4913-.1MMO	Sigma-Aldrich Corp. (USA)
DTT	6908.2	Carl Roth GmbH & Co. KG (GER)
dGTP	D5038-.1MMO	Sigma-Aldrich Corp. (USA)
DMSO	ECL-EMR385050	EuroClone S.p.A. (ITA)
dTTP	T9656-.1MMO	Sigma-Aldrich Corp. (USA)
DMEM	D5796 (Charge RNBF0088)	Sigma-Aldrich Corp. (USA)
EDTA	108418	Merck KGaA (GER)
Ethanol 96%	JB8025.2500PE	J. T. Baker (GER)
Fast Digest Buffer (10×)	B64	Thermo Scientific Inc. (USA)
FBS	10270-106 (Charge 41F5644K)	Life Technologies AG (USA)
G418	ANT-GN5	InvivoGen (CA, USA)
Glucose	G 7528-1KG	Sigma-Aldrich Corp. (USA)
Glycerol	49767	Sigma-Aldrich Corp. (USA)
Glycine	3908.2	Carl Roth GmbH & Co. KG (GER)
HBSS	H6648-500ML	Merck KGaA (GER)
HEPES	9105.4, 500g	Carl Roth GmbH & Co. KG (GER)
Hi-Di Formamide	4311320	Thermo Scientific Inc. (USA)
HPLC water	4218	J. T. Baker (GER)
Hygromycin B	ant-hg-1	InvivoGen (USA)
Kanamycin	K1876-5G	Sigma-Aldrich Corp. (USA)
KCl	104936	Merck KGaA (GER)
$KHCO_3$	4854	Merck KGaA (GER)
KOH	P747.1	Carl Roth GmbH & Co. KG (GER)
Ligase Buffer	B0202S	New England Biolabs Inc. (USA)
Methanol	4627.1	Carl Roth GmbH & Co. KG (GER)
$MgCl_2$ solution (1 M)	AM9530G	Thermo Scientific Inc. (USA)
Midori Green advance	617004	Biozym Scientific GmbH (GER)
Milk, powdered	T145.2	Carl Roth GmbH & Co. KG (GER)

Reagent	Article No.	Manufacturer
NaCl	39573	Carl Roth GmbH & Co. KG (GER)
NaN_3	S2002-100G	Sigma-Aldrich Corp. (USA)
$NaHCO_3$	106329	Merck KGaA (GER)
NH_4Cl	1084	Merck KGaA (GER)
Nonidet P-40	A1694,0250	AppliChem GmbH (GER)
Opti-MEM	51985026 (Charge 1721804)	Thermo Scientific Inc. (USA)
PBS tablets	18912-014	Thermo Scientific Inc. (USA)
Penicillin / Streptomycin	P4333-100ML	Sigma-Aldrich Corp. (USA)
PFA	1.04005.1000	Merck KGaA (GER)
Phosphatase inhibitor	4906837001	Hoffmann-La Roche AG (CHE)
PEI (MW 25000 Da)	23966-2	Polysciences Inc (USA)
Poly-L-Lysine	P2636	Sigma-Aldrich Corp. (USA)
Proteinase Inhibitor	11836 153001	Hoffmann-La Roche AG (CHE)
Protein ladder	LC5925	Thermo Scientific Inc. (USA)
TBE 10x powder	A4348,500	AppliChem GmbH (GER)
SDS	0837-200ML	VWR International (PA, USA)
Sodium acetate	1.06268.0250	Merck KGaA (GER)
Tetracycline Hydrochloride	58346	Merck KGaA (GER)
Tris	37192	Serva Electrophoresis GmbH (GER)
TritonX-100	X100-500ML	Sigma-Aldrich Corp. (USA)
Trizma base	T1503	Sigma-Aldrich Corp. (USA)
Tween 20	P7949-100ML	Sigma-Aldrich Corp. (USA)
Xylene cyanol	X4126	Sigma-Aldrich Corp. (USA)
Zeocin	45-0430	Thermo Scientific Inc. (USA)

3.8. Enzymes

Table 3.8.: List of enzymes

Enzyme	Article No.	Manufacturer
BigDye v3.1	4337457	Thermo Scientific Inc. (USA)
Dnase I	EN0523	Thermo Scientific Inc. (USA)
*Eco*RI FD	FD0274	Thermo Scientific Inc. (USA)
Exonuclease I	EN0582	Thermo Scientific Inc. (USA)
Gateway BP Clonase II Enzyme Mix	11789020	Thermo Scientific Inc. (USA)
Gateway LR Clonase II Enzyme Mix	11791020	Thermo Scientific Inc. (USA)
*Kpn*I FD	FD0524	Thermo Scientific Inc. (USA)
*Not*I FD	FD0594	Thermo Scientific Inc. (USA)
One*Taq* 2× Master Mix with Standard Buffer	M0482S	New England Biolabs Inc. (USA)
One*Taq* 2× Master Mix with GC Buffer	M0483S	New England Biolabs Inc. (USA)
Proteinase K	3115844001	Hoffmann-La Roche AG (CHE)
Shrimp Alkaline Phosphatase	EF0652	Thermo Scientific Inc. (USA)
Trypsin	T3924-100ML	Sigma-Aldrich Corp. (USA)
*Xho*I FD	FD0694	Thermo Scientific Inc. (USA)

3.9. Consumables

Table 3.9.: List of consumables

Consumable	Spec.	Article No.	Manufacturer
96 microwell plates		A62219	Thermo Scientific Inc. (USA)
96 well PCR plates		721979102	Sarstedt AG & Co. (GER)
Bis-Tris Gels	4-12 %	NW04125BOX	Thermo Scientific Inc. (USA)
Cell Culture dish	10 cm^2	833.902	Sarstedt AG & Co. (GER)
Cell scraper		831832	Sarstedt AG & Co. (GER)
Centrifuge tube	50 ml	227261	Greiner Bio-One GmbH (AUT)
Centrifuge tube	15 ml	188271	Greiner Bio-One GmbH (AUT)
Cover glasses	square	6310125	VWR International (USA)
Cover glasses	ø 18 mm	0111580	Marienfeld GmbH & Co.KG (GER)
Cryotubes	1.8 ml	72.379	Sarstedt AG & Co. (GER)
Dispenser tips	1.25 ml	702376	BRAND GmbH + Co. KG (GER)
Dispenser tips	5 ml	6131021	VWR International (USA)
Facial tissues		7730012	GVS Group (GER)
FACS tubes (5 ml)		352052	Fisher Scientific Inc. (USA)
Filtertips	10 µl	701115210	Sarstedt AG & Co. (GER)
Filtertips	200 µl	70760213	Sarstedt AG & Co. (GER)
Filtertips	300 µl	70765210	Sarstedt AG & Co. (GER)
Filtertips	1000 µl	70762211	Sarstedt AG & Co. (GER)
Matrix pipette tips	12.5 µl	7422	Matrix Technologies Inc. (USA)
Micro tube	screw cap	72692105	Sarstedt AG & Co. (GER)
Microscope slide		J3800AMNZ	Thermo Scientific Inc. (USA)
Mini Protean Precast Gel	4-20 %	4568094	Bio-Rad Laboratories Inc. (USA)
NeutrAvidin Agarose Resin		29200	Thermo Scientific Inc. (USA)
Nitril Gloves		D1102-24	WRP (MYS)
Nitrocellulose membrane		LC2000	Life Technologies AG (USA)
Parafilm		PM-996	Bemis Company (USA)
PCR 8-tube stripes	0.2 ml	673210	Greiner Bio-One GmbH (AUT)
PCR 8-cap stripes		373270	Greiner Bio-One GmbH (AUT)
Petri dishes	ø 92 mm	821473001	Sarstedt AG & Co. (GER)
Pipette Tips	1000 µl	70.762.010	Sarstedt AG & Co. (GER)
Pipette Tips	200 µl	70.760.002	Sarstedt AG & Co. (GER)
Pipette Tips	20 µl	30000838	Eppendorf AG (GER)
Precision wipes		7552	Kimberly Clark (USA)
PVDF membrane		LC2002	Life Technologies AG (USA)
Reaction tubes	2.0 ml	72695500	Sarstedt AG & Co. (GER)
Reaction tubes	1.5 ml	72690001	Sarstedt AG & Co. (GER)
Reaction tubes	0.5 ml	72735992	Sarstedt AG & Co. (GER)
Round bottom tubes	14 ml	352059	Corning Inc. (USA)
Serological Pipet	5 ml	356543	Corning Inc. (USA)
Serological Pipet	10 ml	356551	Corning Inc. (USA)
Serological Pipet	25 ml	356525	Corning Inc. (USA)
Six well plates		140675	Thermo Scientific Inc. (USA)
Sterile filter	0.2 mm	16534K	Sartorius AG (GER)
Tris-Acetate Gels	3-8 %	EA03755BOX	Thermo Scientific Inc. (USA)
Weighing pans		KC04.1	Carl Roth GmbH & Co. KG (GER)

3.10. Commercial systems

Table 3.10.: List of commercial systems

Commercial System	Article No.	Manufacturer
BigDye Terminator v3.1 Cycle Sequencing Kit	4337457	Thermo Scientific Inc. (USA)
Gateway BP Clonase II Enzyme Mix	11789020	Thermo Scientific Inc. (USA)
Gateway LR Clonase II Enzyme Mix	11791020	Thermo Scientific Inc. (USA)
GenElute Plasmid Miniprep Kit	PLN70	Sigma-Aldrich Corp. (USA)
Monarch Gel Extraction Kit	T1020S	New England Biolabs Inc. (USA)
Monarch Plasmid Miniprep Kit	T1010 S	New England Biolabs Inc. (USA)
NEBuilder HiFi DNA Assembly Cloning Kit	E5520S	New England Biolabs Inc. (USA)
OneStep RT-PCR Kit	210212	Qiagen N.V. (NLD)
Pierce BCA Protein Assay Kit	23225	Thermo Scientific Inc. (USA)
Plasmid Midi Kit	12143	Qiagen N.V. (NLD)
QIAquick Gel Extraction Kit	28704	Qiagen N.V. (NLD)
SuperScript First-Strand	11904018	Thermo Scientific Inc. (USA)
Western Bright ECL	K12045-D50	Advansta Inc. (USA)

3.11. Bioinformatic tools

Table 3.11.: List of software, bioinformatic tools and databases. URLs to tools and databases: *1 https://www.ebi.ac.uk/Tools/msa/, *2 http://consurf.tau.ac.il, *3 www.ensembl.org, *4 https://gnomad.broadinstitute.org, *5 https://hereditaryhearingloss.org/, *6 www.proteinatlas.org/, *7 www.umd.be/HSF3, *8 http://tmcalculator.neb.com, *9 http://josephroland.com/lab/PEItransfect.html, *10 https://genome.ucsc.edu

Software	Application	Company
Alignment tools*1	Sequence alignment	EMBI-EBI (UK)
AxioVision Release 4.8.2	Microscopy	Carl Zeiss AG (GER)
BD FACSDiva 8.0.1	FACS analysis	BD Biosciences (USA)
Chromas Lite	Sequence analysis	Technelysium Pty Ltd (AUS)
ConSurf Server*2	Conservation analysis	Tel-Aviv University (ISR)
Ensembl*3	Genome annotation	EMBI-EBI (UK)
FlowJo Cytometry	Flowcytometry analysis	Becton, Dickinson & Co (USA)
Gen5 (Version Sept. 2001)	Microplate analysis	Biotek Instruments Inc. (USA)
GnomeAD*4	Genome aggregation data	
Hereditary hearing loss Homepage*5	Hearing loss genes	
Human Protein Atlas*6	Gen expression data	
Human Splicing Finder*7	Splice prediction	Aix Marseille Université (FRA)
Image Lab 5.2	Western Blot analysis	Bio-Rad Laboratories Inc. (USA)
NEB T_m Calculator v1.8.1*8	Primer analysis	New England Biolabs Inc. (USA)
PEI transfection of mammalian cells*9	PEI transfection	Joseph Roland
PRISM7	Statistics, graph design	GraphPad Software (USA)
SeqBuilder	Insilico genome editing	DNA STAR Inc. (USA)
SeqManPro	Sequence analysis	DNA STAR Inc. (USA)
SWISS Model	Protein 3D modelling	University of Basel (CHE)
UCSC Genome Browser*10	Genome browsing	University of CA (USA)

3.12. Devices

Table 3.12.: List of devices

Device	Type	Manufacturer
-80 °C Freezer	KM-DU73Y1E	Panasonic Corp. (JAP)
Biological Safety Cabine	Hera Safe	Heraeus Instruments GmbH (GER)
Biological Safety Cabine	Lamin Air HB2248K	Heraeus Instruments GmbH (GER)
Biological Safety Cabine	Lamin Air LB48C	Heraeus Instruments GmbH (GER)
Blotting Module	Bolt Mini B1000	Thermo Scientific Inc. (USA)
Bright field microscope	Axiovert 40 CFL	Carl Zeiss AG (GER)
Bunsen burner	Phoenix II	Schuett-biotec GmbH (GER)
Cell counting chamber	Neubauer improved	Karl Hecht GmbH & Co. KG (GER)
Centrifuge	Centrifuge 5424	Eppendorf AG (GER)
Centrifuge	Centrifuge 5810R	Eppendorf AG (GER)
Centrifuge	Heraeus Multifuge X3R	Thermo Scientific Inc. (USA)
Centrifuge bottles	B1033-4EA	Thermo Scientific Inc. (USA)
Drigalski spatulas	AL98.1	Carl Roth GmbH & Co. KG (GER)
Erlenmeyer caps	K396.1	Carl Roth GmbH & Co. KG (GER)
Erlenmeyer flask 100 ml	215-1592	VWR International (USA)
Flow Cytometer	FACS Canto II	Becton Dickinson & Company (USA)
Freezer (-150 celsius)	MDF-1156	Panasonic Corp. (JAP)
Fridges		Liebherr AG (CHE)
Gel documentation chamber	Gel stick	Intas S. I. I. GmbH (GER)
Gel documentation chamber	ChemiDoc XRSx	Bio-Rad Laboratirues Inc. (USA)
Gel electrophoresis chamber	700-0136	VWR International (USA)
Gel electrophoresis tank	Mini A25977	Thermo Scientific Inc. (USA)
Gel electrophoresis cell	Mini-Protean Tetra Cell	Bio-Rad Inc. (USA)
Glas pipettes	747715	Brand GmbH & Co. KG (GER)
Heat block	Thermomixer F1.5	Eppendorf AG (GER)
Ice maschine	FM-120EE-50	Hoshizaki Denki K.K. (JAP)
Incubation shaker	Multitron	Infors AG (CHE)
Incubator	Function line T12P	Heraeus Instruments GmbH (GER)
Incubator	MC0-19AIC-PE	Panasonic Corp. (JAP)
Micro centrifuge	Ministar silverline	VWR International (USA)
Microplate shaker	230 V	VWR International (USA)
Microscope	TCS SP8	Leica Camera AG (GER)
Microscope	Axioplan Imaging	Carl Zeiss AG (GER)
Photometric plate reader	Epoch	Biotek Instruments Inc. (USA)
Pipet Aid	Pipetboy	Integra Biosciences (CHE)
Pipettes	Research plus	Eppendorf AG (GER)
Pipettes, electronic	Xplorer plus	Eppendorf AG (GER)
Power supply	PS3002	Life Technologies AG (USA)
Pump		KNF Neuberger GmbH (GER)
Roller mixer	SRT9	Cole-Parmer Ltd.(UK)
Rotor	SLA-150 Super Lite	Thermo Scientific Inc., Sorvall (USA)
Scale	IT1402465	VWR International (USA)
Scale	PC180	Mettler-Toledo Inc. (CHE)
Sequencer	Ap. Bios. Analyzer 3500	Thermo Scientific Inc.,(USA)
Thermocycler	Labcycler	SensoQuest GmbH (GER)
Tube rotator	RS60	BioSan (LVA)
Ultra centrifuge	Superspeed RC2-B	Thermo Scientific Inc., Sorvall (USA)
Ultra pure water system	Purelab flex	ELGA LabWater (UK)
Vortex	Vortex 1	IKA-Werke GmbH & Co. KG (GER)
Water bath	1083	GFL GmbH (GER)

3.13. Buffers and solutions

TE buffer	10 mM	Tris/HCl
	1 mM	EDTA
	Filter sterilize.	
7deaza dNTP mix		Aqua (dest.)
	2.500 mM	dATP
	2.500 mM	dCTP
	2.500 mM	dTTP
	0.625 mM	dGTP
	1.875 mM	7deazaGTP
Gel loading buffer	12 ml	Glycerol
	10 mg	Xylene cyanol
	10 mg	Bromphenol blue
	200 µl	EDTA (0.5 M, pH 8.0)
Sequencing buffer	Homemade 5 ×	Big Dye BDT Sequencing Buffer
pH 9.0, [39]		Aqua (dest.)
	400 mM	Tris
	10 mM	$MgCl^2$
Erythrocyte lysis buffer	155 mM	NH_4Cl
	10 mM	$KHCO_3$
	0.1 mM	EDTA (pH 7.0)
	Adjust pH to 7.4 and filter sterilize.	
Nuclei lysis buffer	10 mM	Tris/HCl
	0.4 M	NaCl
	2 mM	EDTA
	Filter sterilize.	
LB medium	10 g	Bacto-Tryptone
	5 g	Bacto-Yeast extract
	10 g	NaCl
	1 l	ddH_2O
	Autoclave before using.	

LB agar	10 g	Bacto-Tryptone
	5 g	Bacto-Yeast extract
	10 g	NaCl
	15 g	Agar
	1 l	ddH_2O
	Autoclave before using.	
	Add antibiotics to ca. 55 °C warm medium.	
	Pour into petridishes.	
Kanamycin stock solution		Aqua (dest.)
	$100\,mg\,ml^{-1}$	Kanamycin
Ampicillin stock solution		Aqua (dest.)
	$100\,mg\,ml^{-1}$	Ampicillin
	$100\,mg\,ml^{-1}$	$NaHCO_3$
5× KCM buffer		Aqua (dest.)
	0.50 M	KCl
	0.15 M	$CaCl_2$
	0.25 M	$MgCl_2$
PEI stock solution	Heat endotoxin free water to 60 °C	
[224]	$1\,\mu g\,\mu L^{-1}$	PEI
	Let cool to room temperature.	
	Neutralize to pH 7.0 with HCl.	
	Filter sterilize (0.22 µm),	
	aliquot and store at -20 °C.	
Poly-L-Lysine solution		Aqua (dest.)
	100 mM	Boric acid
	$100\,mg\,L^{-1}$	Poly-L-Lysine
	Use NaOH to adjust pH to 8.5.	
	Filter-sterilise.	

Versene		PBS
	5 mM	EDTA
Protein lysis buffer		Aqua (dest.)
	10 mM	Tris/HCl (pH 7.5)
	150 mM	NaCl
	2 mM	EDTA
	1% (v/v)	TritonX-100
	10% (v/v)	Glycerol
	With freshly added:	
	1 mM	DTT
	1 ×	protease inhibitors
	1 ×	phosphatase inhibitors
LDS sample buffer [134]	4 × NuPAGE LDS Sample Buffer is obtained from Thermo Fisher Scientific (USA).	
	Composition of 1 × Sample buffer:	
	106 mM	Tris/HCl
	141 mM	Tris base
	0.51 mM	EDTA
	0.22 mM	SERVA Blue G250
	0.175 mM	Phenol Red
	2% (w/v)	LDS
	10% (v/v)	Glycerol
MOPS buffer [134]	20 × NuPAGE MOPS SDS Running Buffer is obtained from Thermo Fisher Scientific (USA).	
	Composition of 1 × Transfer buffer:	
	50 mM	MOPS
	50 mM	Tris base
	1 mM	EDTA
	0.1% (w/v)	SDS
MES buffer [134]	20 × NuPAGE MES SDS Running Buffer is obtained from Thermo Fisher Scientific (USA).	
	Composition of 1 × Transfer buffer:	
	50 mM	MES
	50 mM	Tris base
	1 mM	EDTA
	0.1% (w/v)	SDS

Tris Acetate buffer [134]	20 × NuPAGE Tris Acetate SDS Running Buffer is obtained from Thermo Fisher Scientific (USA). Composition of 1 × Transfer buffer:	
	50 mM	Tricine
	50 mM	Tris base
	0.1% (w/v)	SDS
Running buffer		Aqua (dest.)
	19.2 mM	Glycine
	25.0 mM	Tris base
	0.1% (w/v)	SDS
Transfer buffer [134]	20 × NuPAGE Transfer Buffer is obtained from Thermo Fisher Scientific (USA). Composition of 1 × Transfer buffer:	
	25 mM	Bicine
	25 mM	Bis-Tris (free base)
	1 mM	EDTA
5x Laemmli buffer		Aqua (dest.)
	0.5 M	DTT
	10% (w/v)	SDS
	0.4 M	Tris-HCl pH 6.8
	50% (v/v)	Glycerine
	dye with bromophenol blue	
TBS buffer (Tris buffered saline)		Aqua (dest.)
	10 mM	Tris/HCl, pH 8.0
	150 mM	NaCl
TBS-T buffer (TBS buffer with Tween 20)		TBS buffer
	0.2% (v/v)	Tween 20
TBS-T BSAazide buffer		TBS-T buffer
	2.00% (w/v)	BSA
	0.02% (w/v)	NaN_3

Blocking buffer		TBS-T buffer
	5% (w/v)	milk powder
HBSS-glucose		HBSS
pH 7.4	$1\,g\,l^{-1}$	glucose
HBSS-glucose with NBD-PE		HBSS-glucose
	5% (v/v)	abs. ethanol
	2 µM	NBD-PE
	Sonicate for 30 sec.	
HBSS-glucose with NBD-PS		HBSS-glucose
	2 µM	NBD-PS
	Sonicate for 30 sec.	
HBSS-glucose with		HBSS
fatty acid free BSA	$1\,g\,l^{-1}$	glucose
	5%	fatty acid free BSA
PBS with EDTA and		PBS
fatty acid free BSA	1 mM	EDTA
	0.5%	fatty acid free BSA
PBS++		PBS
	0.1 mM	$MgCl_2$
	0.1 mM	$CaCl_2$ dihydrate
Biotin solution		PBS++
	$1\,mg\,mL^{-1}$	Biotin
	Bring biotin to RT before adding.	
	Roll solution for 10 min at 4 celsius.	

PBS++ with Glycine and BSA		PBS++
	100 mM	Glycine
	0.3%	BSA
HEPES-KOH		Aqua (dest.)
	20 mM	HEPES
	Use KOH to adjust pH to 7.5.	
	Sterile-filter.	
Protein lysis buffer (Biotinylation)	10 mM	HEPES-KOH
	150 mM	NaCl
	1% (v/v)	Nonidet P-40
	With freshly added:	
	1 ×	protease inhibitors
Highsalt buffer	20 mM	HEPES-KOH
	500 mM	NaCl
	1 mM	EDTA
	0,5% (v/v)	Nonidet P-40

4. Methods

In this chapter the underlying methods for the performed experiments are introduced separated into topics of DNA based procedures, bacteria handling and cultivation, cell culture and protein isolation and analysis. Also the preparation and implementation of the flippase activity assay is described.

4.1. DNA

4.1.1. Isolation of genomic DNA from blood

Genomic DNA from patients and healthy control individuals is isolated from a whole blood EDTA sample. About 10 ml EDTA blood is filled in a 50 ml centrifuge tube and filled with erythrocyte lysis buffer to 45 ml. After mixing the blood is incubated on ice for 15 min to lyse the erythrocytes. During the incubation the blood is routinely inverted until it seems clear and no gas bubbles rise. The lysed blood is centrifuged for 15 min at 1,500 rpm and 4 °C, the supernatant is discarded for specialised waste disposal. The remaining pellet is resuspended in 10 ml erythrocyte lysis buffer and centrifuged again as described above for isolating the leukocytes. The now remaining pellet is resuspended in 5 ml nuclei lysis buffer and then added with 100 µl proteinase-K (10 mg/ml) and 200 µl 20% SDS. The mixture is incubated in a water bath at 37 °C for at least 4 h, usually over night. On the next day the DNA is precipitated by salting out. For this, 1.8 ml 6 M NaCl solution is added to the mix and shaken fiercely. The tube is centrifuged for 15 min at 4,000 rpm and room temperature (RT). The supernatant is filled in a fresh tube and centrifuged again at given conditions. Subsequent to repeated filling in fresh 50 ml centrifuge tubes the supernatant is layered with 2 ml ethanol p.a. (96%). Slow inverting of the tube results in precipitation of the DNA into a fine thread. This thread can be gathered with a glass hook, washed in 70% ethanol, dried with a fuzz free precision wipe and solved in 300 µl TE buffer. The DNA should be kept at 4 °C for at least 7 days to completely solve before measuring the concentration.

4.1.2. cDNA synthesis

The synthesis of cDNA is conducted with the SuperScript First-Strand Synthesis System for RT-PCR (Thermo Scientific Inc., USA) according to protocol. For this isolated DNA-free RNA is first incubated with oligo(dT) primers, which bind to the poly(A) tails of mRNA. After preparing the mixture conditions for the polymerase and inactivating RNAses, the SuperScript II reverse transcriptase synthesises cDNA from template mRNAs. Finally RNase H is used to eliminate the template RNA. The cDNA can then be used to comfortably look at the mRNA status of the cells to the time of RNA isolation, since DNA is more stable at room temperature and therefore, better to handle.

4.1.3. Primer design

Designing of all used primers was performed using the Seqbuilder Software (DNA STAR Inc., USA). The melting temperature (T_m) and recommended annealing temperature were calculated with the NEB T_m Calculator v1.8.1 web tool [171]. Primers were synthesised by Integrated DNA Technologies Inc. (USA). The provided dried primers were solved with TE^{-4} buffer and kept frozen at -20 °C. Aliquots were diluted to 5 pM with ddH_2O and could be stored in the fridge at 4 °C temporarily.

4.1.4. Polymerase chain reaction

The polymerase chain reaction (PCR) is a common method to amplify DNA. Here the specific reaction mixtures and thermocycler protocols for standard amplification as well as special purposes like the amplification of more complex DNA segments and for subsequent sequencing are enlisted.

4.1.4.1. Standard PCR

General amplification of DNA is performed with the Standard PCR protocol (see tables 4.1 and 4.2), for example as PCR for subsequent purification and sequencing. If sufficient for further purposes the reaction volume is divided in half. The usage of Standard buffered or GC buffered One*Taq* 2 × Master Mix is adjusted to the GC content of the PCR product. When it is used in Colony PCR to check transformed colonies on the desired insert, the template volume is replaced with ddH_2O and a single colony is added as template with a pipette tip.

Table 4.1.: 25 µl reaction mixture for Standard PCR amplification

Amount [µl]	**Component**
9.5	ddH_2O
12.5	One*Taq* 2 × Master Mix
1.0	Forward Primer (5 pM)
1.0	Reverse Primer (5 pM)
1.0	Template DNA

Table 4.2.: Thermocycler protocol for Standard PCR amplification

Temperature [°C]	**Time [min]**	
95	3:00	
94	0:30	30 ×
T_m-5	0:30	
68	1 min / kb	
68	5:00	
12	∞	

4.1.4.2. Touchdown PCR

The touchdown PCR protocol is used for the amplification of more complex DNA segments, when Standard PCR does not result in enough product or produces unspecific byproducts. It can be found in table 4.3. The reaction mixture is composed as described for Standard PCR in table 4.1.

Table 4.3.: Thermocycler protocol for Touchdown PCR amplification

Temperature [°C]	**Time [min]**	
95	3:00	
94	0:50	30 ×, -0.5 °C per cycle
T_m+5	0:50	
68	1 min / kb	
94	0:50	30 ×
T_m-5	0:50	
68	1 min / kb	
68	5:00	
12	∞	

4.1.4.3. Sanger sequencing

Sanger sequencing is performed using the BigDye Terminator v3.1 Cycle Sequencing Kit and analysed on the Applied Biosystems® Analyzer 3500, both from Thermo Fisher Scientific (USA). The reaction mixture and the thermocycler protocol are listed in tables 4.4 and 4.5.

Table 4.4.: Reaction mixture for Sanger Sequencing PCR

Amount [µl]	**Component**
6.00	ddH_2O
2.25	5 × BigDye Terminator buffer
0.50	Sequencing Primer (5 pM)
0.25	BigDye Terminator
1.00	purified PCR product

Table 4.5.: Thermocycler protocol for Sanger Sequencing PCR

Temperatur [°C]	**Time [min]**	
96	1:00	
96	0:10	30 ×
55	0:10	
60	4:00	
12	∞	

4.1.5. Agarose gel electrophoresis

Agarose gels are made using 2% agarose in TBE buffer and dyed with 15 µl Midori Green advance (Biozym Scientific GmbH, GER) per 250 ml gel. The DNA samples are mixed with 4 × gel loading buffer and added into the wells. The 2-Log DNA Ladder from New England Biolabs Inc. (USA) is used as a size marker. Electrophoresis is performed at 200 V and about 150 mA.

4.1.6. DNA purification

For some sensitive applications, for example before and after performing a Sanger sequencing on a PCR product, the PCR product has to be purified in oder to get valid results.

4.1.6.1. PCR Purification with ExoSAP

A combination of Shrimp Alcaline Phosphatase and Exonuclease I can be used for purification of the PCR product prior Sanger Sequencing. Shrimp Alcaline Phosphatase dephosphorylates left over dNTPs and Exonuclease I degrades primer remains [11]. The reaction mixture and the thermocycler protocol can be found below in tables 4.6 and 4.7.

Table 4.6.: Reaction mixture for ExoSAP purification

Amount [µl]	**Component**
6.25	ddH_2O
1.00	FastAP (1 U/µl Shrimp Alcaline Phosphatase)
0.25	Exonuclease I (10 U/µl)
7.50	PCR product

Table 4.7.: Thermocycler protocol for ExoSAP purification

Temperatur[°C]	**Time [min]**
37	20:00
85	15:00
4	∞

4.1.6.2. Ethanol precipitation

After Sanger Sequencing the DNA has to be precipitated to get pure DNA for analysis. For this purpose 8 µl ddH_2O and 2 µl 3 M NaAC solution are added to 10 µl Sequencing PCR product. After addition of 50 µl ethanol p.a. (96%) the samples are mixed by vortexing and incubated at room temperature for 15 min to precipitate the DNA. Then the samples are centrifuged at $3.000 \times g$ for 15 min at room temperature and the supernatant is discarded. Afterwards the precipitated DNA gets washed by the addition of 200 µl 70% ethanol and subsequent centrifugation as described before. To dry the DNA the tubes are shortly centrifuged headfirst and without caps at max. $500 \times g$. The sedimented DNA is dried for 5 to 10 min at room temperature and solved in 20 µl Hi-Di formamide. If the protocol is used for purification of DNA products out of the context of Sanger Sequencing the DNA can be solved in ddH_2O or TE buffer.

4.1.6.3. Gel purification

When it is necessary to isolate single bands out of an agarose gel, for example to get rid of unspecific byproducts or after an endonuclease digestion, gel purification can be performed. The desired DNA band is cut out of the gel and purified with the QIAquick Gel Extraction Kit from Qiagen N.V. (Venlo, Netherlands).

4.1.7. Restriction endonuclease digestion

Restriction endonucleases are used to cleave DNA at specific recognition sites. The described reaction mixture in table 4.8 is incubated in a thermocycler for 60 min at 37 °C. Afterwards the enzyme is heat inactivated at 65 °C or 80 °C for 5 -20 min, depending on the used enzyme.

Table 4.8.: 20 µl reaction mixture for DNA digestion

Amount [µl]	Component
18.0 - x µl	ddH_2O
2.0 µl	10 × FastDigest buffer
1 µg	Plasmid DNA

4.1.8. Cloning

Two different techniques are used for cloning. Gateway Cloning was performed for the integration of whole genes into an expression vector, while the replacement of shorter sequence fragments in the middle of genes that were already present in vectors was done with NEBuilder Cloning.

4.1.8.1. NEBuilder Cloning

Cloning of short fragments was performed with the NEBuilder HiFi DNA Assembly Master Mix (New England Biolabs Inc., USA). The underlying principle of this cloning method is the annealing of varied overlapping parts of vector and insert. An exonuclease produces single-stranded 3' overlaps at both ends of the linearised vector and insert, to improve the annealing of both fragments in the correct orientation. A polymerase fills in gaps and a DNA ligase closes the nicks of the assembled DNA. The assembly is conducted according to the manufacturer's protocol with an incubation time of 1 h. The resulting plasmids are used for direct transformation of competent *E. coli* cells (see section 4.2.2).

4.1.8.2. Gateway Cloning

Another method of cloning was Gateway cloning, using the BP and LR Clonase II Enzyme Mixes (Thermo Fisher Scientific (USA). It was performed according the manufacturer's protocol. Gateway cloning is based on the integration mechanism used by Lambda phages to insert their DNA into *E. coli*. The sequence of interest is amplified with overhang-primers that extent it with attB recombination sites. These attB recombination sites match with attP sites in Gateway entry vectors. An entry vector contains a cytotoxic ccdB gene flanked by the attP sides. During the so-called BP reaction the ccdB gene is cut out of the plasmid by phage excisionase and replaced with the insert. For this, the sites attB1 and attP1 as well as attB2 and attP2 specifically attach and the PCR product is integrated by the phage encoded protein Integrase and *E. coli* encoded Integration Host Factor. With this new sites called attL1 and attL2 are build, flanking the inserted sequence. The BP reaction product can directly be used for transformation of competent *E. coli* cells (see 4.2.2).
A second step, the LR reaction, transfers the insert from the Entry vector to a Gateway expression vector. Again the expression vector has matching attR sites flanking the ccdB gene. The LR reaction is a reversed BP reaction. AttL1 and attR1 as well as attL2 and attR2 attach, the enzymes replace ccdB with the insert cut out from the entry clone and create flanking attB sites this way. The LR reaction product can also directly be used for transformation. The selection between clones carrying uncut entry vector and clones with the desired expression vector can be accomplished by taking advantage of the different antibiotic resistances on the vectors.

4.2. Bacteria

4.2.1. Solving bacterial plasmid DNA from filter paper

Plasmid constructs of hATP11A-HA variants, hCDC50A and hCDC50B have been kindly provided by Dr. Hye-Won Shin (Department of Physiological Chemistry, Graduate School and Faculty of Pharmaceutical Sciences, Kyoto University, Japan). The plasmid DNA of hATP11A-HA Isoform 1 WT, hATP11A-HA Isoform 1 E186Q and hATP11A-HA Isoform 1 D414N in the mammal expression vector pCAG as well as HFN-hCDC50A and HFN-hCDC50B in pcDNA3 have been sent on filter paper. Half of the circled spot with DNA was cut out and incubated in 200 µm TE buffer for 30 min [225]. The solved plasmid DNA can be used for transformation of *E. coli*.

4.2.2. Transformation of *E. coli*

Chemically competent KCM *E. coli* cells are thawed and 100 µl cells are added with 20 µl 5 × KCM buffer and 1 µl plasmid DNA, 10 µl solved filter paper plasmid DNA or 10 - 20 µl ligation product. The mix is filled with ddH_2O to 200 µl and blended by pipetting up and down. After 20 min of incubation on ice the cells are heat shocked at 37 °C for 5 min. The addition of 1 ml fresh prewarmed LB medium and shaken incubation for 1 h at 37 °C allows the expression of the plasmids' antibiotic resistance. This is needed for the following selection on agar plates. Thus, the transformed cells are centrifuged for 1 min at 13,000 rpm, the pellet resuspended in 100 µl LB medium and plated on LB agar plates with added antibiotics matching to the plasmids' resistance gene. The plates are incubated at 37 °C over night.

4.2.3. Bacterial over night culture

To grow bacterial over night cultures LB medium is added with antibiotics. Either 1:500 kanamycin stock solution or 1:1,000 ampicillin stock solution are used. The medium is inoculated with bacteria from an agar plate or out of a glycerol stock and incubated at 37 °C and 200 rpm over night.

4.2.4. Bacterial glycerol stocks

Glycerol stocks are made for long term storage of transfected bacteria. 500 µl of an over night culture are mixed with 500 µl 50% glycerol and frozen at -80 °C. For inoculation of new over night cultures the glycerol stock is not thawed, but some frozen bacteria are scraped out of the tube with a pipette tip and cultivated as described above.

4.2.5. Plamid isolation

Plasmid isolation is performed on two different scales. For standard amounts the isolation of plasmid DNA is done with the GenElute Plasmid MiniPrep Kit from Sigma-Aldrich Corp. (USA) or the Monarch Plasmid Miniprep Kit from New England Biolabs Inc. (USA). The Plasmid Midi Kit from Qiagen N.V. (NLD) is used for the isolation of larger amounts of plasmid DNA.

4.3. Cell culture

Cells are handled under sterile conditions. HEK293 and HEK293T cells are cultured with DMEM, which most times is supplemented with 10% FBS, as

well as penicillin, streptomycin and amphotericin B to avoid contamination. If not mentioned otherwise all used solutions are warmed to 37 °C.

4.3.1. Passaging

Cells are cultivated up to 90-100% confluence before diluting and passaging into a fresh culture dish. For this process the medium is removed and the cells washed with PBS. The addition of 1 ml trypsin and 3 min incubation at 37 °C in the CO_2-incubator detaches the cells from the surface of the dish. In order to inactivate trypsin and prevent cell damage, serum containing medium is added. The cell suspension is transferred into a centrifuge tube and the cells pelleted for 10 min at room temperature and $1.000 \times$ g. The supernatant is discarded and the cells resuspended in fresh medium. Depending on the wanted cell density a third to a thirtieth of the cell suspension is used to inoculate a fresh dish with culture medium of the same size as harvested.

4.3.2. Thawing cells

Frozen cells are quickly thawed by short warming up in a water bath at 37 °C without shaking. The cells are added to 10 ml fresh pre-warmed DMEM medium in a 15 ml tube and centrifuged at $80 \times$ g for 4 min to get rid of the freezing medium components. The pellet is resuspended in another 10 ml medium and transferred to a 10 cm dish.

4.3.3. Freezing cells

A plate of confluent cells is trypsinized and peletted at $80 \times$ g. The medium is discarded and the cells resuspended in the residual medium from the tube side. Subsequently the cells are mixed with 1.5 ml growth medium containing 5% DMSO and transferred into a cryovial. For a slow freezing process the vials are placed in a freezing chamber with room temperature isopropanol and cooled down in a -80 °C freezer. Afterwards the cells are stored in a -150 °C freezer.

4.3.4. Transient transfection

Transient transfection is performed using PEI as transfection agent. 0.5×10^6 HEK293 or HEK293T cells per well are inoculated for a 6-well plate. 10 cm dishes are inoculated with 4.0×10^6 cells. After 24 h 0.5 pmol and 2.0 pmol of total DNA respectively are diluted in 300 µl and accordingly 1 ml serum free medium without phenol red in a sterile tube. For this purpose Opti-MEM medium was used. PEI is added as a 3 : 1 mass ratio of PEI and DNA and immediately mixed by pipetting or vortexing. The mixture is incubated at room temperature for 15 min and then added to the cells dropwise. The cells are further incubated at 37 °C in the CO_2-incubator and can be harvested 24 - 96 h after the transfection. For calculation of the volumes for the specific experiments the PEI transfection software by Joseph Roland is used.

4.3.5. Stable Flp-In transfection and creation of a cell line

For the creation of HEK293 cells with stable expression of a gene of interest, HEK293 Flp-In cells (Thermo Fisher Scientific, USA) are preselected with 100 µg/ml zeocin. After a few days the cells can be prepared for transfection with the pOG44 vector and the gene of interest in the pEF5/FRT/V5 vector. pEF5/FRT/V5 is a specific vector for the Flp-In system, which contains Flp recombination target sites for insertion of the target gene into the HEK293 Flp-In DNA, whereas pOG44 encodes for the Flp recombinase itself. After the transfection the cells are passaged to a 25% confluence and selected for successfully stable transfected cells with Hygromycin B without addition of penicillin and streptomycin or amphotericin B.
To create a single cell derived cell line the selection process is prolonged until single cells are spaced on the plate. These are subsequently allowed to grow colonies, which are later transferred to a 24 well plate with filter paper, cultivated without antibiotics and expanded.
In order to check the successful insertion of the gene of interest in place of the former zeocin resistance gene, the expanded single cell derived cell lines are tested for zeocin sensitivity and hygromycin B insensitivity. Further on, the expression of the gene of interest in combination with a V5-tag is checked with ICC and western blotting.

4.3.6. Immunocytochemistry

Previous to the transfection, cells used for ICC are passaged into 6 well plate wells filled with sterile cover glasses to allow the cells to grow on them. 24 - 96 h

after performing the usual transfection protocol the medium is removed and the cells washed with 2 ml PBS. From now on the cells can be handled non sterile and with room temperature PBS.
Incubation with 0.5 ml 4% PFA in PBS for 15 min fixates the cells and is followed by two additional PBS washing steps. The cell membrane gets permeabilised with 1 ml 0.1% Triton-X 100 for 2 min on ice. After another two PBS washing steps the cells are blocked with 1 ml 5% BSA at room temperature for 30 -60 min. For the binding of the first antibody, or a combination of multiple, the antibody is diluted in 5% BSA according to the manufacturer's suggestion or experimentally determined working concentration. 300 µl BSA-antibody solution is given to each well and incubated on a plate shaker over night at 4 °C.
Next day the cells are washed 4 times for 3 min with PBS. The respective secondary antibody or antibodies are diluted in 5% BSA and 500 µl are given to each well. The incubation takes 1 h at room temperature. Because the secondary antibodies are coupled with fluorescent dyes they have to be handled in darkness. Consequently, tubes and wells are wrapped in aluminium foil. After incubation cells are washed 4 times for 3 min with PBS again.
The mounting of the slides has to take place in a shaded room. Tweezers are used to get the cover glass out of the well. The cell free side of the glass is dried with a lint-free wipe. A drop of mounting solution containing DAPI for nuclei staining is put onto a microscope slide and the cover glass gets applied cell side down, so that the mounting solution coats the whole cell area. The cover glass is pressed slightly onto the microscope slide and left to dry. Additionally the dried slide may be fixed with clear nail polish, before examining the staining via fluorescence microscopy.

4.4. Proteins

4.4.1. Protein isolation

For the isolation of proteins out of HEK293 based cell cultures the dishes are handled on ice. The cultures are washed with cold PBS two times. Afterwards 100 µl protein lysis buffer are added for 6 well plates or 300 µl for 10 cm dishes. A cellscraper is used to scrape the cells of the dish and the cell suspension is then transferred into a 1.5 ml reaction tube. After 20 min incubation on ice the proteins are separated from the cell debris by 30 min centrifugation at 14.000 ×g and 4 °C. The supernatant is transferred into a fresh 1.5 ml reaction tube and kept at -20 °C or -80 °C for long term storage.

4.4.2. Protein quantificaion

The Pierce BCA Protein Assay Kit from Thermo Fisher Scientific (USA) is used for the quantification of isolated proteins. BSA standard concentrations and samples are applied to the 96 well plate as duplicates. A volume of 10 µl for the standard concentrations and 2 µl for the samples is used and mixed with 200 µl 50:1 mixture of solution A and B. The assay has to be incubated at 37 °C for 30 min for the peptide bonds to reduce copper ions in order to form Cu^{+}-bicinchoninic acid complexes that absorb at 562 nm. The cooled 96 well plate is analysed with a photometric plate reader (Biotek Instruments Inc., USA). The mean value of the sample results is multiplied by 5 to take the volume differences into account.

4.4.3. SDS-Page

To visualise a protein of interest in the isolated protein solution SDS-Page analysis is done with the Mini Gel Tank and NuPAGE Novex 4-12% Bis-Tris Protein Gels from Thermo Fisher Scientific (USA) according to the manufacturer's protocol. After rinsing the gel wells, 24 µl of each sample mixed with 6 µl 4× Bolt LDS sample buffer are provided to the wells at a total protein amount of 10 µg. For size comparison the SeeBlue Pre-stained Protein Standard (Thermo Fisher Scientific, USA) is used. The separation of the proteins is performed with MOPS or MES buffer at 165 V for about 40 min.

4.4.4. Western blot and protein detection

Subsequently the proteins are wet-blotted from the gel to a nitrocellulose membrane using the Mini Blot Module from Thermo Fisher Scientific (USA) according to the manufacturer's protocol. The blot module is provided with blotting buffer soaked sponge pads and filter paper before adding the gel. Next the nitrocellulose membrane is placed into the module and topped with additional filter paper and sponge pads. The air bubble free and blotting buffer soaked blot module is then transferred to the Mini Gel Tank and blotted at 10 V for 75 min.

Subsequently the nitrocellulose membrane is blocked with 5% milk in TBS-T buffer for 1 h and incubated with the primary antibody against the protein of interest over night at 4 °C on a rolling shaker. If the primary antibody is diluted in 5% milk in TBS-T buffer the membrane does not need to be washed in between, whereas if the antibody is diluted in TBS-T BSAzide the membrane has to be washed three times with TBS-T buffer for 10 min on a plate

shaker. Following the incubation with the primary antibody the membrane is washed again three times with TBS-T buffer for 10 min, before incubating with a horseradish peroxidase coupled secondary antibody diluted with 5% milk in TBS-T buffer for 1 h on a plate shaker. After a final washing step the bound secondary antibodies can be made visible with Western Bright ECL by Advansta Inc. (USA), which is a western blot detection kit containing substrate for the horseradish peroxidase's chemiluminescence reaction. The chemiluminescence can be detected by the ChemiDoc XRSx system (Bio-Rad Laboratories Inc., USA). Molecular weight analysis, normalisation and quantification of protein signal is done with the Image Lab 5.2 software by Bio-Rad Laboratories Inc. (USA).

4.5. Flippase activity assay

The flippase activity assay investigates the translocation of fluorescent labelled phospholipids in cells over time. To compare the activity the mutant hATP11A deletion variant with hATP11A WT and other variants, the method was established and adapted to our needs, based on experiments performed by Takatsu *et al.* [281]. The expression of the used hATP11A-HA variants and their correct subcellular localisation was confirmed via ICC staining and the separation of cell surface proteins with biotinylation, subsequent SDS page and western blot.

4.5.1. Preparation of cells

HEK293 Flp-In CDC50A-V5 cells were transfected with hATP11A-HA pCAG variant vectors or a mock vector for the negativ control, each with six biological replicates. Each transfection population is selected for several weeks with DMEM containing 600 µg/µl G418 to contain only plasmid carrying cells.
For the flippase activity measurement and surface biotinylation six-well-plates harbouring one replicate of every variant are prepared and passaged in a way that results in five plates with 80% confluence for the flippase activity measurement and three plates for surface biotinylation. The experiments are always performed for both tested phospholipids 18:1-06:0 NBD-PE and 18:1-06:0 NBD-PS (Avanti Polar Lipids, Inc., USA) at once.

4.5.2. Cell surface biotinylation and lysis

The cells for surface biotinylation need to be cultivated on Poly-L-Lysin coated plates. For this 1 ml Poly-L-Lysin solution with 10 mg L^{-1} 100 mM borate buffer is added per well and incubated for 1 h at 37 °C. Subsequently the wells are

washed three times with water, before adding the cells.
Three wells with about 80% confluenct cells of one replicate are washed once with cold DMEM to get rid of dead cells that would incorporate biotin. Afterwards the amines from the DMEM that could interfere with the biotinlyation are rinsed off carefully by washing with cold PBS. 1 ml of the fresh prepared biotin solution is added to each well of cells and incubated for 30 min at 4 °C, to prevent internalisation at RT. The reaction is stopped with washing three times with cold PBS++ with 100 mM glycine and 0.3% BSA at 4 °C. In the last washing step, the solution is left in the well for 20 min to be panned at 4 °C in order to quench all free biotin. Afterwards the cells are washed two times with cold PBS++, before the lysis can be started.
For the lysis of the biotinylated cells a special lysis buffer with 20 mM HEPES-KOH, 1% Nonidet P-40, 150 mM NaCl and protease inhibitor is used. The usual Tris based lysis buffer would compete with the biotin at the cell surface. To each well 100 µl biotinylation lysis buffer are added and kept on ice for 15 min. 20 min of centrifugation at maximum speed and 4 °C pelletises the cell debris, so the whole cell protein supernatant can be collected in a clean tube and stored frozen until used for concentration measurement and cell surface protein extraction. This is done simultaneously for every transfected hATP11A-HA variant and repeated for all six biological replicates.

4.5.3. Extraction of the cell surface protein

For the surface protein extraction 25 µl of the thawed supernatants are kept as whole cell protein and the protein concentration is measured.
The rest is used for the extraction of the biotinylated surface protein. Therefore, Pierce NeutrAvidin Agarose Resin (Thermo Fisher Scientific, USA) is warmed to room temperature. 100 µl bead slurry are centrifuged for 1 min at 1000 × g and 4 °C. The supernatant is removed and the bead pellet washed 3 times with biotinylation lysis buffer with centrifugation under the same conditions. After the last cycle of washing and centrifugation, 50 µl buffer are used to create 100 µl of bead slurry in a 500µl tube. The remaining 75 µl of the protein supernatant are pipetted on the beads and filled up with buffer for a half full tube.
To bind the biotinylated protein to the NeutrAvidin, the mixture is incubated with slow rotation over night at 4 °C.
The next day the beads are pelleted at 1000 × g and 4 °C for 1 min. The supernatant with the unbound intracellular protein is removed without removing any beads. Afterwards the beads with the bound surface protein are washed with 250 µl biotinylation lysis buffer three times while rotating them each time

for 5 min at 4 °C. Two washing steps with 250 µl high salt buffer and one with HEPES-KOH follow without rotating. The supernatant is completely removed carefully. To eluate the surface protein from the washed beads, 40 µl 5 × Laemmli buffer is added to the tube, mixed and incubated over night at 4 °C. During this incubation the SDS in the Laemmli buffer has slowly denaturated the protein bound to the NeutrAvidin. To finally remove all protein from the beads the denaturation is extended for another two hours at RT after centrifuging the beads down quickly.
Separation of beads and proteins in Laemmli buffer is accomplished by piercing a tiny hole in the bottom of the tube with a cannula and directly putting the punctuated tube above another clean tube. Together the stacked tubes are centrifuged for 1 min at 500 × g and RT. The Laemmli buffer with the cell surface proteins is pressed into the lower tube, while the beads remain above. The eluated cell surface protein can now be stored at -20 °C or directly used for western blotting.

4.5.4. Analysis of the whole cell and cell surface protein fraction

SDS page and western blotting of the whole cell and cell surface proteins are performed in order to ensure the expression and the transport of the transfected hATP11A-HA variants to the plasma membrane as observed in previous experiments. For this, differing from the general protocol, Mini Protean TGX Stain-Free Precast Gels with 4-20% and the corresponding Mini-PROTEAN Tetra Cell (Bio-Rad Laboratories Inc., USA) were used.
The eluted 40 µl 5 × Laemmli buffer with cell surface protein are diluted with 20 µl biotinylation lysis buffer. Also 12 µl of the earlier separated sample of whole cell protein are denaturated with 3 µl 5 × Laemmli buffer at 37 °C for 30 min.
30 µl of the cell surface protein solution, heated up to 37 °C for better pipetting viscosity, or 12 µl whole cell protein solution of every transfected hATP11A-HA variant were put on the gel. The used marker for size comparison is See-Blue Pre-stained Protein Standard (Thermo Fisher Scientific, USA). The gels were handled according to manufacturers guidelines and run at 200 V for about 40 min. Subsequently the gels were activated at the ChemiDoc XRSx system (Bio-Rad Laboratories Inc., USA) 2 × for 45 sec and blotted according to protocol for 1,5 h directly afterwards. To have a value to compare the loaded protein amount between the different samples, UV light is used to take a picture of the total protein on the blot before blocking and antibody staining.

4.5.5. Flippase activity measurement

For each transfected hATP11A-HA variant of one replicate 5 equal wells with 80% confluent cells are detached from the plates with 250 µl 5 mM versene respectively for about 10 min at 37 °C. After batching and resuspension in 10 ml PBS 2,5 ml cell suspension are aliquoted in 4 2 ml tubes and washed with 500 µl HBSS. For this and all later steps cells are centrifuged at 300 × g and 4 °C for 5 min. The few µl rest volume of all batches are collected and carried along the procedure to form a tube of control cells for FACS standardisation.
After washing the cells are equilibrated in 500 µl HBSS-glucose for 15 min. Upon this step cells are kept on ice all the time.
Phospholipid uptake starts with the addition of 500 µl HBSS-glucose with 2 µM NBD-phospholipid to the cells, except for the control cells. For each of the phospholipids PS and PE two of the four tubes are used to get a duplicate. For PE, 200 µl samples are taken after 0.25 min, 1 min, 4 min, 10 min and 20 min. The same was tried for PS, but then adjusted to 1 min, 2.5 min, 4 min, 6 min and 10 min. The samples are mixed with 200 µl provided ice cold HBSS-glucose with 5% fatty acid free BSA for 10 min to stop the uptake and extract phospholipid from the outer leaflet of the plasma membrane. Lastly the cells are centrifuged for 10 min at 500 × g and 4 °C and resuspended in 150 µl PBS with 1 mM EDTA and 0.5% BSA to get suitable buffer conditions and concentrations for FACS analysis.
$1 * 10^4$ cells per sample are analysed with FACS for FITC fluorescence at 460 nm absorbance and 533 nm emission. Living, single cells are gated and the median fluorescence intensity is calculated.
As mentioned in previous steps, the whole described procedure is performed with all six biological replicates.

5. Results

By different sequencing technologies the cause for the dominantly inherited AS/AN was identified in a large multigenerational family. All family members are carrying a 5,500 bp deletion in the *ATP11A* gene encoding the phospholipid flippase ATP11A. However, pathogenicity of this mutation was not proven, though Immunohistochemistry stainings were performed to verify ATP11A presence in the inner ear prior starting this thesis. To get information on possible disease mechanisms the deletion needed to be characterised further. After identification of the deletion's effect on mRNA and protein level, the consequences for protein interaction, localisation and function had to be determined to finally confirm the heterozygous variant as the genetic cause of the disease.

5.1. Confirmation of biallelic stable mRNA expression

In order to confirm the previously shown stable mRNA expression of both *ATP11A* alleles and make sure that the cDNA aliquot I was using was suitable, my work for this thesis started with the replication of the experiment on biallelic stable mRNA expression (see 1.4.4). The amplification of patient's cDNA with the primers ATP11A_Ex24_25f and ATP11A_Ex28r and sequencing with ATP11A_cDNA_27f again showed the presence of a heterozygous signal for guanine and adenine (figure 5.1). This confirms the existence of stable mRNA of both *ATP11A* alleles, which itself is a prerequisite for the translation.

5.2. Conservation of *ATP11A* exon 29a and 29b

To determine the relevance of the deleted exons of *ATP11A* the evolutionary conservation throughout different species was investigated. A tool used for this is the ConSurf Server (http://consurf.tau.ac.il) [12]. Here amino acids or nucleic acids are scored from 0, unconserved with high variance between species, to 9, extremely conservered. A nucleic acid based Multi Sequence Alignment for 21 eutherian mammals performed with Ensembl (version 90) [1] was analysed with ConSurf and the scores were illustrated as a heat map for convenient comparison (fig. 5.2). Unconserved bases are shown in white and highly conserved ones in

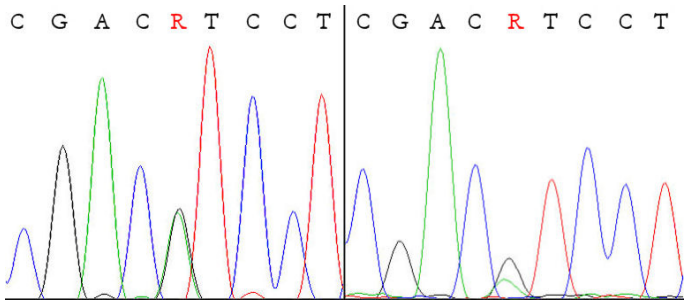

Figure 5.1.: Sequencing of hATP11A exon 28 on genomic DNA template and cDNA template (right). The presence of a heterozygous signal for the SNP rs11616795 on cDNA template rules out complete nonsense-mediated mRNA decay of the mutated transcription.

dark red. For simplification, exons are hereinafter named with their count in the already spliced mRNA. The sequences used for isoform 1 encoded in exon 29 is called 29a, the equivalent of isoform 2, encoded in exon 30 is called 29b and the newly spliced exon of the deletion variant is called 29^{mut}. Exon 29b has variable conservation scores and less conserved regions, while exon 29a has larger regions with high conservation scores of 8 and 9, only interrupted by a few bases with extremely low conservation. Especially the separation in highly conserved bases on the one hand and non-conserved bases on the other hand may point to a selective process and not a random variance. The conserved regions might be necessary for protein function of *ATP11A* isoform 1, whereas the disrupting unconserved bases are seemingly not functionally involved. The random conservation pattern of exon 29b indicates one of two things. The exon is not necessary for protein function or *ATP11A* isoform 2 is either not expressed or not functional at all.

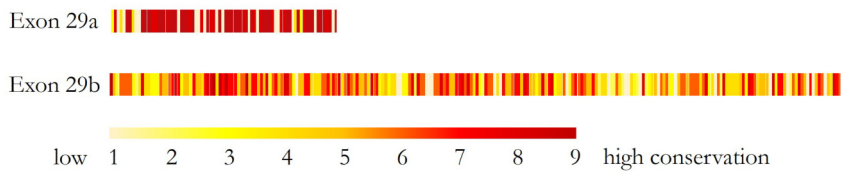

Figure 5.2.: Heat map of the ConSurf conservation of *hATP11A* exon 29a (high) and 29b (low). Multi Sequence Alignment was performed with Ensembl on 21 eutherian mammals. Scores range from 1 - white - unconserved to 9 - dark red - highly conserved.

Since we have a larger deletion, also the tolerance to loss of function mutations is of interest. The Genome Aggregation Database (gnomeAD, version 2.1.1) [108] has constraint metric scores integrated in their database. With this, the tolerance to amino acid variation or loss of function variation can be calculated by comparing the theoretical probability of those variants with the occurrence in the database control population, which excludes people with severe pediatric diseases. Loss of function intolerance is predicted by two scores. The pLI score and the o/e score. Aside genes that are completely tolerant towards loss of function mutations, there are genes which tolerate those variants only at a heterozygous state. A score of pLI $\geq$ 0.9 is considered intolerant to loss of function mutations and indicates haploinsufficiency. This is also the case for *hATP11A* with a pLI score of 0.000. The o/e, which means 'observed divided by expected number of loss of function variants', is 0.33 at an confidence intervall of 90%, meaning that only 33% of the expected number of variants for a gene of this size are found in the database sequences. Taken together *hATP11A* can be interpreted as most likely intolerant to loss of function mutations. Only a few loss of function variants are listed and it can not be ruled out that their carriers are affected by hearing loss at some degree. In the GnomAD database there are two frameshift variants in exon 29b described in 64 and 138 allels respectively (allele frequency of 0.026 and 0.049%). Assuming from the conservation data that the exact amino acid composition of the last exon 29b is not essential, also frameshift mutations in that region might have no effect and for that are tolerated. Another loss of function variant is reported for 47 allels with an allele frequency of 0.021%. It is affecting the splice acceptor site at exon 29a c.3058-1G>T. According to the conservation data this would be more relevant to the protein function, if the mutation altered the protein sequence. The GnomAD database lists the variant only as low confidence loss of function, because there is an alternative in frame AAG splice acceptor six bases after the normal acceptor site that is believed to potentially rescue the splice process with only two amino acids lost.

5.3. Effect of the patient's deletion in *hATP11A* on mRNA level

To examine the effect of the 5,500 bp deletion including the last coding exon of both isoforms on mRNA level a Touchdown PCR was performed. Different reverse primers in the 3' UTR of *hATP11A* were used on control and patient's blood cDNA. The PCR products on control cDNA without deletion were pre-

dicted to have sizes of 5,682 bp, 6,360 bp, 6,963 bp and 8,305 bp respectively. As shown in figure 5.3 the control products of the anticipated sizes were amplified. Amplification of patient's cDNA showed mutated allele bands of about 500 bp, 1,200 bp, 1,800 bp and > 3,000 bp respectively. The size differences between the products match the differences between the control products. In the amplification of the patient's cDNA the amplification of the mutated allele is in favour because of the smaller size. The PCR product of ATP11A_UTR_f and ATP11A_UTR_r2 was the most specific and for this reason used for sequencing. Sequencing shows the use of an aberrant splice site. Exon 28 is followed by another new exon 29^{mut}, starting 171 bp after the deletion. The next stop codon is 114 bp downstream. The alternative splice acceptor site is predicted as such with 89.91% by the Human Splicing Finder web tool [44]. A structural overview of the altered region is shown in figure 5.4. Sequence information is enclosed in the appendix.

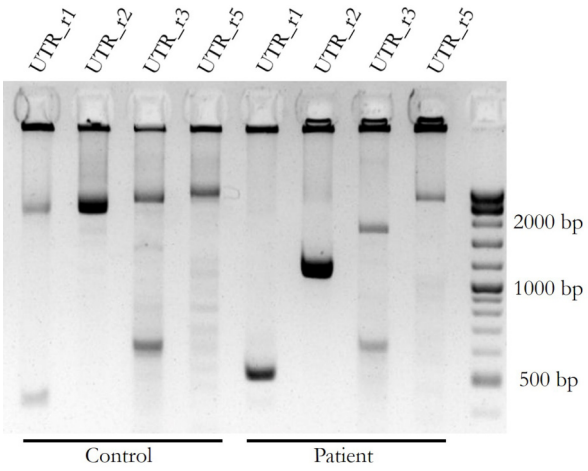

Figure 5.3.: Amplification of *hATP11A* 3' region on control and patient's cDNA. The forward Primer is ATP11A_UTR_f, reverse Primers are ATP11A_UTR_r1, ATP11A_UTR_r2, ATP11A_UTR_r3 and ATP11A_UTR_r5.

Specific reverse primer were designed for the amplification of a part of each *hATP11A* isoform separately including the deletion variant. The primers are listed in section 3.3 as ATP11A_v1_Ex29ar, ATP11A_v2_Ex28_29br and ATP11A_Mut_Ex28_29mutr. These were used to confirm the sequencing finding and get an estimation of the expression level of the variants. Location of the primers and product sizes are illustrated in figure 5.5a.

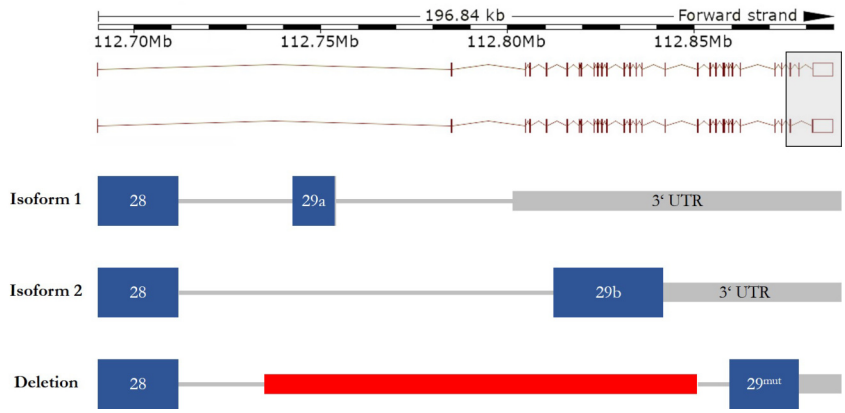

Figure 5.4.: Genomic structure of the 3' region of *hATP11A* with focus on the new exon 29^{mut} usage caused by aberrant splicing. Coding exons of the different variants are marked as blue boxes, whereas introns are shown as thin grey lines. The deletion at the mutated allele is illustrated in red and the beginning of the 3'UTR as a thinner grey box.

The PCR results are presented in figure 5.5b. According to the assumption that isoform 2 plays only a minor role in the cell's ATP11A activity, in the control mostly *hATP11A* isoform 1 is expressed, while only a small amount of isoform 2 and no deletion variant was amplified from control cDNA. In contrast amplification of the patient's cDNA resulted mainly in production of the mutant deletion variant, less *hATP11A* isoform 1 and no detectable isoform 2. All negative controls were empty (not included in the figure).

5.4. Cloning of *hATP11A* isoforms in tagged expression vectors

In addition to the available pcDNA3 based plasmid constructs of human *ATP11A* isoform 1 WT, the two point mutation variants hATP11A-HA E186Q and D414N and HNF-hCDC50A pcDNA3, also *hATP11A* isoform 2 and the mutant deletion variant were needed for further experiments.
The template DNA for amplification of the desired sequences of the variants was commercially synthesised as gene fragments with a size of about 1,500 bp including the HA-Tag of the hATP11A-HA Isoform 1 pCAG construct. Detailed sequence information is attached in the appendix. To receive the plasmid backbone, the hATP11A-HA Isoform 1 pCAG plasmid was digested with restriction enzymes to cut out the part that needed to be replaced with the new sequences. The insert sequences of *hATP11A*-HA isoform 2 and the mutant

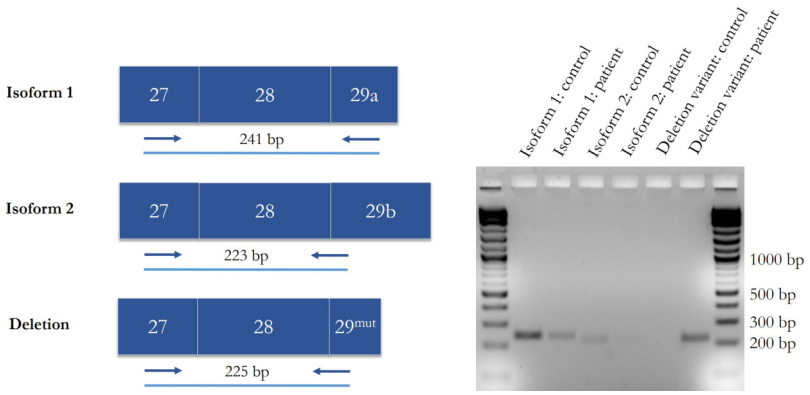

(a) Primer locations. The forward Primer is ATP11A_Ex27f, reverse Primers are ATP11A_v1_Ex29ar, ATP11A_v2_Ex28_29br and ATP11A_Mut_Ex28_29mutr respectively.

(b) Agarose gel of the raw relative quantification of *hATP11A*.

Figure 5.5.: Raw relative quantification of *hATP11A* in control and patient's cDNA. In healthy control cDNA less *hATP11A* isoform 2 and no deletion variant can be amplified. In patient's cDNA mainly the deletion variant is found.

deletion variant were amplified from the gene fragments with primers that resulted in overlapping regions of vector backbone and inserts. After purification, backbone and insert were combined using the NEBuilder Cloning method, followed by transformation of competent *E. coli* cells.

In the same way an additional artificial variant of *hATP11A* was cloned to investigate if the missing exon 29a or the artificial exon 29_{mut} added by the mutation is pathogenic. This time the insert template was not synthesised, but directly amplified from the hATP11A-HA Isoform 1 pCAG plasmid. This way a plasmid with a *hATP11A* variant ending after Exon 28, called hATP11A-HA until ex28 pCAG was made.

For cotransfection analysis of *hATP11A* Isoform 1 WT and *hATP11A* deletion variant, both variants need to have identifiable tags. For this purpose the vector pcDNA3.1(-) Myc/His was used to amplify the Myc/His-Tag with overlapping bases to the pCAG vector. NEBuilder Cloning inserted the Myc/His-Tag between *hATP11A* Isoform 1 WT and the HA-Tag, which no longer is expressed in the new vector due to a stopcodon after the Myc/His sequence.

As mock control an empty vector backbone of pCAG called MCS-HA pCAG was constructed. To also get a useful vector for further cloning, the insert was replaced by a multiple cloning site. This multiple cloning site was synthesised

as gBlocks Gene Fragments with homologous ends for NEBuilder coning. The *hATP11A* isoform 1 WT sequence was removed from the hATP11A-HA Isoform 1 WT pCAG vector with restriction endonuclease digestion and subsequent gel purification, before the plasmid was assembled via NEBuilder cloning.
In order to use the Flp-In system for generation of stable cell lines, Gateway Cloning was performed with *CDC50A* as an insert. The HNF-hCDC50A pcDNA3 vector was used as a template for the amplification of *CDC50A* with the primer that added attB recombination sites to the gene sequence. The *CDC50A* fragment was inserted in to entry vector pDonr211. Successfully cloned pDonr211 CDC50A plasmid was used for a following LR reaction, moving *CDC50A* into the pEF5/FRT/V5 Flp-In vector to receive the finished pEF5/FRT hCDC50A-V5 plasmid for transient transformation of HEK293 cells. The received colonies of all cloned constructs were analysed using colony PCR with two different primer pairs, which could identify the specific variant and the correct location of the insert. Over night cultures of positive clones were grown, the plasmid DNA isolated and the gene of interest coding area sequenced to exclude additional mutations during the cloning process. Glycerol stocks were created for storage. Vector maps of all non commercially available plasmids used can be found in the appendix.

5.5. Subcellular localisation of hATP11A isoforms

In order to investigate the subcellular localisation of the deletion variant of hATP11A-HA at the plasma membrane, HEK293T cells were cotransfected with three plasmids. In addition to the different variants of hATP11A-HA pCAG, tdTomato-ER-3 was used as a fluorescent marker for the ER. To see differences in transportation, the transfection was performed with and without HFN-hCDC50A pcDNA3 to ensure the presence of enough CDC50A for proper transport from the ER to the plasma membrane. The results are shown in figures 5.6 and 5.7. Each panel compares the cotransfection with HNF-hCDC50A pcDNA3 (left) with the cotransfection without HNF-hCDC50A pcDNA3 (right). All cells shown on the left were checked for the expression of HNF-hCDC50A, yet it is not included in the merged picture for better clarity. Without CDC50A cotransfection all hATP11A-HA variants colocalise with the ER marker (all panels on the right side). With hCDC50A hATP11A-HA Isoform 1 WT can be found at the plasma membrane. Some hATP11A-HA still colocalises with the ER probably because of the overexpression. Similar findings could be observed for the non functional protein hATP11A-HA Isoform 1 E186Q, although it is transported to the plasma membrane. As expected the transport deficient variant hATP11A-

HA Isoform 1 D414N completely colocalises with the ER, comparable to the transfection without HFN-hCDC50A pCAG. The two variants hATP11A-HA Isoform 2 and the deletion variant, which have not been characterised so far, are localised at the plasma membrane. Taken together, my experiments show that the use of exon 29b in isoform 2 or 29^{mut} in mutant ATP11A does not alter the interaction of the protein with hCDC50A and its correct intracellular transport.

It is unclear if hATP11A undergoes homodimerisation. Therefore, it was checked whether the simulation of a heterozygous state via cotransfection of hATP11A-His/Myc Isoform 1 WT and hATP11A-HA deletion variant has an impact on protein transport and localisation. Different tags are used to distinguish the variants in the immunocytochemistry staining. *hCDC50A*-Flag expression was not tested, but the difference in subcellular localisation between the contransfection with HFN-hCDC50A pCDNA3 (left side of figure 5.8) and without (right side) resembles previous results. In the presence of hCDC50A both variants are mainly localised at the plasma membrane. Accordingly, the expression of WT and deletion variant in the same cell does not impair the transport.

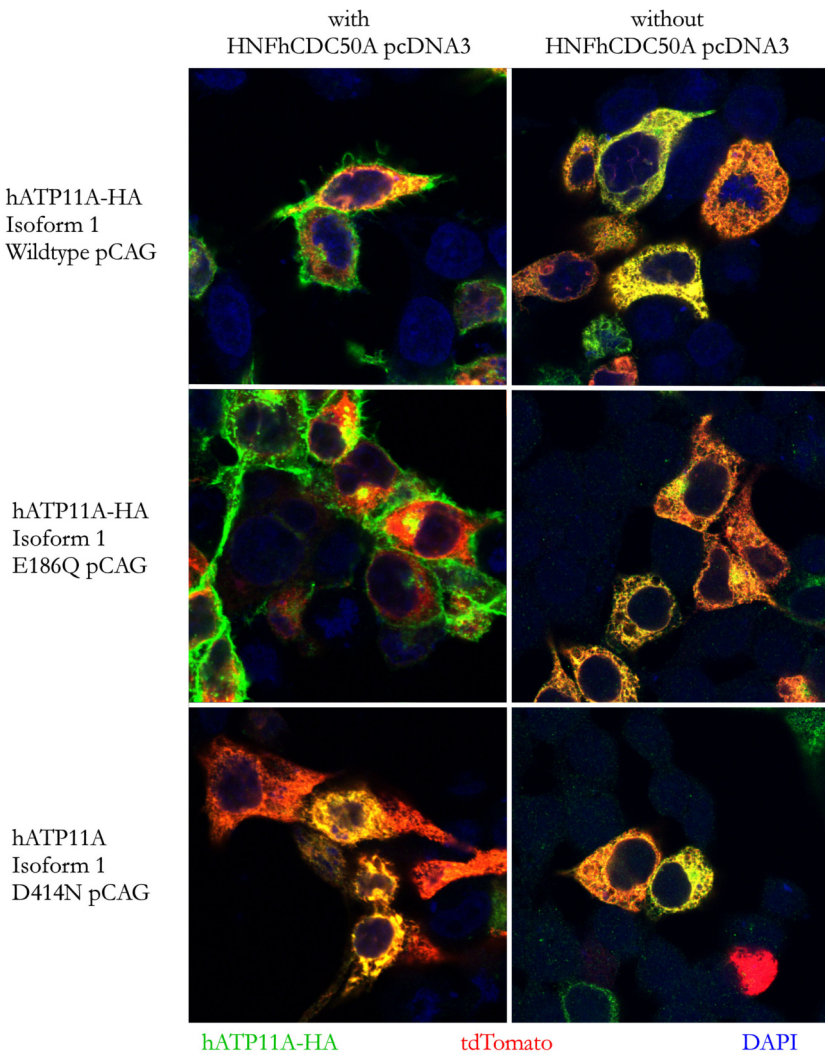

Figure 5.6.: Part 1: Immunocytological staining of HEK293T cotransfections for hATP11A-HA location studies with tdTomato-ER, an hATP11A-HA pCAG variant and with or without HNF-hCDC50A pcDNA3. Staining was performed using Monoclonal Anti-Flag M2 F3165 (1:500) and Alexa Fluor 633 Goat anti-Mouse IgG A21052 (1:1000) for HNF-hCDC50A and Anti-HA rabbit H6908 (1:666) and Alexa Fluor 488 Goat anti-Rabbit IgG A11008 (1:1000) for hATP11A-HA. Nuclei were stained with DAPI. The cells shown on the left were checked for the expression of HNF-hCDC50A, yet it is not included in the merged picture for better clarity. Each arrangement compares the cotransfection with HNF-hCDC50A pcDNA3 with the cotransfection without HNF-hCDC50A pcDNA3.

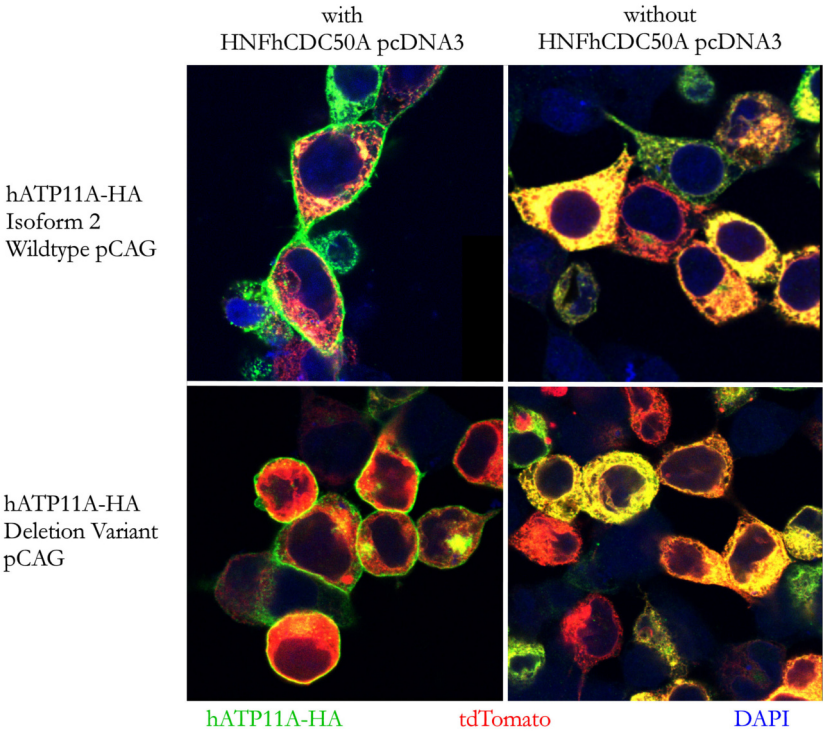

Figure 5.7.: Part 2: Immunocytological staining of HEK293T cotransfections for hATP11A-HA location studies with tdTomato-ER, an hATP11A-HA pCAG variant and with or without HNF-hCDC50A pcDNA3. Staining was performed using Monoclonal Anti-Flag M2 F3165 (1:500) and Alexa Fluor 633 Goat anti-Mouse IgG A21052 (1:1000) for HNF-hCDC50A and Anti-HA rabbit H6908 (1:666) and Alexa Fluor 488 Goat anti-Rabbit IgG A11008 (1:1000) for hATP11A-HA. Nuclei were stained with DAPI. The cells shown on the left were checked for the expression of HNF-hCDC50A, yet it is not included in the merged picture for better clarity. Each arrangement compares the cotransfection with HNF-hCDC50A pcDNA3 with the cotransfection without HNF-hCDC50A pcDNA3.

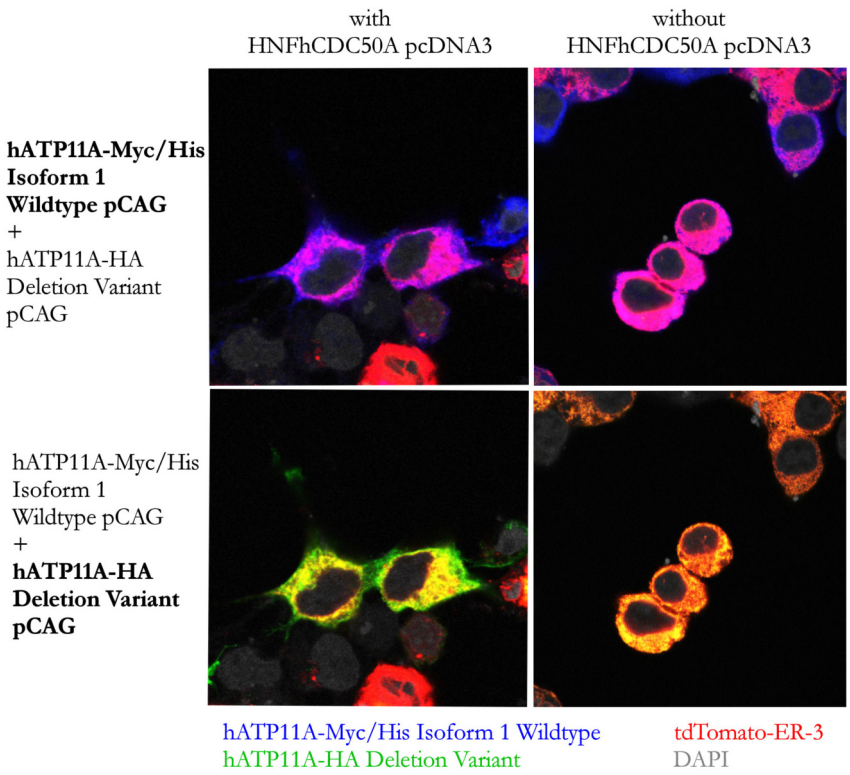

Figure 5.8.: Immunocytological staining of HEK293T cotransfections simulating a heterozygous state for hATP11A location studies with tdTomato-ER, hATP11A-His/Myc Isoform 1 pCAG, hATP11A-HA deletion variant pCAG and with or without HNF-hCDC50A pcDNA3. Staining was performed using Anti-HA rabbit H6908 (1:666) and Alexa Fluor 488 Goat anti-Rabbit IgG A11008 (1:1000) for hATP11A-HA deletion variant and Anti-C-Myc mouse M5546 (1:500) and Alexa Fluor 633 Goat anti-Mouse IgG A21052 (1:1000)for hATP11A-Myc/His Isoform 1. Nuclei were stained with DAPI. To show the effect of missing hCDC50A for a cotransfection of hATP11A-His/Myc Isoform 1 pCAG and hATP11A-HA deletion variant pCAG, the absence of hCDC50A on the right side of the panels is compared to the presence of hCDC50A on the left side. The localisation of the hATP11A-HA variants is made visible by merge pictures of tdTomato with anti-Myc staining for hATP11A Isoform 1 (upper part) and with anti-HA staining for hATP11A-HA deletion variant (lower part).

5.6. Flippase activity assay

Since transportation of ATP11A is not changed in the patient according to my immunocytochemistry experiments, an alteration in the functionality is another potential consequence that might result in the phenotype. A fluorescence based assay was adapted and established to judge the flippase activity of several hATP11A variants. To investigate the activity of the patient's hATP11A deletion variant and also hATP11A Isoform 2 WT more comprehensively, not only those, but also hATP11A-HA Isoform 1 WT, E186Q and D414N, as well as a negative mock control were analysed. And in addition a truncated hATP11A variant, ending after the sequence coded in exon 28, is evaluated as well. It resembles the deletion variant, as it also misses exon 29, but lacks an artificial ending after exon 28. This experimental strategy enables a differentiation, if the missing exon 29 alone or the additional exon 29^{mut} causes the possible different behaviour in the assay.
Human *CDC50A* was stably integrated into HEK293 cell DNA. A single cell derived cell line expressing *hCDC50A* was then transfected with different *hATP11A*-HA variants and used for the flippase activity assay.

5.6.1. Creation of a stable HEK293 Flp-In hCDC50A-V5 cell line transiently expressing *hATP11A*-HA

Stable integration of *hCDC50A* into HEK293 Flp-In cells was performed with the vector pEF5/FRT/V5, which was specially created for the usage with the Flp-In transfection system. After the initial antibiotic selection process, two isolated cells survived and grew colonies. Subsequent analysis and selection of the cells showed that colony 2 on the one hand still reacted sensitive to 100 µl/ml Hygromicin B to a certain degree and on the other hand partly survived cultivation with 100 µl/ml Zeocin. This colony had probably not derived from a single cell and was not selected properly. Colony 1 performed as expected for a transfected and selected single cell colony and, therefore, was used for further inspection. Immunocytochemistry was performed, expoiting the V5 tag of the transfected *CDC50A*. Confocal imaging showed equally stained cells all expressing a comparable amount of CDC50A (see fig. 5.9a). After protein lysis of colony 1 cells and western blotting, protein detection showed distinct bands at the estimated size (see fig. 5.9b).
Cells of the HEK293 Flp-In hCDC50A-V5 cell line were transfected with the different hATP11A-HA pCAG variants previously used for the determination of the subcellular localisation, an additional variant ending after exon 28 and

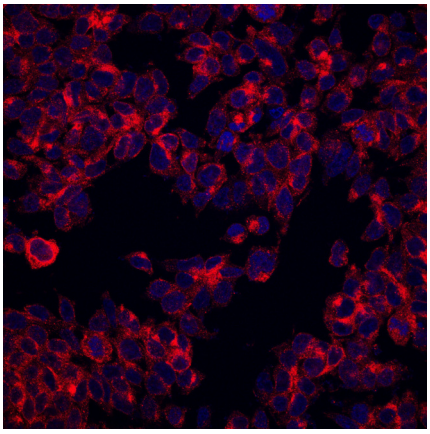

(a) Confocal imaging of HEK293 Flp-In hCDC50A-V5. hCDC50A-V5 was stained using V5 tag monoclonal antibody R960-25 (1:500) and Alexa Fluor 633 Goat anti-Mouse IgG A21052 (1:1,000). Imaging was done with Leica TCS SP8 confocal laser microscope (Leica Microsystems GmbH, Wetzlar, Germany).

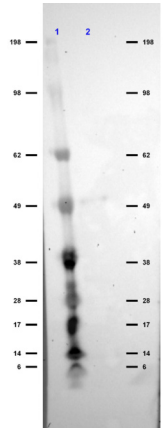

(b) Western blot of hCDC50A-V5 (44.96 kDa) in HEK293 Flp-In hCDC50A-V5 lysate. The horseradish peroxidase tagged V5 tag monoclonal antibody R961-25 (1:5,000) (Thermo Scientific Inc., USA) was used for detection. Despite its smaller size CDC50A runs in broad bands at 50 kDa, because of the heterogeneous structure of the oligosaccharide chains [211].

Figure 5.9.: Expression analysis of the generated cell line HEK293 Flp-In hCDC50A-V5. hCDC50A is expressed in all cells.

a mock vector. Six biological replicates of every hATP11A-HA pCAG variant were made and selected with 600 µg mL^{-1} G418 for several weeks.
When performing the isolation of cell surface protein and the flippase activity assay, the transfected cells were tested on their expression of *hATP11A*-HA and the correct protein translocation with ICC. The ICC stainings showed overexpression of hATP11A-HA with the expected location, previously examined by subcellular localisation experiments. The new variant of hATP11A-HA ending after exon 28 was found to be transported to the plasma membrane.

5.6.2. Surface biotinylation

Since it was decided against normalisation on cell surface hATP11A-HA protein, as described later in the results of the flippase activity measurement, the surface biotinylation, cell surface protein isolation and subsequent western blotting was only used as another pre test. It was employed to ensure that all protein variants are expressed and translocated as expected from the earlier performed immunocytochemistry findings. Exemplary blots are shown in figure 5.10.

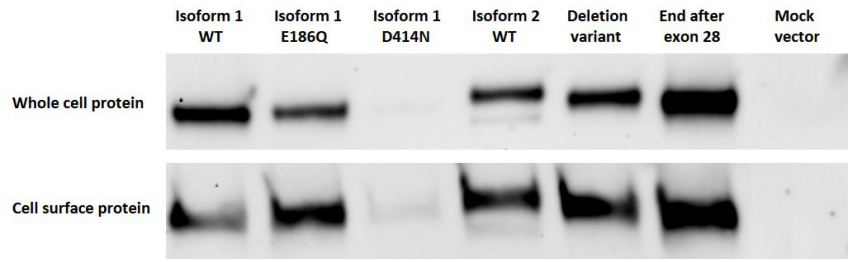

(a) Western blots of all wells number 2 of every transfected hATP11A-HA variant. The whole cell protein blot was exposed for 240 s and the cell surface protein blot for 60 s.

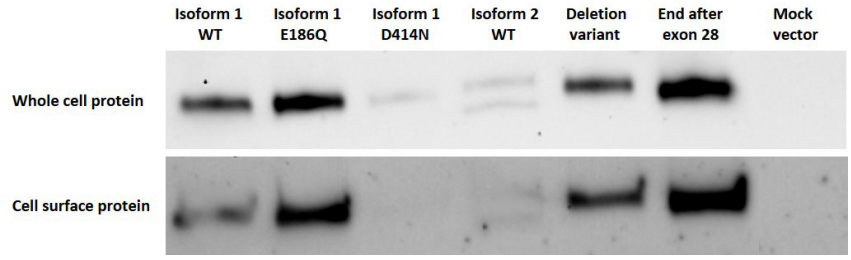

(b) Western blots of all wells number 3 of every transfected hATP11A-HA variant. Both the whole cell protein blot and the cell surface protein blot was exposed for 240 s.

Figure 5.10.: Exemplary western blots of whole protein and cell surface protein fractions. hATP11A-HA variants were detected with an 1:1,000 dilution of rabbit anti-HA antibody H6908 from Sigma-Aldrich Corp. (USA) and 1:2,500 goat anti-rabbit antibody with HRP conjugate 32460 from Thermo Scientific Inc. (USA). Although hATP11A expression levels differ between the variants and the transfections while the whole protein level is constant, all variants are generally expressed and translocated as expected. hATP11A-HA D414N levels are probably lower because of degradation in the ER [292].

Despite quite consistent results for the total protein amount, the band intensity of the hATP11A-HA variants in the whole cell protein blots differed between each other and also between different wells transfected with the same variant. Especially hATP11A-HA isoform 1 D414N bands are faint in comparison. Nevertheless, equivalent to the results of the previous subcellular localisation experiments, all variants are expressed and all but hATP11A-HA D414N get translocated to the plasma membrane.

5.6.3. Flippase activity measurement

The flippase activity of different hATP11A-HA variants is tested for the phospholipids PS and PE. In order to avoid falsifications by endocytosis of the phospholipids, the experiments were performed on ice.
The FACS measurements were gated to first excluded not living cells and in a second step set a threshold gate to divide fluorescing cells from unfluorescing ones by using untreated cells as a baseline. The detailed gating process is shown at the example of hATP11A-HA Isoform 1 WT after 1 min in figure 5.11. The median fluorescence intensity of the gated cell populations was used for all further calculations. The time point adjustment for the samples taken from the NBD-PS treated cells resulted in only four measurements for 20 s and 20 min. This is too little to be used for further statistics, so they were left out.

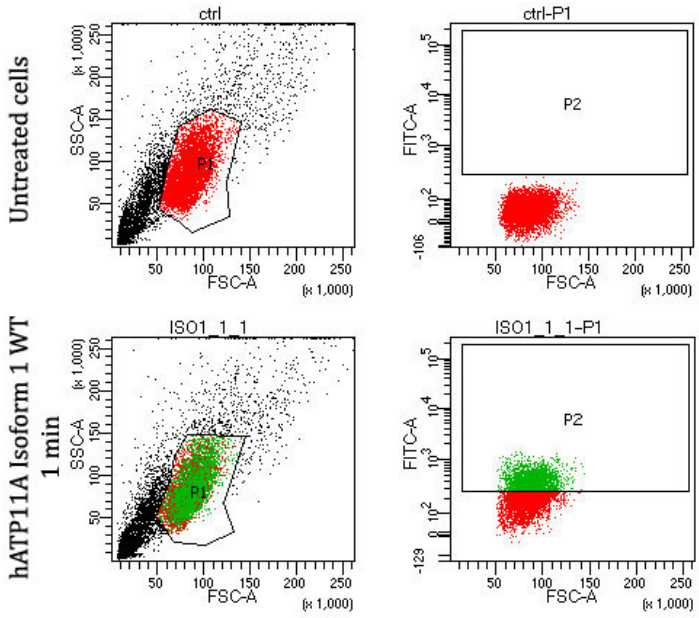

Figure 5.11.: Exemplary gating process of the FACS data. Every sample as well as the untreated cells are first divided in living cells and debris using the sidescatter (SSC-A) and forwardscatter laser (FSC-A). P1 represents the population of living single cells. On the right, only P1 population cells are plotted with their fluorescence intensity (FITC-A). The untreated cells are used to set a threshold gate to divide fluorescing and unfluorescing cells. The fluorescing population is called P2 and is automatically used for detecting fluorescence above the threshold in all samples. P2 cells are shown in green, whereas cells below the threshold are shown in red.

Outliers were identified by the ROUT method of the Prism Graph Pad software with a Q coefficient of 1%. For NBD-PS only two values of the deletion variant were found, whereas for NBD-PE there were two values for the mock vector, one for the deletion variant and five values at time point 20 s spreading over several variants, showing that such an early sample for PE might not be useful and too susceptible to second wise deviation from the protocol.
The rest of the median fluorescence measurements were used to calculate an algorithmic mean and the standard derivation per time point and transfected *hATP11A*-HA variant. The statistical significance was analysed with t-Tests with the Holm-Sidak method ($\alpha = 0.05$) using the Prism Graph Pad software again. Each time point was analysed individually without assuming a consistent standard derivation.
The one outlier for the hATP11A-HA deletion variant in the NBD-PS data does only alter the median and standard derivation at 6 min ever so slightly. The significance level is not changed by this. Therefore, the interpretation of the data is the same for both calculated versions, shown in figures 5.12 and 5.13.
The fluorescence intensity of the cells transfected with the different hATP11A-HA pCAG plasmids clearly forms two groups after NBD-PS treatment. hATP11A-HA Isoform 1 E186Q, D414N, Isoform 2 WT and the deletion variant perform similar to the mock vector in terms of NBD-PS transport.
hATP11A-HA Isoform 1 WT and the variant ending after exon 28 reach significantly higher fluorescence intensity. These variants transport NBD-PS from the surrounding into the cell. While Isoform 1 WT seems to slow down the transport after the 6 min sample, the variant ending after exon 28 keeps on flipping NBD-PS with a steady rate. This difference between the hATP11A-HA Isoform 1 with and without exon 29a is, however, not significant.
It might be suspected that after treatment with NBD-PE similar results can be observed as seen for NBD-PS treatment. This is not the case. The incorporation of NBD-PE occurs much slower compared to NBD-PS. Consequently, the last sample is taken after 20 min instead of 10 min. The development of the fluorescence intensity over time after the NBD-PE treatment is shown in figures 5.14 and 5.15. The first one shows the whole data, the second one is cleared from outliers as described before. Again, the difference between both is very small. When looking at the relative intensities of the variants, one could estimate three groups of NBD-PE incorporation. The first one consists of hATP11A-HA Isoform 1 E186Q, Isoform 1 D414N and Isoform 2 WT. These ones seem to have almost no incorporation at all, the differences between the time points all are approximately within the size of the standard derivation. Isoform 2 fluorescence

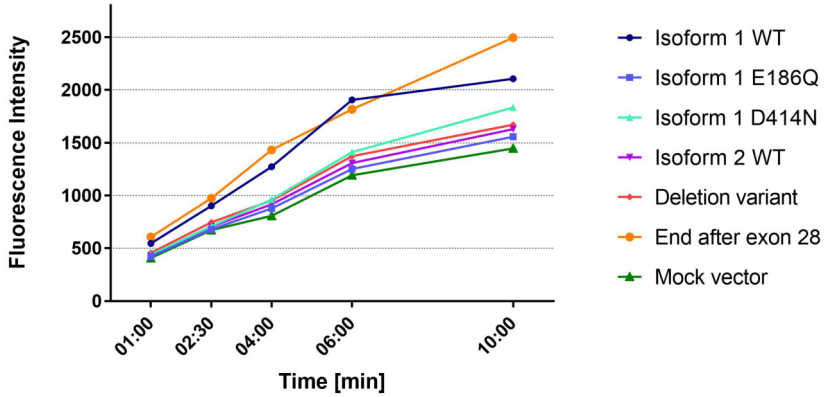

(a) Linegraph of NBD-PS intake over time in HEK293T cells stably overexpressing CDC50A and transfected with different hATP11A-HA pCAG variants, including outliers. The sample time points are marked with symbols. The connection between the points is extrapolated from those to better show the grouping in functioning and non functioning flippases. Error bars and significance levels are left out for visual clarity.

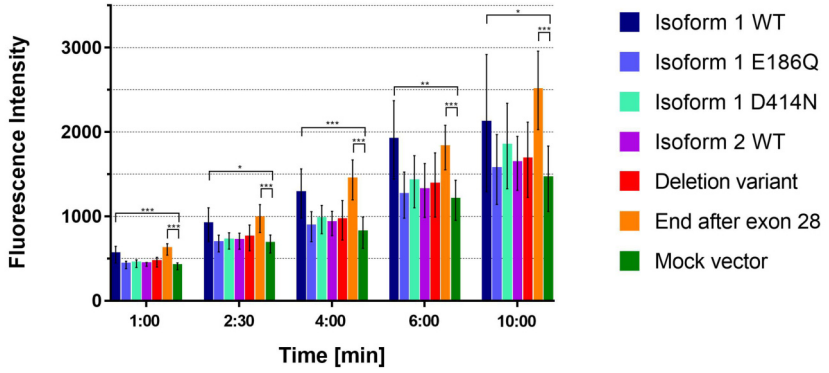

(b) Bargraph of NBD-PS intake in HEK293T cells stably overexpressing CDC50A and transfected with different hATP11A-HA pCAG variants at each measured timepoint, including outliers. Error bars show the standard derivation. Significance levels: * < 0.05, ** < 0.01, *** < 0.001.

Figure 5.12.: Mean median fluorescence of NBD-PS, including outliers. The variants can be grouped in functioning ones (Isoform 1 WT and End after exon 28) and non functioning ones (Isoform 1 E186Q, Isoform 1 D414N, Isoform 2 and the patients' deletion variant).

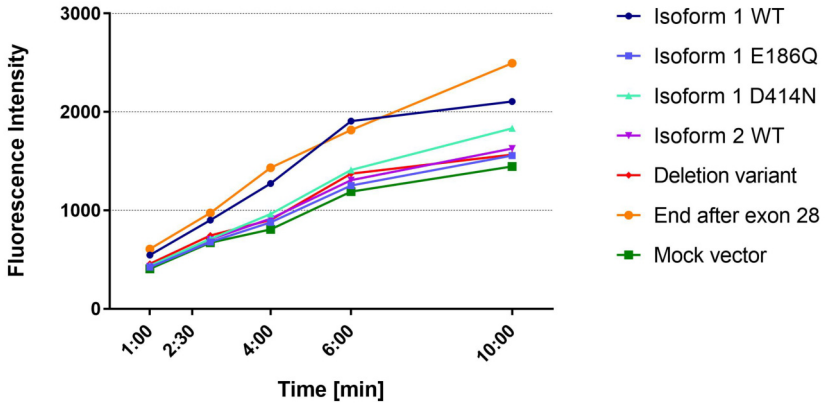

(a) Linegraph of NBD-PS intake over time in HEK293T cells stably overexpressing CDC50A and transfected with different hATP11A-HA variants, without outliers. The sample time points are marked with symbols. The connection between the points is extrapolated from those to better show the grouping in functioning and non functioning flippases. Error bars and significance levels are left out for visual clarity.

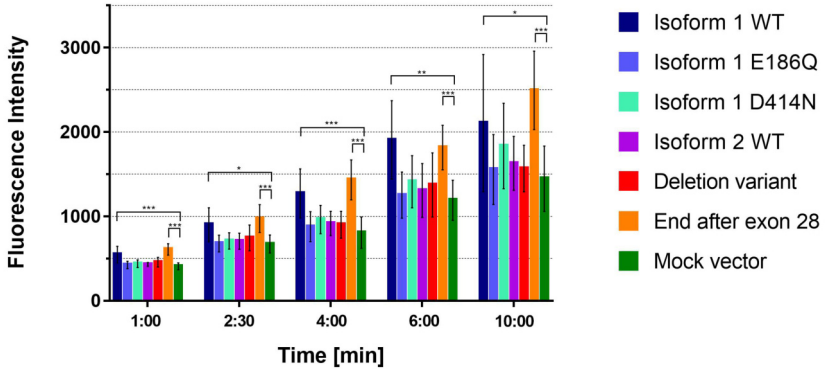

(b) Bargraph of NBD-PS intake in HEK293T cells stably overexpressing CDC50A and transfected with different hATP11A-HA variants at each measured timepoint, without outliers. Error bars show the standard derivation. Significance levels: * < 0.05, ** < 0.01, *** < 0.001.

Figure 5.13.: Mean median fluorescence of NBD-PS, without outliers. The variants can be grouped in functioning ones (Isoform 1 WT and End after exon 28) and non functioning ones (Isoform 1 E186Q, Isoform 1 D414N, Isoform 2 and the patients' deletion variant).

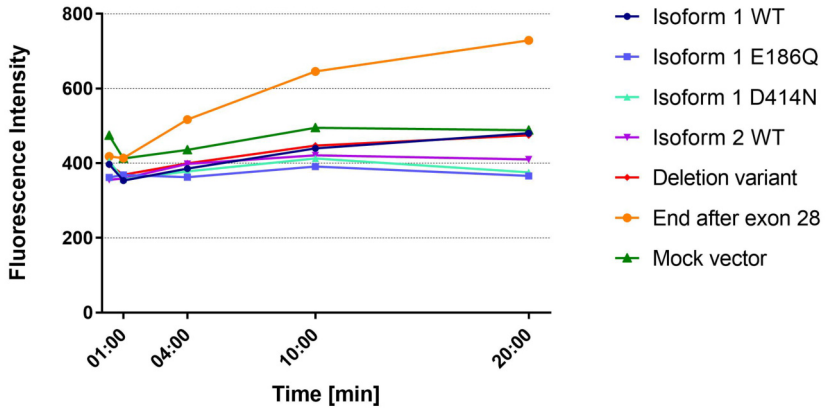

(a) Linegraph of NBD-PE intake over time in HEK293T cells stably overexpressing CDC50A and transfected with different hATP11A-HA pGAG variants, including outliers. The sample time points are marked with symbols. The connection between the points is extrapolated from those to better show the grouping in functioning and non functioning flippases. Error bars and significance levels are left out for visual clarity.

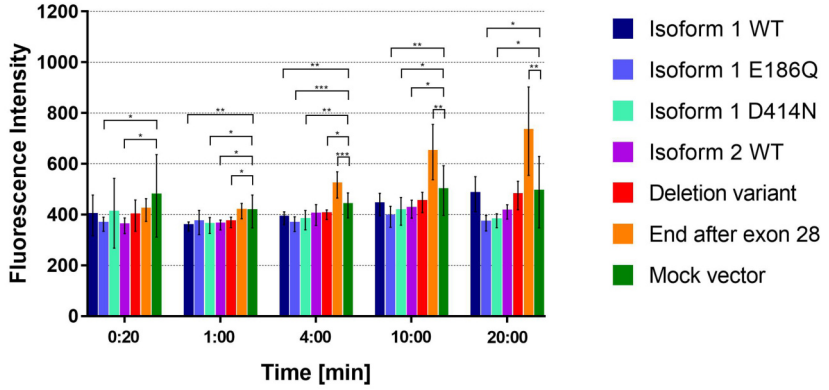

(b) Bargraph of NBD-PE intake in HEK293T cells stably overexpressing CDC50A and transfected with different hATP11A-HA pGAG variants at each measured timepoint, including outliers. Error bars show the standard derivation. Significance levels: * < 0.05, ** < 0.01, *** < 0.001.

Figure 5.14.: Mean median fluorescence of NBD-PE, including outliers. The data of the Mock vector is not conclusive. However, the other variants can be grouped in (1) non functioning (Isoform 1 E186Q, Isoform 1 D414N and Isoform 2), (2) functioning (Isoform 1 WT and the patients' deletion variant) and (3) overactive (Ending after exon 28).

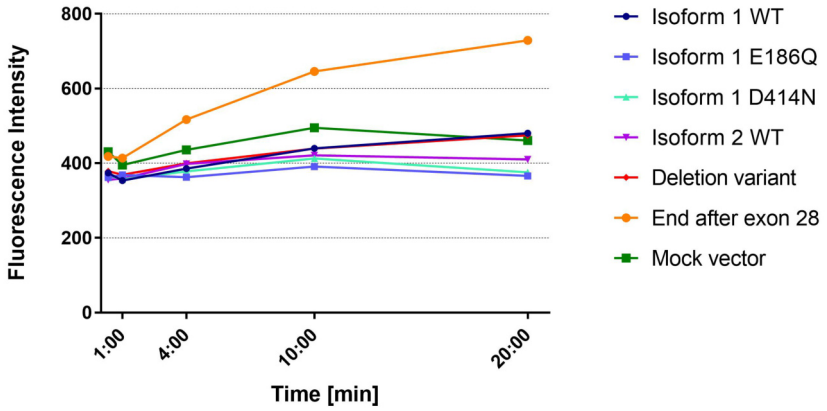

(a) Linegraph of NBD-PE intake over time in HEK293T cells stably overexpressing CDC50A and transfected with different hATP11A-HA pCAG variants, without outliers. The sample time points are marked with symbols. The connection between the points is extrapolated from those to better show the grouping in functioning and non functioning flippases. Error bars and significance levels are left out for visual clarity.

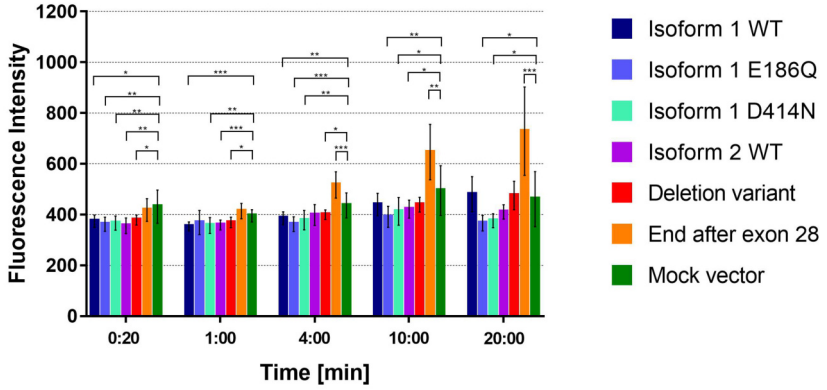

(b) Bargraph of NBD-PE intake in HEK293T cells stably overexpressing CDC50A and transfected with different hATP11A-HA pCAG variants at each measured timepoint, without outliers. Error bars show the standard derivation. Significance levels: * < 0.05, ** < 0.01, *** < 0.001.

Figure 5.15.: Mean median fluorescence of NBD-PE, without outliers. The data of the Mock vector is not conclusive. However, the other variants can be grouped in (1) non functioning (Isoform 1 E186Q, Isoform 1 D414N and Isoform 2), (2) functioning (Isoform 1 WT and the patients' deletion variant) and (3) overactive (Ending after exon 28).

intensities do not exceed those of the loss of function variant Isoform 1 E186Q and the loss of transport variant Isoform 1 D414N.
A second group form hATP11A-HA Isoform 1 WT and the deletion variant. In the beginning they are not distinguishable from group 1, but at 20 min the fluorescence intensity increases significantly above the starting value.
Clearly distinguishable from those are cells transfected with hATP11A-HA pCAG ending after exon 28. The incorporation of NBD-PE grows rapidly from the start and reaches much higher fluorescence intensities.
The cells transfected with the mock vector do not fall in group 1, as would have been suspected for only endogenous flippase activity, but have fluorescence intensities above the hATP11A-HA Isoform 1 WT and deletion variant cells. Stricter handling of the outliers, with a Q coefficient raised to 5%, decreases the value for 20 min to the level of the not incorporating group 1, but the other time points still have raised intensities.

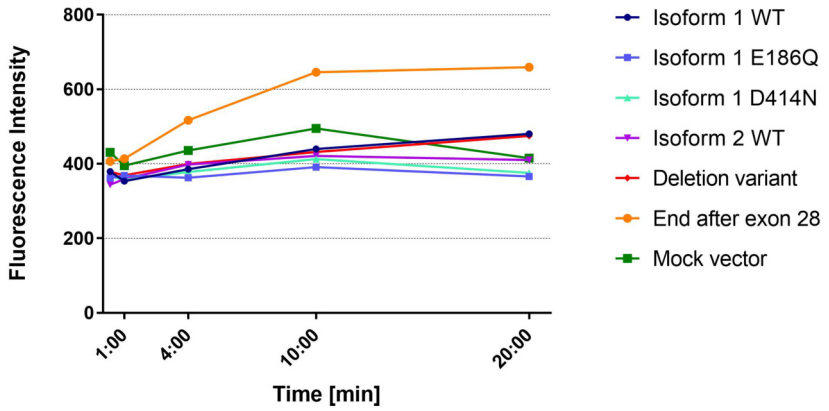

Figure 5.16.: Linegraph of NBD-PE intake over time in HEK293T cells stably overexpressing CDC50A and transfected with different hATP11A-HA pCAG variants, without outliers calculated with a Q coefficient of 5%. The sample time points are marked with symbols. The connection between the points is extrapolated from those to better show the grouping in functioning and non functioning flippases. Error bars and significance levels are left out for visual clarity. Stricter handling of outlier data points does not alter the interpretation.

High significance especially at the end of the measurements, can mainly be seen for the variant ending after exon 28. The fluorescence intensity through incorporated PE is higher compared to all other variants. This in part validates the findings of the elevated, yet not statistically significant, translocation of NBD-PS for the hATP11A variant ending after exon 28, compared to the WT.

6. Discussion

In a family affected by autosomal-dominant progressive, non-syndromic AS/AN, a 5,500 bp deletion at the 3' region of *ATP11A* was identified. It spans the last coding exon of both *ATP11A* isoforms. The phospholipid flippase encoded by ATP11A isoform 1 is an ubiquitously expressed transporter for PS and PE. Together with CDC50A it forms a complex which maintains the phospholipid gradient across the plasma membrane.
In this thesis the deletion was found to result in the usage of an alternative last coding exon 29^{mut}. Since the subcellular localisation of this mutant ATP11A deletion variant did not differ from that of ATP11A isoform 1 WT, the flippase activity was analysed in order to identify a loss or gain of function. Also isoform 2, which is suspected to be an evolutionary remnant due to a lower expression level and less conservation of the last coding exon compared to isoform 1, was found to localise to the plasma membrane. Including isoform 2 in the flippase activity assay allows for a comprehensive evaluation.
In the following chapter the results of this flippase activity assay are interpreted and put into scientific context. Therefore, possible genetic mechanisms leading to hATP11A hypoactivity or loss of function and a phenotype representation for the deletion variant are discussed and compared. Also molecular pathomechanisms are considered on the base of phenotypical, cellular and molecular characteristics of other ATPase loss of function models and studies on ATPase inactivation or the influence of disturbed membrane asymmetry.

6.1. The influence of *ATP11A* exon usage on flippase activity

The flippase activity of different hATP11A-HA variants is tested and compared based on the translocation of fluorescent phospholipids across the plasma membrane. For this purpose the phospholipids NBD-PS and NBD-PE are used, as Takatsu *et al.* [281] previously found that hATP11A Isoform 1 WT only flips PS and PE, but not PC and sphingomyelin (SM). I examined hATP11A-HA Isoform 1 WT, hATP11A-HA Isoform 2 WT, the mutant hATP11A deletion variant and an artificial, truncated variant ending after coding exon 28 and

missing the 29^{th} exon completely, which is the one in that the other variants differ. hATP11A-HA E186Q and hATP11A-HA D414N, which are known loss of function and loss of transport variants respectively, are used as negative control, as well as a transfected mock vector. All of those should only show a basal translocation rate caused by the endogenous hATP11A protein in the HEK293 cells. Additional phospholipid intake via endocytosis is ruled out, since the experiments were performed on ice, where the flippase is still active but endocytosis is blocked [281].

Both in the western blot analysis of whole cell protein or cell surface protein, as well as in the fluorescence measurements of the flippase activity assay, there is a variation among each hATP11A-HA variant. However, the variation found between the fluorescence intensities of the assay is not congruent with the variation found in the intensity of the western blots of whole cell protein or cell surface protein fractions of that specific set of replicates. Consequently, it is not likely that the exact amount of overexpressed hATP11A-HA variant protein influences the NBD-phospholipid intake, as long as there is expressed hATP11A-HA variant protein at all.

Accordingly, the results obtained from the western blots are only used for a rough estimation on *hATP11A*-HA expression and protein transport, but not for quantification in reference to the flippase assay. Nevertheless, despite similar amounts of whole protein, *hATP11A*-HA D414N shows consistently lower levels of expression compared to all other variants in all replicates. In their study on ATPase - CDC50A complexation during transport from the ER, similar findings regarding D414N variants were made by Tone *et al.* [292]. Presumably the D414N variant gets degraded in the ER due to lower stability or disturbed interaction with CDC50A.

It was thought about additional normalisation of the data. Like performed by Takatsu [281], the first way could have been the normalisation on present hATP11A-HA on the cell surface, detected in the cell surface western blots. While this results in reasonable data for variants that are transported to the plasma membrane, it blows the relative NBD-PS intake of less well transported variants, accompanied by the endogeneous intake, out of proportion. In addition, there is no evidence that an overrepresentation of hATP11A above the standard level at the cell surface also increases the incorporation of phospholipids above the standard level. There is the possibility that after reaching the correct phospholipid asymmetry at the membrane the activity of hATP11A is downregulated and the intake stops. That way, the massive overexpression and overrepresentation at the plasma membrane had no impact on phospholipid

intake and the normalisation on it would be misleading. This postulation is affirmed by the fact that the variation of hATP11A-HA overexpression measured in the whole cell protein and cell surface protein fraction western blots is not congruent with the variation of NBD-phospholipid intake.
Without normalisation on cell surface hATP11A-HA the decreased translocation to the plasma membrane of a variant can also be included in the assessment of loss of function, not only the enzymatic activity.
The second way of normalisation could have been on the mock vector's fluorescence intensity as the basal NBD-phospholipid intake of the cells' endogeneous hATP11A. With the standard deviation error for all data, the NBD-phospholipid intake values of some samples with non functioning hATP11A-HA variants was even lower than that of the Mock vector. This would result in normalised values below the artificially created zero activity baseline of the mock vector. Since this way of normalisation would not calculate relative differences between the NBD-PS intake of the different hATP11A-HA variants, the data remains unnormalised.
When interpreting the flippase assay, the fluorescence intensities of transported NBD-PS can be categorized in two groups. The first group consists of hATP11A-HA Isoform 1 E186Q, D414N, Isoform 2 WT and the deletion variant, which all resemble the mock vector's intensity. Due to the lack of transfected *hATP11A*-HA in the mock vector cells, the growing fluorescence intensity through incorporated NBD-PS in these samples must be caused by the endogenous hATP11A in the HEK293T cells. The absence of additional NBD-PS transport was expected for cells transfected with the artificially created hATP11A-HA E186Q loss of function and D414N loss of transport proteins. Equivalent findings for hATP11A E186Q are described by Takatsu *et al.* [281] in their study on phospholipid flippase activities and substrate specificities. The graphs for this thesis' experiments show that cells with hATP11A-HA Isoform 1 D414N have a slightly higher mean fluorescence intensity. This indicates that the loss of transport is not complete, but instead some of the functional flippase is still transported to the plasma membrane. This is not statistically significant, though, and not supported by other literature by now.
Similarly noticeable, but also not statistically significant, is a minimally higher fluorescence intensity of the deletion variant, using exon 29^{mut}, compared to the mock vector. Following only the statistic significance, the mutant protein has to be interpreted as a loss of function variant for PS transport. Nevertheless, the slightly higher fluorescence intensity in addition to the predicted loss of function intolerance for hATP11A by the Genome Aggregation Database, opens the

discussion for an only drastically reduced function instead of a complete loss. The lack of frameshift or stop mutations with an elevated allele frequency in hATP11A indicates that those type of mutations are usually lethal. Therefore, the hypothetical remaining flippase activity of the hATP11A deletion variant would better match this observations and explain the non-lethality. Hence, despite the missing statistical significance, in this thesis the result for the deletion variant is further referred to as hypoactivity or hypofunctionality. This does not rule out a complete loss of function, but takes the pLI score into consideration. All discussion of possible pathomechanisms in this chapter are applicable for both hypoactivity and complete loss of function.

As previously assumed because of the lower mRNA expression rate of *ATP11A* isoform 2 in blood and the lower conservation of exon 29b, the so far untested isoform 2 shows no flippase activity for NBD-PS despite being transported to the plasma membrane. This coincides with the estimation that *hATP11A* isoform 2 WT is probably an evolutionary remnant and not used for phospholipid flipping at the plasma membrane.

The second group contains hATP11A-HA Isoform 1 WT and the artificial variant ending after exon 28. They both reach significantly higher fluorescence intensities compared to that caused by the mock vector's basal NBD-PS transport. The NBD-PS transport of hATP11A-HA Isoform 1 WT seems to reach a plateau after 6 minutes, whereas the variant ending after exon 28 further incorporates NBD-PS into the cell with a steady state. However, since those differences are not significant, no assumptions about the necessity of exon 29a for the inactivation of hATP11A, for example after reaching a certain amount of PS at the plasma membrane or in the cell can be made. Nonetheless, the data reveals that not the loss of exon 29a is the cause for the hypoactivity of the mutant deletion variant, but the new exon 29^{mut}.

Due to a much slower incorporation of NBD-PE, the growth of the fluorescence intensity differs substantially between measurements with NBD-PS and NBD-PE. The slower flippase reaction of PE was already described by Segawa *et al.* [243], who found v_{max} lower for PE compared to PS and an overall higher affinity for PS based on a higher K_m when performing a Michaelis Menten kinetics analysis. Comparing the relative fluorescence intensities of the hATP11A-HA variants, three groups could be differentiated. The first one is build by hATP11A-HA Isoform 1 E186Q, D414N and Isoform 2, which almost shows no incorporation of NBD-PE. This indicates that the basal flippase activity for NBD-PE of the endogenous hATP11A of the HEK293 cells is very low compared to that for NBD-PS, measured previously. The intensities of hATP11A-HA Iso-

form 2 again do not exceed those of the loss of function variants E186Q and D414N. This further supports the hypothesis of *hATP11A* isoform 2 as an evolutionary remnant.

hATP11A-HA Isoform 1 WT and the deletion variant form the second group. For the first part of the experiment their fluorescence intensities resemble those from group 1. Only after 20 minutes it increases significantly above the basal level. It would be interesting to have additional sample time points up to 60 min after NBD-PE treatment for those variants, to see if the intensity further increases. At first glance, the usage of exon 29^{mut} instead of exon 29a does not seem to have the same diminishing impact on PE transport that it has on PS transport. This further supports the hypothesis of a rest activity of the mutant protein instead of a complete loss of function. An explanation for the lack of influence on PE translocation comes to mind when directly comparing the fluorescence intensity levels of the incorporated NBD-PE to those of NBD-PS. The affinity and therefore the translocation efficiency was so low, that over the time of the complete experiment the average levels of fluorescing NBD-PE only reach the level that PS incorporation achieved after 1 minute. It seems that hATP11A is translocating so little NBD-PE overall, that neither the overexpression of *hATP11A* Isoform 1 WT nor the hypofunctionality in the mutant deletion variant does result in fundamental changes of NBD-PE incorporation, which can be maintained e.g. through hATP11C, hATP8A1 and hATP8A2.

Consistent with the fluorescence intensity profile from the incorporation of NBD-PS, the hATP11A-HA variant ending after exon 28 forms a third group in which the intensity increases rapidly from the start and reaches much higher levels compared to all other variants. This supports the previous finding that not the loss of exon 29a is the cause for the hypoactivity of the deletion variant, but the additional exon 29^{mut}. The significant difference in the flippase activity of hATP11A-HA Isoform 1 and the variant ending after exon 28 further indicates that exon 29a is involved in a regulatory mechanism causing some sort of inactivation or downregulation.

Not plausible in the case of the NBD-PE treatment experiments seems the behaviour of the cells transfected with the mock vector. The cells transfected with the mock vector have fluorescence intensities above the hATP11A-HA Isoform 1 WT and deletion variant cells. This would either imply additional NBD-PE incorporation in the mock vector cells other than the endogenous activity or downregulation of the endogenous hATP11A activity in all other cells except for the ones transfected with the plasmid hATP11A-HA until ex28 pCAG. Both explanations are not likely and since the mock vector transfected cells are the

same as used for the NBD-PS experiments, the cells themselves can not be the cause. The NBD-PE solution was made fresh for every experiment and the same batch was used for all hATP11A-HA variants within one experimental line. Thus, incorrect mixed NBD-PE solutions would have affected all variants similarly and the discrepancies would most likely been identified as outliers. With an Q coefficient of 1% this is not the case. Only the value for the 20 min sample decreases slightly below the intensities of hATP11A-HA Isoform 1 WT and the deletion variant. The same is true for a Q coefficient raised to 5%, see figure 5.16. Here the value for 20 min decreases to the level of the not incorporating group 1, where it would be suspected, but the other time points still seem to have raised intensities. Considering the low incorporation rate of PE compared to PS, the differences between the mock vector cells and the overexpressed hATP11A variants might rather stem from the combination of low intensities, in particular at the earlier time points, and the low amount of samples per time point, resulting in deceptive low standard derivation. Overall the flippase activity measurements for NBD-PE are not perfectly conclusive. Replication of the experiments with NBD-PE and the addition of later sample taking time points are necessary to confirm these tendencies and assumptions.
Taken together, the assay shows several significant observations about ATP11A's flippase activity and the role of its last coding exon.
(i) The experiments confirm a higher flippase activity of hATP11A for NBD-PS compared to NBD-PE.
(ii) Cells transfected with hATP11A-HA Isoform 2 do not exhibit flippase activity exceeding the basal activity of the endogenous protein. This suggests *hATP11A* isoform 2 to be an evolutionary artefact, which is not used for phospholipid flipping at the plasma membrane.
(iii) The mutant deletion variant of hATP11A-HA does show almost no flippase activity. A slight elevation of fluorescence levels above the basal translocation in addition to the predicted loss of function intolerance indicates that the replacement of exon 29a with exon 29^{mut} results in hypoactivity of the protein.
(iv) The hATP11A-HA variant ending after exon 28 is overly active. The missing exon 29a seems to have some regulatory function, that affects the flippase activity through downregulation or inactivation.
Since PS plays a very important role in many cellular functions, it is possible that the substantial reduction or loss of flippase activity caused by the 5,500 bp deletion in the 3'-region of *ATP11A* is the reason for the hearing loss. Plausible ways in which the deletion could result in hypofunctionality and in which this may inflict auditory function need to be discussed further.

6.2. Discussion of possible C-terminal regulation of hATP11A activity

The deletion in *ATP11A* analysed in this thesis is the first described mutation in a coding region of a gene causing dominantly inherited, non-syndromic AS/AN. To date there is only a single other report of dominantly inherited AS/AN in one family caused by a heterozygous mutation in the gene *DIAPH3* [114, 238]. In *DIAPH3* the mutation occurs in a highly conserved part of the 5'UTR (c.-172G>A). This interrupts a GC box element consensus sequence for transcription factor binding. Consequently the gen expression of *DIAPH3* is increased, so the mutation potentially alters the transctiptional regulation and leads to gain of function. The overexpression of *DIAPH3* has been shown to reduce sound-evoced potentials in Drosophila [238] as well as induce hearing loss and stereocilia defects in mice [239].
In contrast the 5,500 bp deletion in *ATP11A* is not located in a transcription regulatory region, but directly influences the splicing pattern of *hATP11A*. The mutation does not lead to nonsense-mediated mRNA decay. Instead it alters the protein structure of hATP11A in a way that the last exon is replaced by an artificial new exon trough aberrant splicing. As discussed, the altered protein loses flippase function at least for one of its two substrates, namely PS. Experiments with a *hATP11A* variant only missing the last exon without the addition of the exon 29^{mut} showed that the reduced functionality does not occur due to the missing exon 29a, but is caused by the new exon 29^{mut}. The flippase activity for the variant ending after exon 28 was elevated even higher than the one of hATP11A Isoform 1 WT for both PS and PE. The question arising from this is why the missing exon has such an effect on flippase activity and how the artificial exon can lead to at least partial loss of function.

6.2.1. C-terminal targeting signals

Exon 29a of *hATP11A* Isoform 1 WT contains 75 bp before the stop codon. This translates to 25 amino acids. The whole exon 29a gets translated to a part of the 41 amino acid stretching cytoplasmic C-terminus. which does not code for any catalytic core domains, but might inhibit a regulatory unit. On top, there are some indications for C-terminal regions with targeting function in ATPases.
The amino acid sequences of ATP9A and ATP9B have a 75% similarity. While both localise to the TGN, ATP9A additionally localises to endosomes. When the N-terminal cytoplasmic region of ATP9A is replaced with the diverging N-

terminal cytoplasmic region of ATP9B the localisation changed and the chimeric protein also was localised exclusively at the TGN. This indicates a Golgi targeting signal at the N-terminus [280]. Most known targeting signals determining the localisation of mammalian proteins are at the N-terminus [57], but there are some exceptions [168]. In theory such a targeting signal for the plasma membrane could be coded in the deleted hATP11A exon 29a or in the aberrant exon 29^{mut}, resulting in abnormal localisation and consequently, loss of the original function. ICC staining, cell surface protein western blotting and finally the flippase activity assay of hATP11A ending after exon 28 and the deletion variant performed in this thesis speak against this hypothesis of a targeting signal in the missing exon. For both variants the protein is still transported to the plasma membrane at least in HEK cell culture.

Recently Takayama *et al.* [283] found that the three C-terminal splice variants of ATP11C differ in their localisation. The variant called ATP11C-b localises to a specific region of the plasma membrane in polarised cells, whereas ATP11C-a and ATP11C-c are distributed on the entire membrane in polarised and non-polarised cells. They found the C-terminal residue sequenz LLXYKH in ATP11C-b to be the responsible targeting signal. In some tissues ATP11C loss can be compensated by ATP11A, due to their similar protein sequence [243]. The amino acid sequence between the two human ATPases begin to differ after their 28th exon, the same place the splicing of the isoform variants takes place. Exon 29a of hATP11A isoform 1 has a high similarity to the last exon of hATP11C-c (isoform 4), making hATP11A isoform 1 and hATP11C-c corresponding isoforms (see figure 6.1). Exon 29b of hATP11A isoform 2 has no matching exon in hATP11C. Also the targeting signal LLXYKH has no corresponding residues in hATP11A isoforms or the deletion variant. Therefore, this finding has no direct indication for abnormal hATP11A transport. Rather the conclusion would be that hATP11A isoform 1 should also be distributed in the entire plasma membrane irregardless of the polarisation of the cell and that HEK293 cells are a suitable test system. Nonetheless, it slightly raises the likelihood of another so far unknown localisation site working in similar ways at the natural or aberrant hATP11A C-terminus. Transport that is only altered in polarised cells would not have been detected in HEK cell culture transfected with the hATP11A deletion variant, but could disturb hATP11A localisation at the plasma membrane of polarised IHCs in the patient.

Localisation studies performed with chimeric proteins showed that the N-terminal region of hATP10B proteins and the C-terminal region of hATP11B contain localisation sites important for intracellular trafficking to the endosomes,

```
ATP11A isoform 1    TKSQCLSVEQSTIFMLSQTSSSLSF----      25
ATP11C-c            VTKRLPSSGTSAIFMLSQTSSNHSFSWSE      29
                    ...:  *   *:*********. **
```

Figure 6.1.: Alignment of the protein sequence of hATP11A isoform 1 exon 29a and hATP11C3 isoform 4 exon 29 (www.clustal.org/omega)

while flippase activity and phospholipid specificity were not affected. When the terminal regions were expressed as peptides they distributed in the cytosol, so no direct interaction with the endosomal membranes are happening to establish the localisation. In contrast, fusing those terminal regions to Lyn11-EFFP-FRB, a protein that is usually localised at the plasma membrane, results in translocation to intracellular endosomal compartments, while fusion with the other terminal regions of hATP10 and hATP11 proteins did not change the localisation. This suggests that the N-terminus of hATP10B and the C-terminus of hATP11B contain the endosomal targeting signal responsible for their specific protein localisation. The assumed targeting signal in the hATP10B is the ETTPLL sequence that is similar to the di-leucine motif [DE]XXXL[LI]. The di-leucine motif is a typical sorting motif in intracellular trafficking of transmembrane proteins. The replacement of the Leucine residues with Arginine in fusion proteins resulted in abnormal localisation to the plasma membrane [175]. A similar targeting mechanism using a C-terminal di-leucine motif, which can be switched on and of by phosphorylation is present in hATP11C. Here the change of localisation to endosomal structures is used as a regulatory mechanism to induce the loss of flippase activity at the plasma membrane. A more detailed explanation follows in the next section on C-terminal regulatory mechanisms. Taken together, the reported relocation of proteins with mutated di-leucine motif and the finding of this thesis, that all C-terminally altered hATP11A variants are still transported to the plasma membrane, indicate that at least in the last 25 amino acids of hATP11A there is no alternative targeting mechanism. The localisation to the plasma membrane is the default if it is not overwritten by the endosome targeting signal as happening in hATP11B.

6.2.2. C-terminal regulatory domain mechanisms

There is a great variety in the regulatory mechanisms of P4-ATPasen. A thing a lot of them have in common is the location of the responsible domain in the cytosolic C-terminus of the protein.
In plant H^+ pumps there is a C-terminal regulatory domain of about 100 amino

acids [206, 184, 247]. The phosphorylation and dephosphorylation of an included threonine residue is used to regulate the ATPase activity. The unphosphorylated domain is thought to interact with an inhibitory site in the cytoplasmic domains, thus inactivating the protein [186]. Another C-terminal regulatory domain is present in yeast H^+ pumps. The domain is about 40 amino acids long and has little homology to the one in plants. It is suspected to interact with a different inhibitory site, since the reaction on adding synthetic domain peptide is directly opposed [184, 119]. The ATPase gets activated by the phosphorylation of serine and/or threonine [75]. While the mutation of the yeast phosphorylation residues renders the ATPase inactive, the complete deletion of the regulatory domain locks the protein in a constitutional active state in yeast as well as plants [189, 207, 247, 206]. However, there is no sequence similarity between the C-terminus of hATP11A and the plant or yeast H+ pump.

Another case of C-terminal regulation in P-ATPases is known from plasma membrane Ca^{2+} pumps. In human plasma membrane Ca^{2+} pumps the regulatory C-terminus varies between the different isoforms, while their catalytic unit remains similar. This leads to different affinities and thus inhibition / activation intensities [200]. The phosphorylation of the inhibitory region of Ca^{2+} pumps with protein kinase C was found to add to their activation with calmodulin, but has only little effect on its own [311].

Despite this minor role in Ca^{2+} pumps and the fact that there is no sequence similarity to a calmodulin-binding site or the PDZ domain binding site in the hATP11A C-terminus, a phosphorylation dependent autoinhibitory C-terminus could be a main regulatory domain in hATP11A, like it is in H^+ pumps of plant and yeast. Presuming this would be the case, the results of the flippase activity assay could be well described in the boundaries of the inhibition model. In WT hATP11A the flippase activity could be regulated via the phosphorylation of the C-terminus. Phosphorylation prediction performed with the NetPhos 3.1 Server of the Technical University of Denmark [19], shown in figure 6.2, reveals several possible phosphorylation sites at the ATP11A isoform 1 C-terminus. Of those predicted sites five residues are possible interaction sites for protein kinase C, which is responsible for the phosphorylation of the Ca^{2+} pumps' inhibitory region. Nevertheless, as also the activation through phosphorylation is supposed to work through steric hindrance of the binding of the inhibitory site and the catalytic core, the phosphorylation with any other kinase could probably have the same activating effect.

As described before, the loss of 25 of the 41 amino acids of the C-terminus in the variant of hATP11A ending after exon 28 leads to an overactive protein.

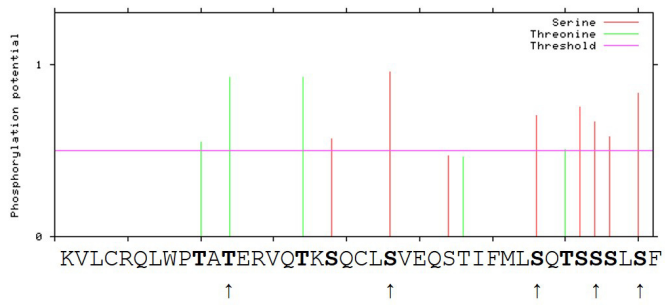

Figure 6.2.: Pediction of phosphorylation sites in the hATP11A isoform 1 C-terminus performed with the NetPhos 3.1 Server of the Technical University of Denmark [19]. Serine and threonine residues with phosphorylation probabilities above the prediction threshold are printed in bold letters. Phosphorylation sites with possible protein kinase C interaction are marked with arrows.

Without an inhibitory domain binding to the catalytic core the flippase would be permanently activated. In the case of the deletion variant of hATP11A ending with exon 29^{mut} it can be hypothesised that the altered sequence is still able to perform the inhibitory interaction with the catalytic core, but the activation through phosphorylation does not take place. That way the flippase would be permanently inactive. Looking at the predicted phosphorylation sites of exon 29^{mut} in figure 6.3 it is noticeable that the altered sequence lacks the multitude of phosphorylation sites at the downstream end. In the upstream part of the C-terminus, the first two threonine sites coded in exon 28 stay the same. Afterwards only one serine and one threonine phosphorylation site are predicted, of which only the latter is associated with protein kinase C. This fits to the assumption that phosphorylation of the presumed inhibitory region is absent or at least diminished.

In contrast to the broad knowledge upon ion flipping P4-ATPases, the regulation mechanisms of phospholipid flipping P4-ATPases remained unclear until recently. Mechanisms were discovered for the yeast flippase Drs2p, hATP11C and hATP8A1. In yeast the PS and PE flipping Drs2p forms a heterodimeric complex with Cdc50p, which is in an autoinhibited state when no activator is present. The activation is triggered by phosphatidylinpsitol-4-phosphate (PI4P) [167, 290]. The C-terminal inhibitory domain of Drs2p acts in compliance with the model of the catalytic cycle of the human P4-ATPases described in section 1.5.6, only here the interaction of the catalytic core and the regulatory C-terminus is inhibitory rather than activating (see fig. 6.4).

It fills a groove between the N-domain and the A- and P-domain, interacting

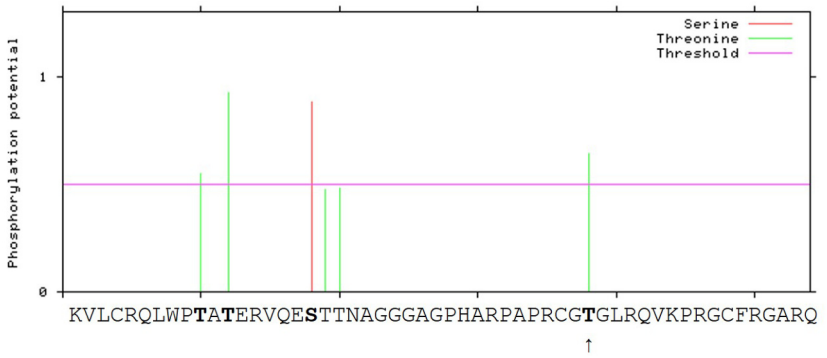

Figure 6.3.: Pediction of phosphorylation sites in the hATP11A deletion variant with exon 29^{mut} performed with the NetPhos 3.1 Server of the Technical University of Denmark [19]. Serine and threonine residues with phosphorylation probabilities above the prediction threshold are printed in bold letters. Phosphorylation sites with possible protein kinase C interaction are marked with arrows.

with all three. This interaction stabilises the conformational state and inhibits ATP binding. Also the forced distance between the N-domain and the P-domain prevents phosphorylation of the P-domain. [10, 339]. In Drs2p the N-terminal region has an additional regulatory effect. It forms hydrophobic interactions with the A-domain that are suspected to cause a small inhibition.

Through the binding of PI4P to a positively charged region of the transmembrane domain, a proximal helix switch upstream of the inhibitory domain is twisted 90 ° and thus the inhibitory peptide disengages from the catalytic core domains. This results in further conformational changes, the PI4P is released and the catalytic cycle is activated [10].

A recent study by Takatsu *et al.* [282] found that the human phospholipid flippase hATP11C is endocytosed upon Ca^{2+}-dependent protein kinase C activation. The phosphorylation of the C-terminal Ser1116 creates a functional di-leucine motif, that is used as a signal for endocytosis of hATP11C into early endosomes and recycling endosomes. This decreases the flipping of PS at the plasma membrane and to a lesser extend also the flipping of PE. The minor influence on PE translocation of loss of hATP11C inactivation in their study and hypoactivity of hATP11A in this thesis indicates that those two P4-ATPases are either no essential flippases for PE distribution across the plasma membrane and the translocation is compensated by ATP8A1 and ATP8A2 or the affinity for PE is generally that low that only little PE gets translocated and no significant effect can be noticed through loss of their ATPase activity. Nevertheless,

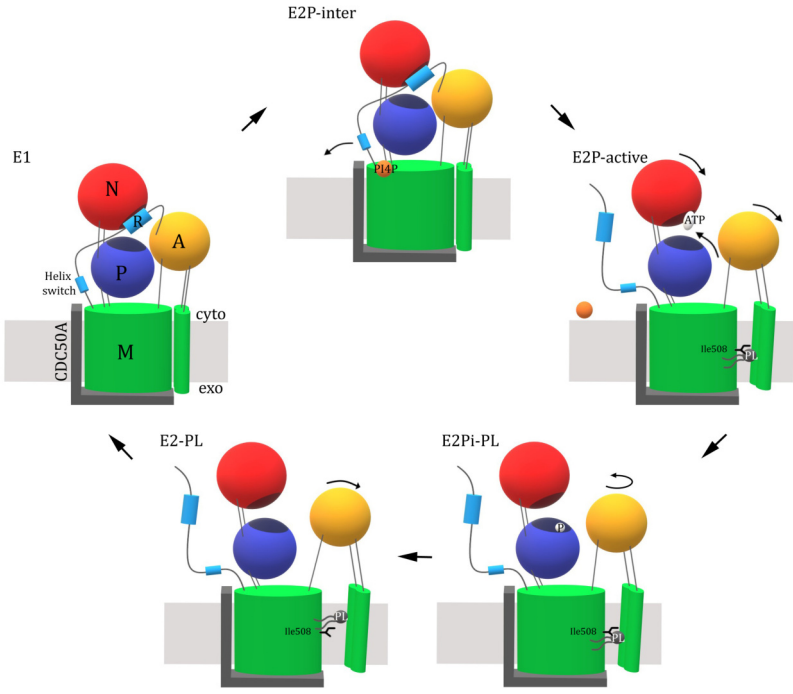

Figure 6.4.: Schematic model of the catalytic cycle of the complex Drs2p-CDC50A [10, 290]. The color scheme is inherited from that of figure 1.10. E1: Starting state, the C-terminal R-domain (light blue) wraps around the catalyic core domains (red, blue and yellow) and block the ATP binding site with an inhibitory peptide. E2P-inter: Intermediate state, PI4P (orange) binds to a positively charged pocket in the transmembrane region and activates the flippase. E2P-active: The helix switch (light blue) rotates 90 ° away from the cytosolic domains and thus disengages the inhibitory peptide. The core domains rotate, enable targeting of the ATP binding site and open a hydrophobic cleft. The phospholipid enters and is blocked by Ile508. PI4P diffuses away. E2Pi-PL: The phosphorylation site of the P-domain (blue) gets phosphorylated, the A-domain (yellow) turns further. E2-PL: Further movement of the A-domain results in an open hydrophobic cleft. The phospholipid passes the Ile508 blocking and can be transported to the cytoplasmic leaflet. Afterwards the flippase shifts back to the E1 starting state.

the permanent activation of hATP11A through the deletion of the inhibitory domain in the variant ending after exon 28, enables such a gain in phospholipid flipping activity that not only PS, but also PE translocation increases significantly.

However, the deactivating reaction to phosphorylation of the C-terminus in hATP11C is directly opposed to the activation of the human plasma mem-

brane Ca^{2+} pumps. Due to the high sequence similarity between hATP11A and hATP11C it could be assumed that the same internalisation would happen for hATP11A. In contrast, Takatsu *et al.* showed an increased surface level of hATP11A upon protein kinase C activation with PMA treatment. Although ATP11A also has a C-terminal sequence that could be interpreted as similar to the di-leucine motif, it apparently is no sufficient signal for endocytosis upon protein kinase C activation. The alignment of the C-terminal regions of hATP11A and hATP11C used by Takatsu *et al.* is performed with EMBOSS Needle [222]. A similar structure of alignment is received by only a few of the sequence alignment tools provided on the homepage of EMBL-EBI. The other do not interpret the residues STIFML of hATP11A as similar to the SVRPLL di-leucine motif of hATP11C (see different alignments in figure 6.5). While the SVRPLL sequence of hATP11C can be phosphorylated to mimic a typical [DE]XXXL[LI] di-leucine motif of transmembrane proteins, the phosphorylated STIFML sequence of hATP11A still lacks the first of the two leucine residues, that was found to be essential for endocytosis induction [282].

```
EMBOS Needle:
hATP11A       ------------KVLCRQLWPTATERVQTKSQCLSVEQSTIFMLSQTSSSLSF--
hATP11C       VLKNVRRRSARRNLSCRR-----------ASDSLSARPSVRPLLLRTFSDESNVL
                           :: **:            *:.**.. *.  :* :* *. *

T-Coffee:
hATP11A       KVLC--RQLWPTATERVQTKSQCLSVEQSTIFMLSQTSSSLS--F
hATP11C       V-LKNVRRRSARRNLSCRRASDSLSARPSVRPLLLRTFSDESNVL
                *   *:  .  .   :  *:.**.. *.  :* :* *. *  :
Clustal Omega:
hATP11A       ------------KVLCRQLWPTATERVQTKSQCLSVEQSTIFMLSQTSSSLSF
hATP11C       VLKNVRRRSARRNLSCRRASDSLSARPSVRPLL-------LRTFSDESNVL--
                           :: **:   : : * ..:          :  :*: *. *
```

Figure 6.5.: Protein sequence alignments of the hATP11A and hATP11C C-terminus performed with different EMBL-EBI alignment tools [138]. EMBOSS Needle [222] (as done by Takatsu *et al.* [282]), T-Coffee and Clustal Omega were used. The supposed di-leucine motif is marked in bold letters.

During the cryo electron microscopic research on the catalytic cycle of P4-ATPases the C-terminal regulatory mechanism of human ATP8A1 was discovered to be yet different from those described above [97]. While the main mechanism is still sterical hindrance through interaction between the catalytic core and the C-terminal regulatory domain, there seems to be no PI4P and no phosphorylation involved. The hATP8A1 regulatory domain consists of a conserved GYAFS motif and a short helical domain (SQSEVIR). The phenylalanine (F) of the GYAFS motif is recognised by a loop region in the N-domain and stacks there with another phenylalanine of the ATP-binding site. That way the E2P

state is stabilised and the N- and A-domain are kept apart. In accordance to the findings for hATP8A1, Chalat *et al.* [30] showed that hATP8A2 mutants with a C-terminus truncated by 33 amino acids including the GYAFS motif and the short helical domain have a reduced flippase activity, while mutants with a deletion of the complete C-terminus exhibit no change in activity. They propose that there is an autoinhibitory domain upstream of the 33 residues, which is suppressed by an anti-autoinhibitory domain at the exteme C-terminal end of the protein. Hiraizumi *et al.* [97] suspect that the GYAFS motif and the short helical domain could positively regulate the activity by keeping the N-domain and the A-domain apart and thus enabling the rotation of the A-domain for both hATP8A1 and hATP8A2. This combination of an autoinhibitory and an anti-autoinhibitory domain would be a newly discovered mechanism that was never described before for another P-ATPase.

There are several factors eliminating the possibility of this regulatory mechanism for hATP11A. While the phenylalanine of the ATP-binding site is conserved among hATP11A and hATP11C, the C-terminal region of those two P4-ATPases are shorter than that of hATP8A1, so the GYAFS motif and the short helical domain are missing. Also, when the extreme end of the C-terminus, coded by exon 29a, is deleted in the experimental procedure of this thesis, the protein is still active. For this reason not only an anti-inhibitory domain but also a potential autoinhibitory domain had to be coded upstream of the splice site. Accordingly, when exon 29a is replaced by exon 29^{mut} in the deletion variant, both the autoinhibitory and the anti-autoinhibitory domain potentially corresponding to the GYAFS motif would still be missing and the flippase should remain active. Since the experiments show a reduced activity for the deletion variant, a similar combination of two counteracting domains can not be the underlying mechanism for hATP11A, excluded the case in which the WT exon contains a substitute for the GYAFS motif and the aberrant exon itself coincidentally contains another autoinhibitory domain.

It would be more reasonable to suspect a mechanism similar to that proposed for Drs2p (see fig. 6.4). In this hypothesis the aberrant C-terminal region of the deletion variant would still be able to fold between the P- and N-domain to some extend. Thus the phospholipid flipping activity is blocked. Yet, the equivalent to the helix switch motif of the WT protein that would be necessary for activation could be missing. A comparison of the C-terminal protein sequences of Drs2p and hATP11A does align the helix switch motif with a amino acid sequence of the deleted exon 29. Even though the medium sequence similarity does not immediately indicate an identical switch domain for hATP11A, a sim-

ilar mechanism could be possible. This way the alternative C-terminus would lead to permanently decreased activity.
However, the cytoplasmic C-terminal region of hATP11A is with 41 amino acids a lot shorter than for example that of Drs2p with 135 amino acids. Considering that the inhibition is suspected to work through steric hindrance of some kind, the strength of the inhibition could also be purely dependent on the length of the C-terminal region. Following this hypothesis the relatively short 41 amino acid terminus of hATP11A dampens the flippase activity, but does not prevent phospholipid translocation completely. The usage of exon 29^{mut} instead of exon 29a, which elongates the usually 41 amino acid long cytoplasmic C-terminal region to 54 amino acids, could strengthen the inhibitory interaction with the catalytic core domains and thus deactivate the protein stronger compared to the wild type.
Both mechanisms have in common, that upon truncation of the complete exon 29a without replacement, the remaining part of the C-terminus is probably to short to still interact with the catalytic domains and the activity is restored.
So in summary, all four P4-ATPases hATP8A1, hATP8A2, hATP11A and hATP11C that have a substrate specificity for PS and PE share a very conserved amino acid sequence for the greatest part of the protein. Yet their N- and C-terminal regions, including the regulatory domains, differ substantially and their activity seems to be regulated by different mechanisms. Both hATP8A1 and hATP8A2 are known to be positively modulated by the GYAFS motif, which suppresses a supposed autoinhibitory domain, that is thought to work like the autoinhibitory domain of ion transporting P4-ATPases through steric inhibition of the ATP or phospholipid binding at the catalytic core. In contrast hATP11C is negatively modulated by its C-terminal di-leucine motif. Upon phosphorylation it acts as a targeting signal for endosomal transport and retention.
It can be assumed that the C-terminal region of hATP11A also harbors a regulatory domain. The way of achieving the regulation and the resulting reaction that inhibits or enables phopholipid flipping could possibly be still different from the other human P4-ATPases displayed above, since the required motifs from hATP11C and hATP8A1/2 are missing in hATP11A. As speculated, the most suitable hypothesis seems to be a mechanism similar to the one of yeast Drs2p flippase, shown in figure 6.4, or a simple steric inhibition regulated via the length of the C-terminal region. This multitude of different regulation approaches could have been emerged from the need of the cell to prevent PS exposure on the cell surface in non apoptotic cells.

A similar assumption is made by Segawa *et al.* [243] in their work on the cleavage of hATP11A and hATP11C by caspases and subsequent PS exposure by scramblases in apoptotic cells. Despite hATP11C having a higher PS and PE flipping activity compared to hATP11A, in most tissues both are expressed and in a lot of them hATP11A even is the preferred one. Only in the liver there is mainly hATP11C present. While hCDC50A deficient cells lose the ability to flip PS and PE almost completely and expose PS on the cell surface, hATP11C deficient cells still have enough flippase activity to maintain plasma membrane asymmetry, probably through compensation by hATP11A [242]. So in non apoptotic cells expressing both hATP11A and hATP11C one active form is enough to avoid PS exposure.
During the activation of some cell types the intracellular Ca^{2+} level at the plasma membrane can transiently rise up to more than 100 µmol [141, 223, 147]. This would be enough to activate phospholipid scramblases and at least reduce flippase activity [18]. Would the inactivation of hATP11A through Ca^{2+} induced protein kinase C work the same way and would be similar efficient as the inactivation of hATP11C, the activation of the cells would lead to PS exposure, apoptosis and engulfment by phagocytes. Only if a single regulatory mechanism just results in the incomplete inactivation of flippase activity, the survival of the cell can be assured and PS and PE can be translocated back into the inner leaflet once the Ca^{2+} level reaches normal concentrations.

6.3. Discussion of a molecular pathomechanism

The assay results showed that the deletion variant of hATP11A, in which the exon 29a is replaced by exon 29_{mut}, is hypoactive regarding the intake of PS at the plasma membrane. Since hATP11A is present almost ubiquitously and the plasma membrane asymmetry is essential throughout the whole body, it has to be addressed why a heterozygous substantial reduction of hATP11A's PS flipping activity can cause hearing loss, but has no visible effect in other organs and tissues.
Here, findings from other ATPase defects and studies on the role of PS and other phospholipids in the plasma membrane can be used for a detailed analysis of possible molecular pathomechanisms.
It has been demonstrated that *ATP11C* loss does not lead to PS exposure on the cell surface, while the loss of *CDC50A* does. The missing flippase activity probably gets compensated by ATP11A in some tissue [243, 282]. This might be true the other way round, too. Andersen *et al.* [2] suggests that some cells

can compensate with other P4-ATPases while others can't. The knockout of *ATP8A1* in mice for example has only impact on hippocampal neurons but not on erythrocytes, where *ATP8A2* is believed to compensate for the loss [131]. Knockout mutant mice producing no ATP11C show defects only in erythrocytes, hepatocytes and B-cell progenitor cells, which are cell types that do not express compensating ATP11A [145, 41, 244]. With compensation by ATP11C a heterozygous hypoactivity of ATP11A might not lead to an altered membrane composition in most tissues. Though, there is the possibility that this is not true for the inner ear. Perhaps there is no or less ATP11C in some inner ear cells to compensate a decreased ATP11A flippase function in general, due to transient expression patterns during development or due to inactivation in certain cellular processes. This could lead to locally restricted disturbance of the usual membrane asymmetry and PS exposure on the cell surface. However, this is not described yet. It would be needed to check this hypothesis with stainings of the inner ear. Preferentially cross sections of healthy cells could be compared to those with the deletion variant of hATP11A, for example in a mouse model. In the following sections I discuss scenarios in which a lack of compensatory flippase activity seems plausible and examine cellular processes in which the diminished hATP11A function could influence the hearing ability.

6.3.1. Cell shape and stability

As described in section 1.1 on anatomy and functioning of the auditory system, the shape and stability of hair cells and supporter cells is of great importance for mechanotransduction in the hearing process.
A possible reason for hearing loss could therefore be deformation of the hair cells due to general stability loss by the potentially altered membrane composition. In red cell mebrane it was shown that PS in the cytosolic leaflet interacts with actin filaments to strengthen the cytoskeleton and membrane stability [140]. The influence of the membrane composition on stability is also believed to be the reason for the BRIC phenotype induced by loss of ATP8B1 function, mentioned in section 1.5.7 [194]. If for example the stability of hair cell stereocilia is compromised, they might not withstand the mechanical stress during signal transduction for long.
Studies also showed that an disturbed phospholipid asymmetry at the plasma membrane is able to interfere with phosphatidylinositol generation [91, 251], which itself is important for mechanotransduction and maintainance of stereocilia bundles [74, 98].
In addition, the cell shape can be influenced by the phospholipid composition of

the plasma membrane. The bilayer couple hypothesis says that a local imbalance of the number of phospholipids in one leaflet of a lipid bilayer compared to the opposite leaflet will produce an expansion of that leaflet area. In order to minimise its energy state and to maintain the hydrophobic interaction between the leaflets, the bilayer has to bend [248]. Several experimental approaches with phospholipids show this effect on membrane curvature [45]. Focusing on the role of ATPases in this, mutations in mice *Atp11c* have been shown to alter the morphology of erythrocytes [330]. The exogenous expression of *hATP10A* in HeLa cells causes elevated PC transport to the cytosolic leaflet, which results in a strong inward bending of the plasma membrane, subsequent changes in cell shape, decreased cell size and inhibited focal adhesion [152, 163]. This extended bending could not be detected for cells expressing the loss of function mutant *hATP10A* E203Q or the PS / PE flippase *hATP11A* [278]. The fact that overexpression of *hATP11A* does not lead to extended membrane bending in HeLa cells has been explained with the limited amount of PS and PE in the exoplasmic leaflet, which prevents an extreme imbalance of lipid mass between the layers [278]. Consistently, artificial sequestration of PS in the cytosolic leaflet of HeLa cells also caused bending and inhibited cell spreading and focal adhesion, so the previous lack of bending indeed has to be caused by missing overtransport to the cytosolic leaflet or the additional transport back to the exoplasmic leaflet [152]. However, in contrast to overexpression, a lowered amount of ATP11A could effect the cell negatively. For example did the addition of PS to the exoplasmic leaflet of erythrocytes induce outward membrane bending, which could be normalised by translocation to the cytosolic leaflet [245].

At the cytosolic leaflet PS is thought to not only interact with cytoskeletal proteins, but to be essential for Rac1 [66] and Cdc42 [62] signalling pathways, which are both important regulators of cell motility and polarity among others. Translocating the necessary PS to the exoplasmic leaflet could disturb the signalling and thus influence the cell shape.

Altered cell shapes of hair cells and supporting cells could have fatal consequences on hearing. The distance between hair cell stereocilia bundels and the tectorial membrane is delicate and essential for correct signal transduction. Do hair cells not reach the tectorial membrane due to changed membrane bending, no action potential can be evoked and the signal gets lost. Additionally most of the supporting cells have a distinct pillar shape to held the hair cells in their place. Alterations in their shape might have a similar effect, as the importance for correctly developed supporting cells was shown in a caspase-deficit mouse model [279].

Therefore, the balanced phospholipid transport provided by PS flippases, such as hATP11A, seems to be essential for the cell shape, mechanical stability and maintainance by influencing the intensity of membrane curvature [78], interaction with the cytoskeleton, signalling proteins and phosphatidylinositol generation.

6.3.2. Disturbed endo- and exocytosis

Following studies also display an effect of phospholipid flippase activity on exo- and endocytosis, consistent with P4-ATPase function in yeast [241] and findings of disturbed intracellular vesicular transport upon loss of endosomal ATPase function, discussed later [340]. The sole presence of PS in the cytosolic leaflet is not sufficient, but flippase activity for PS or PE is needed to generate a phospholipid abundance in the cytosolic leaflet in order to enable endocytosis, presumably due to its effect on membrane curvature. The importance of flippase activity is also emphasised by the finding that in yeast the depletion of cells of PS through knockout of the PS synthase *cho1* does not inhibit endocytosis, while the double knockout of *cho1* and *cdc50a*, needed for the flippase complex, did [284]. It has often been observed that PS flipping is necessary for the recuitment of membrane fission and vesicle forming proteins. Examples of this and other ways in which flippase activity in different cell types affects endocytosis and vesicular trafficking are summarised in a commentary by Panatala *et al.* [190]. However, the theory that the flippase complex directly interacts with components of the vesicle forming machinery, seems to be false. Proteins of the vesicle forming machinery have been observed to efficiently assemble on TGN membranes of a yeast *drs2* deletion strain, but were not sufficient to induce membrane bending needed for vesicle budding in the absence of Drs2 [135, 31]. The finding that the incorporation of additional exogenous PS and PE to the cytosolic leaflet of human K562 cells enhances endocytosis, while the additional incorporation of phospholipids that stay in the exoplasmic leaflet inhibits it, rather support the assumption that these effects are based on changes in membrane curvature [63].
In dissected organ of Corti, apparently healthy hair cells show PS externalisation and blebbing at the apical plasma membrane, which did not result in apoptosis, whereas induced apoptosis resulted in PS exposure on the entire surface of those cells [251, 250]. The exposure of PS could not be inhibited with adding caspase inhibitors, nor did the morphology change to apoptotic features, so it can be assumed that the regional exposure of PS has another reason that inducement of phagocytosis. Instead PS exposure was further induced in the hair cells with

increasing the level of Na^+ or cAMP. It is believed by Shi *et al.* [251] that the elevated level of cAMP, induced by Na^+ influx, increases the exocytosis rate or inhibits flippase activity, resulting in exposed PS, as the regulation of exocytosis by cAMP has been reported previously [82]. Alternatively they discuss that elevated Na^+ levels could result in an overactive Na^+ / Ka^+-ATPases, which diminishes ATP levels needed for PS-ATPase function. Both hypothesis have in common that due to the high exocytosis rate at the apical membrane of hair cells and the resulting rapid membrane turnover [246, 81, 80], PS-ATPases might not keep up against the physiological externalisation [251]. This reported blebbing, interpreted to be a form of elevated exocytosis as a result of PS externalisation, fits to the findings on the influence of membrane curvature on endo- and exocytosis and its connection to PS localisation in the plasma membrane.

Small changes in membrane curvature through impaired hATP11A function might be enough to have an influence on hearing through altered endo- and exocytosis. In healthy cells exo- and endocytosis happens at a much higher rate in IHCs compared to OHCs [81, 80]. This could indicate why the patients phenotype represents with AS/AN rather than cochlear hearing loss. Also especially at the synaptic ribbon of the inner hair cells a well coordinated balance of exo- and endocytosis is essential. For the fine tuned hearing process the precise timed and ultra fast release of high rates of glutamate and other synaptic proteins upon activation is provided there. At the same time, fast clearance of the release site, as well as compensatory membrane building, vesicular recycling and vesicle pool replenishment are needed to maintain the process. As described in section 1.3.2, a problem with this is also the underlying reason for AS/AN caused by OTOF loss of function [150]. An imbalance at one of those sites might lead to impaired signal transduction and could subsequently result in slow but progressive loss of hair cells and spiral ganglion neurons [121, 270, 8, 230]. However, the process of exo- and endocytosis at the inner hair cells' apical membrane and synaptic ribbon is not yet fully understood [191], but it can be presumed that PS dependent membrane curvature plays a vital role as it seems to do in other cell types.

6.3.3. Activation of apoptosis

The well regulated inactivation of flippases through caspases, mentioned previously in section 1.5.7, is important for selective apoptosis. Both ubiquitinously expressed plasma membrane ATPases *ATP11A* and *ATP11C* contain caspase-3 cleavage sites, which are cleaved during apoptosis to inactivate them [242, 243].

The deactivation alone is not sufficient to continue with apoptosis, when only the Ca^{2+}dependent TMEM16F scramblase of healthy cells is active. Only the activation of the additional scramblase Xkr8 by caspase-3 enables further transport of PS to the exoplasmic leaflet. Without counteraction of the deactivated ATPases, the retention of PS in the cytosolic leaflet can not be maintained and PS is exposed on the cell surface [277]. The exposed PS now acts as a scaffold for proteins linking the apoptotic cell to macrophages for subsequent engulfment, the so-called efferocytosis. There are several proteins involved in this linking and their expression and usage is seemingly tissue specific [162]. One of them, MFG-E8, contains a RGD motif which can bind to macrophages and links it to PS via its factor VIII-hologous domains [88]. Another, the TIM4 receptor, is expressed in various resident macrophages and binds to PS via an IgG domain [288]. Experiments indicate that TIM4 can only recruit apoptotic cells by binding to exposed PS, but does not induce engulfment. However, it has been shown that TIM4 strongly enhances the efferocytosis activity mediated by TAM receptors and the homologous glycoproteins Protein S and GAS6 [331, 173, 139]. In macrophages expressing both TIM4 and TAM receptors this enhancement is necessary to induce efferocytosis at all [331]. The TAM receptor family consists of the tissue specific expressed receptor kinases TYRO3, AXL and MERTK [128, 226, 77, 269, 309] and most macrophages expresses one of them [331]. Protein S and GAS6 bind to the TAM receptors and also recognise PS in a Ca^{2+} dependent manner [165, 3] to build a bridge between the apoptotic cell and the macrophage. Their affinity to PS is much lower compared to that of TIM4, which suggests that efferocytosis is activated by a combined process of 'tethering' (TIM4) and 'tickling' (TAM) [263] that uses exposed PS as an anchor.

Based on this role of PS in the induction of efferocytosis it is easy to imagine disturbed apoptosis through defects in PS flippases at the plasma membrane. This has been shown for hemizygous male *Atp11c -/+* mice that express no *ATP11C*. The consequence is a severe deficit of circulating B cells [329, 255]. The reason has been found to be the engulfment of B cell progenitors by bone marrow macrophages, because they are not able to counterbalance transient PS exposure [244]. During the B-cell development early B cell progenitor cells loose the expression of *hATP11A* and use hATP11C as their only plasma membrane flippase. Whith this missing, there is no PS flippase activity counteracting the usually transient exposure of PS performed by scramblase TMEM16F and the apoptotis inducing PS signal gets mimicked [244]. A similar problem could be true for hypofunctionality of hATP11A. As described above, hATP11C can

be transiently inactivated through Ca^{2+} induced protein kinase C as described above [282]. With the hATP11A deletion variant hypoactive, the remaining rest activity of hATP11A might not be enough to balance scramblase activity during the transient inactivation and an apoptosis like state is induced.
To shed light on why this could be problematic especially in the inner ear it is worth to notice that in mammals the precise frequency mapping of spiral ganglion neurons is not present at birth, but rather develops gradually during a postnatal ripening process [52, 257, 202]. During this process afferent neurons projecting to the wrong frequency are eliminated by apoptosis [174, 172], while type I spiral ganglion neurons, which project to both OHCs and IHCs during the embryonic development [52, 258, 100], are pruned [reviewed in 42]. During pruning the connection between type I cells and OHCs are eliminated, but the projections to IHCs remain [202, 71, 258, 322]. The reduction of cochlear neurons happens prior hearing onset from postnatal day 4 to 6 in rat [229, 205] and gerbil and coincides with findings of apoptotis. These apoptotic cells are mainly located at the periphery of the spiral ganglion [53], so they are thought to project to outer hair cells [14, 22].
There are multiple ways discussed in which neuronal pruning can be induced. For some cell types caspase induction seems plausible [reviewed in 240]. Recently it has been suggested that a certain threshold of caspase activity divides between morphogenic pruning and complete cell death by apoptosis [68]. If type I spiral ganglion cells undergo a similar caspase regulated pruning during their developmental ripening, it is possible that the hypoactivity of hATP11A in the patient could shift the threshold of necessary caspase activity. Lower levels of caspase then are sufficient to inactivate the remaining PS flippases and thus induce pathogenic apoptosis instead of pruning the type I spiral ganglion to project only to the IHC.
Similarly, the greater epithelial ridge, supporting cells of the IHCs, are remodelled by caspase-3 mediated apoptosis between postnatal day 7 to 13 in mice [279, 199]. A corresponding process in humans seems likely. Also here the diminished hATP11A activity in patients could interfere with normal development of the inner ear. Pathogenic loss of supporting cells might subsequently result in degeneration of IHCs and thus to hearing loss.
A second hypothetical way of the induction of pathogenic apoptosis in the patient could be linked to the sole presence of macrophages and apoptotic factors in the periphery of spiral ganglion neurons and IHCs during the apoptotic remodelling of innervation or supporting cells. If the lowered ATP11A activity in patients' type I spiral ganglion cells, IHCs or supporting cells results in PS ex-

posure through their general or developmental ATPase expression pattern, the present apoptosis machinery could bind to it and induce pathogenic apoptosis. A connection between the ripening of the spiral ganglion neurons and hearing loss has also been proposed by Stapelbroek *et al.* [265]. In their study with *Atp8b1* deficient mice degeneration of hair cells was only noticeable after postnatal day 4, the time at which the reduction of cochlear neurons is supposed to start. Human neuronal connections are remodelled until puberty [107]. Despite the developmental cochlear remodelling of gerbil and rat inner ear seem to reach adult state earlier, it is not specifically known when human cochlear development is fully completed and if there is additional modification that could cause apoptosis later in life. Should this development also last until puberty, the progressing nature of the described hearing loss in *hATP11A* deletion patients with onset in the first two decades of life is relatable. Anyhow, also the diminished signal through less surviving type I neurons innervating to IHCs after one single initial pruning process or degenerated IHCs though the loss of supporting cells could lead to slow progressive loss of IHCs. Further progression to more frequencies and signs of cochlear disfunction could be interpreted as additional loss of spiral ganglion neurons and supporting cells as a secondary consequence of hearing loss due to missing input signals for those cells, too [121, 270, 8, 230]. Gasdermin E, another identified deafness gene, highlights the connection of hearing loss and apoptosis regulation [123, 144]. Different reported mutations cause the skipping of exon 8 and result in a gain of function for the protein [179]. It has been shown that this gain of function leads to elevated pyroptosis [306, 321], a form of secondary necrosis [249]. This presumably causes the progressive, symmetrical, non-syndromic sensorineural hearing loss through abnormal cell death in the inner ear [40]. Patients develop hearing loss starting at the high frequencies at an age of 5 to 15 years and progress to middle and lower frequency loss later in life [179]. This is concordant with the progression of hearing loss studied in this thesis. However, in contrast to that the speech perception of patients with Gasdermin E mutations is compromised only slowly. This indicates that the cells affected by the induced cell death are not inner hair cells, synapses or auditory nerve cells, but other cells of the inner ear, causing cochlear dysfunction instead of AS/AN [179]. Why only those cells are affected is not clear. Nonetheless, this specific non-syndromic phenotype as a result of a gain of function of an ubiquitinously present protein, suggests that a similar mechanism caused by partial loss of hATP11A flippase activity could also terminate in a locally isolated phenotype of the inner ear, possibly due to a special relationship between inner ear cells and apoptosis.

6.3.4. Neurite degeneration and regeneration

Similar to its involvement in axonal pruning during inner ear development, PS exposure is associated with developmental neurite degeneration in the context of tissue homeostasis and prevention of neuroinflammation [316, 235, 161, 231, 253] The activation of scramblase Xkr8 and the translocase ABC1 during axon degeneration results in PS exposure of mouse dorsal root ganglion neurons in vitro [316]. PS exposure on neurites can also be artificially induced through physical injury, knockout of PS flipping ATP8A and scramblase overexpression in *Drosophila* [235]. Scramblase overexpression and *CDC50* knockout have also been associated with neurite shortening, degeneration and in part subsequently lowered neurite counts in mice [37], without complete cell loss. In contrast, overexpression of the ATPase and *CDC50A* resulted in enhanced neurite outgrowth [340, 328]. These results will be analysed more detailed in section 6.4.2 on ATP8A mouse models.
The PS exposure induced upon axon injury does not always have to lead to degeneration. It has been shown that in *C. elegans* caspase induced CED-7 floppase based PS exposure after axon injury acts as a signal to enable axonal reconnection and fusion [99, 170]. On the cell surface TTR-11 binds to integrin and PS, which activates the integrin to initiate the axon regeneration via the INA-1 - CED-10 pathway [99]. Although details of the distinction which pathway is chosen are still unclear, it is interesting to notice that proteins known for their role in apoptosis, are also able to promote axon regeneration.
It is plausible that an imbalance in the initiating exposure of PS on the axon surface could disturb the mechanism differentiating between degeneration and regeneration. An elevated rate of degenerating spiral ganglion axons in the patients which otherwise would have been regenerated would both explain the AS/AN phenotype and the progressive behaviour.

6.3.5. Interaction with intracellular and membrane bound proteins

When PS gets exposed at the plasma membrane, the resulting problem is not only an abundance in the exoplasmic leaflet, but there also remains insufficient PS at the cytoplasmic leaflet of the plasma membrane. This PS is important for the electrostatic properties of the inner leaflet and interaction of the membrane with many intracellular and membrane bound proteins [reviewed in 129, 264]. The most common ways are penetration of the membrane with hydrophobic residues, unspecific electrostatic interaction with the negatively charged mem-

brane, interaction with the PS headgroup through specific PS recognition motifs or a combination of those. While most of the proteins interacting with PS are thought to be important for structural purposes, like cytoskeleton and membrane stability, a part of them might also be signalling proteins [264].
The interaction of proteins with the plasma membrane is determined by the presented composition of phospholipids and often times by the presence of Ca^{2+} as a cofactor. This way the interaction can be controlled in intensity and timing by the amount and moment to which specific phospholipids are transported to a certain place at the membrane and the activity of Ca^{2+} channels and transporters [129]. By modulating the phospholipid composition of the inner leaflet, the electrostatic properties can be used to regulate the activity of interacting proteins. This mechanism is called the 'electrostatic switch' [149]. Recently a related mechanism, the 'flip-flop switch' was proposed to regulate the activity of the Ca^{+} channel PIEZO1 during myotube formation. Ca^{+} influx was completely lost in CDC50A deficient mouse myoblasts and significantly diminished in ATP11A deficient mouse myoblasts. It is thought that PS headgroups exposed at the outer leaflet inhibit PIEZO1 activity and that recovery of PS to the cytosolic leaflet by ATP11A is essential for activation [295]. While PIEZO1 and also PIEZO2 are not the mechanosensitive channels of hair cells needed for mechanotransduction and PIEZO2 only plays a role in hair cell development as well as after tip-link breakage [325], similar switch mechanisms still might control other protein activity essential for hearing.
Consequently, an altered distribution of PS through diminished ATP11A function might influence the activity and interaction of the plasma membrane with intracellular and membrane bound proteins. This could result in a variety of disturbed pathways. Interaction with the plasma membrane, and also PS in particular, is associated with a multitude of protein functions and there are probably many more to uncover. Therefore, without additional information about cellular changes upon ATP11A reduction or loss of function, it is hardly possible to speculate on a single pathway that might be causing the sensorineural hearing loss.
As one example of many possibilities, PS interacts with protein kinase C [274, 310]. Through the interaction, protein kinase C-β gets activated and acts as a docking site for other signalling proteins [332]. Also synaptotagmin, a presynaptic protein that acts as a Ca^{2+} sensor to regulate exocytosis of neurotransmitters, was found to interact with PS [275, 337]. Both proteins are associated with pathways that are essential for correct signal transmission and neuronal function, which could possibly lead to AS/AN.

6.3.6. Impaired calcium level threshold and transporters

Calcium ion influx is a central part of the signal transduction of IHCs. When the mechanical signal of a soundwave evokes small changes in the membrane potential of IHCs, ultimately Ca^{2+} channels are opened at their active zone at the synaptic pole. Ca^{2+} enters the IHC and binds to otoferlin [228, 17]. Otoferlin subsequently interacts with the SNARE complex protein and allows the fusion of stored synaptic vesicles with the presynaptic membrane. This way the neurotransmitter VGLUT-3 is exocytosed [212]. At the same time, Ca^{2+} binds to synaptotagmin-IV in the vesicle membrane and increases its affinity for presynaptic membrane phospholipids, which accelerates the exocytosis. The released glutamate activates AMPA receptors of the postsynaptic spiral ganglion neurons and induces action potentials that are transmitted further to the auditory cortex. The remaining glutamate is then rapidly taken up by transporters in supporting cells to avoid overstimulation [72].
Recently it has been found that the Ca^{2+} level of cells regulates the differentiation between cell survival, apoptosis and autophagy [122], like it was previosly described for the caspase-3 level [68]. This is not surprising, since Ca^{2+} is involved in caspase-3 regulation [155, 180] and scramblase activation [276]. The finding indicates that the non-syndromic hearing loss phenotype with its specific location at the IHCs, synapse or auditory nerve, could stem from Ca^{2+} levels during activation locally reaching dimensions that are sufficient for transient hATP11C inactivation and scramblase activation. The consequence would be the same as described for lowered caspase-3 thresholds. The diminished hATP11A activity in the patients' cells could not counteract scramblase activity during the transient hATP11C inactivation and the normally healthy process could for example tip to apoptosis inducement, if the PS exposure is not cleared fast enough.
In hair cells PMCA transporters are present to normalise the intracellular Ca^{2+} concentration after activation [50, 79, 315]. In rat organ of Corti *Atp2b2*, coding for PMCA2, is highly expressed at the OHC stereocilia and to a lower level at IHC stereocilia tips. Two other PMCAs, PMCA1 and PMCA3 are only present in IHCs. PMCA3 is mainly located at their cuticular plate, the apical surface and to some extend at the basolateral plasma membrane, while *Atp2b1*, coding for PMCA1, is expressed at the basolateral membrane of IHCs, but not at the stereocilia [50]. It has been reported that *Atp2b2* mutant mice experience early onset hearing loss due to degeneration of cochlear hair cells [270, 117, 48]. It has also been found that a disturbed membrane composition, which is clearly possible with decreased hATP11A activity, could influence the transporting

efficiency of PMCA Ca^{2+} transporters [285]. The study was performed with the protein PMCA4 from erythrocytes. It is suspected, but not proven that all those Ca^{2+} transporters react the same to changes of the plasma membrane composition [285] and it is not clear if they are able to compensate for each other. Anyhow, if the transporter activity is lowered in a way that enough Ca^{2+} is retained in the IHC, signal transduction could be disturbed and the projecting spiral ganglion neurons might be degenerated. Additionally with higher Ca^{2+} levels ATP11C could be inactivated and scramblases activated, which would cause even more disturbance of the membrane asymmetry and let the process escalate faster.

6.4. Evidence from P4-ATPase loss of function mouse models

In order to find direct evidence for the cellular consequences of P4-ATPase loss of function in general and specifically for auditory cells, mouse models are useful. There is only a single report on loss of ATP11A itself. A study on placental defects in embryonic lethal mouse mutants found muscular ventricular septal defects in *Atp11a*$^{-/-}$ embryos [201]. There seems to be a certain threshold of ATP11A activity necessary for development and survival that can not be compensated by other P4-ATPases.
However, based on published phenotypes of other P4-ATPase loss of function models, assumptions can be made for ATP11A. To hypothesize which of the discussed possible pathomechanisms is most plausible for the hearing loss phenotype through partial hATP11A loss of function, some mouse models already mentioned in section 1.5.7 'Diseases related to P4-ATPases' are examined again with respect to the findings of this thesis. Two models, ATP8A2 and ATP8B1 loss of function and knockout, are associated with sensorineural hearing loss [37, 265], while ATP11C loss of function models are interesting in regard of protein homology, expression pattern and localisation [256, 329, 256, 255, 5].

6.4.1. ATP8B1 loss of function

ATP8B1 is a PS and PC specific phospholipid flippase localised to the plasma membrane [252]. Reduced and complete loss of function is known to result in a spectrum of liver diseases, with the gravity depending on the degree of loss of function. Patients with a more severe phenotype also develop extrahepatic symptoms, one of those being sensorineural hearing loss [265, 182].
Among other tissues, ATP8B1 is expressed in the stereocilia of hair cells, while

there is no ATP8B1 at the spiral ganglion neurons or supporting cells [265]. For human patients the onset of hearing loss is in the first two decades of life, like it is for patients with hATP8A2 or hATP11A mutations. In the loss of function mouse model [265] first deficits are noticable on cellular level at P16 and progress until 6 month of age. The measurements and latencies of the ABR testing revealed no retrocochlear origin. Also the TEOAE was normal, so the defect is indicated to be on OHC level.
Indeed, cellular degeneration starts at the basal OHC stereocilia. Subsequently the OHCs are completely lost and the surrounding supporting cells degenerate as a secondary consequence. Later the OHCs' spiral ganglion cells degenerate, probably as a consequence of missing input signals. From there on the cell loss progresses to IHCs and all spiral ganglion cells. No analysis were made of the apoptosis level, PS exposure or vesicle trafficking, so all of the theories mentioned above could be relevant. Concordant with those theories, Stapelbroek *et al.* [265] hypothesise that the altered membrane composition could result in mechanical instability of the stereocilia. This would have the consequence that they could not stand the constant mechanical stress at the tectorial membrane. Other hypothesis are the inhibition of Ca^{2+} transporters and a disturbed PI generation through PS asymmetry, which itself inhibits maintenance and mechanotransduction.
The findings from the ATP8B1 loss of function mouse model give only little inside that is portable to ATP11A loss of function. While the onset of hearing loss and the progressing phenotype is fitting, the problem is based on OHC loss instead of IHC or spiral ganglion loss. The reason for that might be a different expression of *ATP8B1* and *ATP11A* in the inner ear, whith *ATP8B1* hypothetically beeing expressed at the OHCs' stereocilia and *ATP11A* at the IHC stereocilia. Anyhow, the specific pathomechanism could not be determined further.

6.4.2. ATP8A2 and ATP8A1 loss of function

ATP8A2 is a PS and PE specific phospholipid flippase expressed at the plasma membrane, but also at the TGN and in late and recycling endosomes [252]. Loss of ATP8A2 function has been reported to cause cerebellar ataxia, mental retardation and dysequilibrium syndrome, but is also associated with loss of sight and hearing [178]. In mice it was shown to be expressed in brain, spiral cord, testis and photoreceptors of the retina [28, 36, 340, 37]. It probably is also expressed in the inner ear, but there is no proving data yet. In an *Atp8a2* knockout mouse line and the *wl/wl* mouse line, which has ATP8A2 loss of function

due to a deletion in exon 22 [340], the onset for ataxia and neurodegeneration is at about P12 [37]. Degeneration at the eye could be observed only after day 14 when *Atp8a2* is first expressed in that tissue. The degeneration manifests with shortened outer segments of the photoreceptor, but with overall normal structure. The outer segments of photoreceptors have a high turnover, in which the tip is phagocytosed and new membrane is added constantly to maintain the length [126, 273]. Due to that high turnover there is no pronounced phospholipid asymmetry at the plasma membrane [94]. Experiments revealed that phagocytosis at the outer segment was normal, no PS was exposed on the surface and the PS content of the membrane was overall decreased [37, 340]. It is assumed that this stems from defects in vesicle trafficking from the Golgi to the inner segment of the photoreceptor, caused by loss of ATP8A2 function in the TGN and the endosomes. This results in inefficient disc morphogenesis necessary to maintain the correct outer segment length. Subsequent photoreceptor degeneration is a secondary consequence of outer segment defects, as was reported previously [92, 101]. The hypothesis of disturbed transport is supported by findings in regard to axon degeneration causing other pathologies of the ATP8A2 loss of function phenotype. In mice the degeneration of axons upon ATP8A2 loss of function happens without cell loss, elevated caspase activity or apoptosis, but decreased axonal transport of phosphorylated neurofilament was found and proclaimed to be the reason of degeneration [340]. It was also found that while the overexpression of *ATP8A2* and *CDC50A* resulted in enhanced NGF-induced neurite outgrowth, reduction of CDC50A activity through RNA interference reduced neurite outgrowth in PC12 cells. The same was true for rat hippocampal neurons. The enhanced outgrowth represented with longer, but not more neurites [328].

With respect to the hearing loss phenotype the *Atp8a2* mouse models showed a disturbed startle reflex and an elevated ABR threshold. The inner and outer hair cells were intact, but spiral ganglion neuron loss was observed, in corcordance with the ABR findings [37]. However, it is not clear if transport defects are also the reason for the spiral ganglion cell loss. PS exposure was not analyzed for the inner ear cell membranes, where there is a phospholipid asymmetry under normal circumstances. Levano [131] reported PS exposure in hippocampal neurons, even so there was no abnormal morphology or apoptosis in ATP8A1 deficient mice with delayed hippocampus dependent learning. Transferred from the homology of ATP8A1 and ATP8A2, PS exposure is likely to also happen in similar tissues with membrane asymmetry upon ATP8A2 loss of function.

Since it is not the hair cells that degenerate, which would be the photoreceptor

corresponding cell type in the ear, but the spiral ganglion cells, it is feasible to think of an alternative mechanism. For ATP8A1 deficient hippocampal neurons changes in morphology and apoptosis were already ruled out, so other consequences of an altered phospholipid composition are also a possible explanation for spiral ganglion neuron degeneration. Suitable seems to be the hypothesis of an imbalance in endo- and exocytosis at the ribbon synapse of otherwise healthy looking inner hair cells, disturbed signal transmission and subsequently a loss in spiral ganglion neurons.
While the imbalance of endo- and exocytosis at the ribbon synapse is a valid possibility also for ATP11A hypofunctionality, a direct involvement in intracellular vesicular trafficking is rather unlikely, since ATP11A is not expressed at the TGN or endosomes [252]. At the same time, the finding that PS exposure in hippocampal neurons does not result in apoptosis indicates that induced apoptosis of spiral ganglion neurons is most likely also not the reason for hearing loss in the patients. For loss of ATP8A1 mice hippocampal neuron morphology remained healthy as well as hair cell morphology in ATP8A2 deficient mice. This lets draw the conclusion that changes in cell shape of hair cells, supporting cells or spiral ganglion neurons are also in ATP11A hypofunctionality not the reason for hearing loss. However, the expression pattern and intracellular localisation of ATP11A and ATP8A1 /ATP8A2 differ, so there also can be differences in the effects on cellular function [252].

6.4.3. ATP11C loss of function

Since ATP11C has the highest sequence similarity to ATP11A of all the P4-ATPases, transports the same substrates and is also located at the plasma membrane [252], it is very interesting to look at studies of the several available ATP11C loss of function mouse models, even when there is no hearing loss involved.
The *ambrosius* mouse strain and the 18NIH30a strain harbor splice site mutations in intron 27 and 26 respectively, resulting in shortened proteins [329]. In the *emptyhive* strain, mice have a stop mutation at position Q655Ter in *Atp11c*, so about half of the protein sequence is missing [256]. The *spelling* strain contains a missense mutation in exon 12 [255]. All those proteins seem to be inactive.
The gene coding for ATP11C is located on the X chromosome, so while male mice are hemizygous, heterozygous female mice carry a mutation that is either expressed or suppressed depending on random X inactivation in each cell.
Homozygous female and hemizygous male mice with the *ambrosius Atp11c* loss

of function mutation develop a B cell deficiency syndrome, whereas heterozygous female mice present no noticeable phenotype. The affected pro-B cells exhibit a lower PS translocation to the inner leaflet of the plasma membrane, with rest flippase activity probably provided by other PS flippases in the membrane. Also the amounts of pro-B cells and B cells were reduced. Those numbers where not affected by supressing apoptosis, so the reason for cell loss is not the induction of apoptosis through PS exposure. Instead ATP11C seems to be important for the differentiation of B lymphocytes from the pro-B cell stage onwards. Pro-B cells and pre-B cells were unresponsive to artificially induced differentiation with IL-7, a regulatory hematopoietic growth factor for B-lymphocyte development [329].

While some abnormalities like hepatocellular carcinoma and anemia only occurred in the *ambrosius* strain [329] and an enlarged gall bladder or death of dystocia in homozygous female mice was only reported for the *emptyhive* and *spelling* mouse strains, B cell deficiency and hyperbilirubinemia were found in all ATP11C loss of function mouse models regardless of the mutation and were further explored in following studies [256, 255].

In *emptyhive* and *spelling* strains, the B cell deficiency could be demonstrated to arise from failure in B cell development at the adult stage [255]. In the fetal liver of mutant mice B cells could still be generated, but in the adult bone marrow differentiation stopped at pro-B cell stadium. On those undifferentiated bone marrow lymphocytes no PS exposure was detected. As in the *ambrosius* model, again blocking of apoptosis did not result in a higher B cell count, so the development is stagnating independent from apoptosis. It suggests itself that ATP11C could be involved in signalling pathways that are important for adult, but not fetal B cell development, like IL-7 and IL-7R signalling. Anyhow, those also interfere with T cell development and Igll1 expression, while ATP11C loss of function does not [255]. Since B cell progenitors of the *ambrosius* mouse model did not respond to stimulation with IL-7 [329], the interference with only B cell differentiation could still be a valid explanation, if ATP11C is only involved in some downstream branches of IL-7 and IL-7R signalling or there is a transient downregulation of IL-7 and IL-7R activity during which ATP11C is essential for compensation [255]. For example, similarly to IL-7, ATP11C could be important for sustaining the expression of *Ebf1*, which is involved in the regulation of early B cell development [26].

Bypassing intermediate stages of B cell development through additional expression of the signalling factor BCR partially corrected B cell deficiency, so ATP11C also could be involved in an earlier stage of that pathway [255].

However, a pathomechanism based on disturbed PI asymmetry in the plasma membrane [70] as suspected by Stapelbroek *et al.* [265] for ATP8B1 is unlikely in this case. Experimentally enhanced and decreased PI availability did not change the phenotype, so neither direct modification of PI asymmetry by transport through ATP11C nor indirect modification through influence on PI generation are plausible causes for stagnant B cell development [255].
Hyperbilirubinemia was also studied in detail in the context of the *emptyhive* and *spelling* mouse models [256]. It was found that the liver function and histology of affected mice showed only minor pathology and that the hyperbilirubinemia stems from effects on nonhematopoietic cells. When fed with a cholic acid enriched diet, the cholic acid was elevated in the serum and became toxic. It seems ATP11C has a function in preventing colestasis, as *Atp11c* mutant mice develop mild cholestasis similar to other PFIC and BRIC mouse models, that can be changed to a more severe development with inducing diets [320]. However, their hyperbilirubinemia declines progressively with age. The reason for this is still unclear. It might be caused by behavioral differences in young and ageing mice or with substrate competition of ATP11C, resulting in increased dependence on ATP11C activity in younger mice [256]. Hypothesis on the underlying causes for the hyperbilirubinemia are related to findings for ATP8B1 loss of function. The canalicular membrane asymmetry is known to be important for the formation of bile [260] and the structural stability to withstand the detergent effects of bile [194], so loss of ATP11C function could have the same effect as loss of ATP8B1, since both flip PS at the plasma membrane. Also the noted involvement of P4-ATPases in vesicular trafficking is taken into account, as ATP11C might mediate trafficking of other canalicular transporters as well [256].
Investigation of the anemic phenotype of *ambrosius* ATP11C loss of function mice showed an opposing pathology for erythrocytes compared to lymphocytes [330]. Erythrocyte development was normal, but the shape was altered and the lifespan shortened, resulting in anemia in hemizygous male and homozygous female mice. In the early developmental stages a significantly slower PS intake was shown for *Atp11c* mutant cells compared to WT erythrocytes. Since in healthy WT erythrocytes PS internalisation reduces with cell maturity, the differences declined progressively. Nevertheless, while WT cells showed no PS externalisation, the amount of mutant cells showing externalisation increased with cell age. Based on the bilayer couple hypothesis [248] mentioned above, the stomatocytotic cell shape could be caused by the altered phospholipid asymmetry of the plasma membrane. Other possible reasons are the misregulation

of sterol absorption and excretion or disturbed interaction with cytoskeletal proteins and the membrane.
Recently a single human male patient with a hATP11C loss of function mutation has been reported [5]. The patient has hemolytic anemia with normal shaped erythrocytes. The mutation site T418 is located near the phosphorylation site D412, the equivalent of D414 in hATP11A, which is important for interaction with CDC50A. This leads to a 10 fold decreased PS intake in mature erythrocytes compared to control. It is unclear whether the remaining PS flippase activity stems from ATP11C itself or from other flippases present at the plasma membrane. Activity measurements of the mother's erythrocytes exhibited two populations, one with normal and one with decreased intake, reflecting on random X-chromosome inactivation.
Regardless of the minimal PS internalisation, PS was retained in the cytoplasmic leaflet of the plasma membrane nevertheless. Only senescent cells near the end of their life cycle, which have Ca^{2+} induced scramblase activity, show PS externalisation. This indicates that it can not be externalised without additional scramblase activation, even without efficient flippase activity. However, the percentage of PS exposing cells among the senescent erythrocytes was higher in the patient compared to control and the heterozygous mother. Erythrocytes of the patient and WT cells with induced scramblase activation exposed PS to a similar extent, so PS retention to the cytoplasic leaflet is most likely regulated by scramblase activity rather than ATP11C activity, although ATP11C loss of function seems to facilitate PS exposure upon scramblase activation in erythrocytes [5].
There are some differences in the anemic ATP11C loss of function phenotype between mice and the human patient. In mice erythrocytes develop stomatocytosis, while the patient's cell maintain a biconcave shape. While the patient's erythrocytes have a 10 fold decreased PS intake, but only expose PS at the end of their lifespan, mice erythrocytes expose PS early on, but only show reduced PS internalisation in early developmental stages. Both mutations should result in loss of ATP11C function, so the differences probably are caused by the compensation by other PS flippases. In mice only *Atp11c* mRNA was found in erythroblasts, so in the early stages there probably is no compensatory flippase activity left, which results in PS exposure and an abnormal shape. In human erythrocytes *hATP11A* and *hATP11C* are expressed at similar levels, so a loss of hATP11C function does not leave the cell without any PS flippase activity to maintain shape and PS retention to the cytoplasmic leaflet, regardless of the diminished PS intake.

The ruling out of apoptosis as a reason for B cell deficiency and anemia in the ATP11C loss of function mutant mice indicates again that apoptosis might not be directly involved in producing the hearing loss phenotype of patients with an *ATP11A* mutation. The studies on ATP11C loss also showed that PS exposure on the plasma membrane is not present in every cell type, despite deminished PS intake. Arashiki *et al.* [5] suspects scramblases to be the regulating instance of PS retention in human erythrocytes. This, however, does not have to be the same for other cell types. *ATP11A* mutant cells from types with higher membrane turn over or a high amount of endocytosis could possibly have not enough PS flippase activity left to internalise the PS added to the outer leaflet that way, especially when missing a compensatory flippase.

6.4.4. Conclusions for ATP11A

Taken together the studies on P4-ATPase loss of function mouse models and human patients make some pathomechanisms more likely than others.
The PS exposure on the plasma membrane of cells with diminished PS flippase activity is highly dependent on the cell type and P4-ATPase expression pattern. While in *Atp8a2* deficient mice photoreceptors show no sign of PS exposure, but the PS content of the membrane is overall diminished [37, 340], hippocampal neurons of *Atp8a1* deficient mice expose PS [131]. Mice erythrocytes lacking ATP11C activity expose more and more PS while aging, [330] and in contrast human erythrocytes display PS externalisation only in senescent cells at the end of their lifespan [5]. As suspected above, cells with high membrane turn over and an immense rate of endo- and exocytosis, like it happens at the synaptic ribbon of hair cells, might not compete with the natural addition of PS at the outer leaflet of the plasma membrane and fail to internalise it, if the PS flippase activity is decreased through partial loss of function. In particular this could be true for cell types specialised on the expression of a single PS flipping P4-ATPase.
The involvement of apoptosis as a direct consequence of missing flippase activity and the exposure of PS on the cell surface was ruled out in many cases [340, 131, 329, 255]. It is reasonable to hypothesize that also for a substantial heterozygous reduction of ATP11A function direct induction of apoptosis is not the reason for hearing loss. Nevertheless, elevated apoptosis during developmental stages of the organ of Corti, axon degeneration or degeneration and subsequent engulfment of inner ear cells as a secondary consequence of another pathomechanism are still valid theories.
One of those other pathomechanisms that is supported by the loss of function

studies is a diminished mechanical stability [265, 194, 330]. High sheer stress, like bending of hair cell stereocilia at the tectorial membrane, could lead to damaged and degenerated cells that are subsequently lost by apoptosis as a secondary consequence. This would fit the progressive character of the patients' hearing loss better than apoptosis during developmental stages of the organ of Corti, even though the initial loss of only a few cells through elevated apoptosis could lead to a disturbed signal transmission to spiral ganglion neurons and further cell loss later in life.

The theory of a disturbed generation of PI through the altered asymmetry of the plasma membrane as a reason for failing maintenance and mechanotransduction in hair cells, as proposed for ATP8B1 loss of function [265], seems unlikely, since PI levels did not influence the anemia phenotype in ATP11C loss of function [255]. A diminished Ca^{2+} transporter activity, which was hypothesized by Stapelbroek *et al.* [265] was not examined in any of the studies. However, a comparable involvement in intra- and intercellular signalling pathways, possibly via altered protein interaction with the membrane [264, 129] or vesicular trafficking are thought to be potential explanations for many P4-ATPase loss of function phenotypes, like stagnant B cell differentiation and axon degeneration through disturbed axonal transport [329, 340]. A similar mechanism could very well be present in ATP11A hypofunctional cells, too.

Altered asymmetry and amounts of phospholipids in the inner and outer leaflet of the plasma membrane could also influence the cell shape as described in the bilayer couple hypothesis [248]. Upon ATP8A1 loss of function hair cells and hippocampal neurons exhibit a normal morphology [131]. Anyhow, this does not directly indicate a similar morphology upon ATP11A hypoactivity, since ATP8A1 is also located in endosomes [252] and might not be the main PS flippase at the plasma membrane of cells in the inner ear.

A difference worth mentioning is that heterozygous loss of *ATP8A1*, *ATP8A2*, *ATP8B1* and *ATP11C* is most often not sufficient for a disease phenotype, except for some mild cases of cholestasis caused by heterozygous mutations in *ATP8B1* [47, 103]. Generally, there seems to be enough flippase activity left, probably also via compensation through each other. Only loss of both *ATP8A1* and *ATP8A2* is lethal in mice [131]. For *hATP11A* already a heterozygous hypoactivity of PS flippase function is resulting in a hearing loss phenotype. This could be explained by the expression pattern of P4-ATPases in the tissue. Most cell types express a variety of P4-ATPases, so a heterozygous loss of one of them does not result in a major disturbance of PS transport [243, 317]. The exact ratio of expressed P4-ATPases in the ear has not been examined so far.

However, the outstandingly high preferential expression of *ATP11A* with over 80% in the kidney [317] indicates that the same is true for the inner ear. The early embryogenesis of the innear ear and the kidney are based on the same transcription factors and gene expression patters from mesodermal induction. This results in many structural and functional similarities between the tissues. Through disease studies a lot of genes have been identified that play an important role in both ear and renal function [reviewed in 102, 293], so *ATP11A* could be one of them, despite a renal phenotype was only described for patient 9 (11 years old), which has chronic renal failure with hypertension besides a frequently relapsing nephrotic syndrome. With preferential expression of *ATP11A* there potentially would be not sufficient compensatory ATPase function with hATP11A hypofunctionality in some or even all inner ear cells.

7. Summary and Outlook

A family presented with autosomal dominant inherited non-syndromic sensorineural hearing loss, which was clinically further classified as an auditory synaptopathy / auditory neuropathy. No linkage to the known AUNA1 locus was found, but another common haplotype at a locus subsequently called AUNA2 was identified [124]. Whole genome sequencing revealed that all patients carried a 5,500 bp deletion in the gene *ATP11A* located within the linkage region. Within this thesis the identified mutation was shown to result in aberrant splicing of the last coding exon of both *ATP11A* isoforms. Instead of the highly conserved exon 29a of isoform 1 or exon 29b of isoform 2, a novel exon 29^{mut} was created as shown by comprehensive mRNA analyses. The novel exon begins at an alternative splice acceptor site 171 bp downstream of the deletion in the 3' UTR of ATP11A and ends with a stop codon after 114 bp. This deletion variant of *ATP11A* was shown to be expressed on mRNA level in the patient, while the level of isoform 1 and 2 are reduced. Similar to the wild type hATP11A isoform 1, studies in HEK293 cells overexpressing the deletion variant revealed its localisation at the plasma membrane when coexpressed with hCDC50A. After establishing a flippase activity assay, I could show that the activity for PS transport of the deletion variant was severely diminished and showed comparable levels to known loss of function controls and the mock vector. Despite the data not being significant, the activity of the mutant deletion variant seems not to be lost completely. The fluorescence intensity presents slightly above that of the known loss of function variant E186Q or the mock vector. This matches the predicted loss of function intolerance of *hATP11A* by the Genome Aggregation Database, according to which even a heterozygous complete loss of function can be assumed to be lethal.

Isoform 1 seems to be the only physiologically important isoform of hATP11A. Human ATP11A isoform 2 seems to be an evolutionary remnant, as exon 29b is not only less conserved and isoform 2 hardly expressed in human blood cDNA, but also my experimental data indicates a low PS flippase activity of this splice variant. The results for the translocation capability of the different hATP11A variants for PE were not fully conclusive. The experiment needs to be redone with a larger sample size and longer incubation time between sampling, to

investigate also the slower incorporation of PE into the cytoplasmic leaflet. However, the results of the earlier samples show similar fluorescence levels for the hATP11A isoform 1 and the deletion variant. This further supports the hypothesis of an incomplete loss of function and indicates that the cellular level of incorporated PE is not as severely affected by the patient's mutation as the level of PS, probably caused by the lower affinity of hATP11A for PE and the resulting lower translocation in general.

However, in the assay a highly elevated PS and PE transport activity of a hATP11A variant ending after exon 28 showed that the diminished activity is not caused by the loss of exon 29a, but by the creation of the alternative exon 29^{mut}. Comparisons with the C-terminal regulatory mechanism of other P4-ATPases and insights from recent studies in P4-ATPase mechanics indicate that the aberrant splicing disturbs the normal regulation of hATP11A activity. The C-terminus fills a groove between the N-domain and the A- and P-domain, that stabilises the conformational state. Depending on the ATPase this results either in inhibition or enabling of ATP binding and phosphorylation of the P-domain.

The simplest interpretation of my data suggests that the inhibitory properties of the hATP11A cytoplasmic C-terminal region purely depend on its length. The 41 amino acid terminus of the WT minimally interacts with the catalytic core and only dampens the flippase activity to some extend, whereas the elongated 54 amino acid terminus of the hATP11A deletion variant interacts more firmly and prevents phospholipid translocation to a higher degree. In contrast, the deletion of exon 29a without substitution results in an only 16 amino acid short C-terminal sequence, which can not interact with the catalytic core. Therefore, the activity of this variant is even higher than that of the WT.

Another possible model mechanism would be similar to that of yeast Drs2p flippase, where the C-terminus has an autoinhibitory function that can be interrupted by interaction with PI4P. Upon binding, a helix switch turns, the C-terminus disengages and the catalytic cycle is activated. For hATP11A a model like this could likewise explain the activity changes in both the deletion variant and the variant ending after exon 28. Like before, without any exon 29 the C-terminus is not long enough to fill the groove and stabilise the inactive conformation and the protein is permanently active. Exon 29^{mut} elongates the C-terminus enough for interaction with the other domains and inactivation of the catalytic cycle. Though, with a potential equivalent sequence of the helix switch, located in exon 29a, missing, the C-terminus can not disengage and the flippase remains deactivated.

The first theorised mechanism would better support the suggested hypoactivity of the mutant protein, while the second better matches to a complete loss of flippase function. Insights in the mechanism of hATP11A phospholipid flipping through investigation of the crystal structure could clarify those hypothesis. Also mutation studies looking for a helix switch or an interaction site at which the autoinhibition can be regulated and checking whether other C-terminal sequence length have an inactivating effect would shed further light on the detailed mechanics of hATP11A regulation.

The multitude of P4-ATPases with their different expression patterns, cellular localisation and regulatory mechanisms makes it possible to adjust the flippase activity and the processes depending on it to the needs of each tissue, cell type and developmental stage. Nevertheless, some of them have overlapping function and when expressed in the same cell they can compensate for each other.This delicate combination of role allocation and cooperation makes the reduced or lost function of a single P4-ATPase not lethal. Despite the ubiquitous expression of low levels of most P4-ATPases most tissues are not affected, either because they do not use that ATPase as their main flippase for a specific function or the loss can be compensated by another one that is also expressed. However, if the defect P4-ATPase is essential for the cell type, several pathomechanisms depending on the specific role can emerge.

Human ATP11A translocates PS and PE from the exoplasmic to the cytoplasmic leaflet of the plasma membrane and is expressed in most tissues to some extend, but not necessarily as the main PS transporting flippase, while in the kidney it was found to act almost as a solo PS flippase. High similarities between the kidney and inner ear development during early embryogenesis and subsequent resemblance in structure and functionality indicate a similar expression pattern for P4-ATPases, too. This may explain sensorineural hearing loss deriving from the hATP11A hypoactivity in the patients. Possibly the inner ear cells are even more dependent on hATP11A compared to renal cells. That would justify the lack of a renal phenotype in all of the affected patients except patient 9 and indicate why even a heterozygous reduction of hATP11A function is sufficient to cause hearing loss, while other P4-ATPase related diseases are only caused by homozygous or hemizygous mutations most of the time. A proteomic analysis of the expressed P4-ATPases and the relative expression pattern through the developmental stages of inner ear cells, as well as knowledge about the specific phospholipid composition and distribution of their plasma membrane would be useful for more accurate hypothesis and targeted experiments.

The cell dependent fine tuning of flippase activity can also be estimated by the differing extent of PS exposure on the cell surface in cells deficient of a P4-ATPase. While some cells types only show diminished flippase activity, but no major changes in the phospholipid asymmetry of the plasma membrane, other cell types are more prone to expose PS at certain developmental stages or even accumulate PS in the exoplasmic leaflet all the time. Those differences become not only obvious between different cell types, but also between species with variation in the P4-ATPase expression pattern. Therefore, deduction from other ATPases, cell types or model organisms, might not be accurate to speculate on the effect that partial loss of hATP11A activity has on PS exposure of auditory cells.

In any case, there are findings that exposure of PS in neurons and at the apical site of hair cells did not lead to apoptosis. Moreover, studies of different PS flipping P4-ATPases conclusively show that suppression of apoptosis in flippase deficient cells did not alter any phenotype. Hence it can be assumed that the direct induction of apoptosis does not cause the progressive hearing loss.

Also the interference with intracellular transport, as proposed for the ATP8A1 and ATP8A2 loss of function phenotype, does not seem to be the reason for hATP11A based hearing loss, since *ATP11A* WT and the mutant variant do not localise to endosomes and the TGN in the presence of CDC50A, as shown with the ICC stainings. Thus, a direct involvement in intracellular transport is unlikely.

Nevertheless, an altered PS distribution in the plasma membrane could influence the balance between axon degeneration and regeneration or endo- and exocytosis , as well as the functionality of Ca^{2+} transporters and the cell shape and stability. In addition PS is also thought to interact with other cytoplasmic and membrane bound proteins involved with signalling in the cytoplasmic leaflet. This opens a broad field of possible ways in which normal cellular function and thus hearing could be disturbed.

In order to identify which of the discussed pathomechanism causes the progressive AS/AN of the patients, an in vivo model, for example a mouse model, may be applied. The most obvious question to adress is the PS distribution across the membrane, which may be answered by comprehensive annexin V staining of inner ear cross sections of WT and ATP11A deficient mice. Comparative cross sections at multiple ages can furthermore be used for a general inspection of morphological differences and cell loss of inner ear cells. This could help to define the start of a possible degeneration, pinpoint to the cells that are initially affected and characterise the progressive development.

Although further research of the molecular and cellular consequences and the discussed pathomechanism of diminished hATP11A function in the human inner ear is needed, this thesis was able to characterise a pathological splice variant of *hATP11A* caused by a 5,500 bp deletion in a family with sensorineural hearing loss and demonstrate its hypoactive PS flippase function. In addition it was possible to gather some insights on the regulatory mechanism that is suspected to give rise to the reduction of flippase activity through comparison with another C-terminally truncated variant.

Determination of the primarily affected cells and the progression of this specific hearing loss phenotype would lead to a better understanding of this novel pathomechanism. With the identification of the role of hATP11A in auditory function, further awareness of the general molecular mechanism of hearing will be achieved. The examination of a specific genetic defect in a family with AS/AN results in basic insights in inner ear physiology. Detailed knowledge of the different factors that are involved in hearing will be implemented in developing more personalised medical and social treatment of patients with AS/AN in the future.

Bibliography

[1] B. L. Aken, P. Achuthan, W. Akanni, M. R. Amode, F. Bernsdorff, J. Bhai, K. Billis, D. Carvalho-Silva, C. Cummins, P. Clapham, *et al.* Ensembl 2017. *Nucleic acids research*, 45(D1):D635–D642, 2017.

[2] J. P. Andersen, A. L. Vestergaard, S. A. Mikkelsen, L. S. Mogensen, M. Chalat, and R. S. Molday. P4-atpases as phospholipid flippases - structure, function, and enigmas. *Frontiers in physiology*, 7:275, 2016.

[3] H. A. Anderson, C. A. Maylock, J. A. Williams, C. P. Paweletz, H. Shu, and E. Shacter. Serum-derived protein s binds to phosphatidylserine and stimulates the phagocytosis of apoptotic cells. *Nature immunology*, 4(1): 87–91, 2003.

[4] H.-J. Apell. How do p-type atpases transport ions? *Bioelectrochemistry*, 63(1-2):149–156, 2004.

[5] N. Arashiki, Y. Takakuwa, N. Mohandas, J. Hale, K. Yoshida, H. Ogura, T. Utsugisawa, S. Ohga, S. Miyano, S. Ogawa, *et al.* Atp11c is a major flippase in human erythrocytes and its defect causes congenital hemolytic anemia. *Haematologica*, 101(5):559–565, 2016.

[6] S. Arlinger. Negative consequences of uncorrected hearing loss-a review. *International journal of audiology*, 42:2S17–2S20, 2003.

[7] J. Attias and E. Raveh. Transient deafness in young candidates for cochlear implants. *Audiology and Neurotology*, 12(5):325–333, 2007.

[8] K. B. Avraham, T. Hasson, K. P. Steel, D. M. Kingsley, L. B. Russell, M. S. Mooseker, N. G. Copeland, and N. A. Jenkins. The mouse snell's waltzer deafness gene encodes an unconventional myosin required for structural integrity of inner ear hair cells. *Nature genetics*, 11(4):369–375, 1995.

[9] Axelsen, Kristian B. P-Type ATPase Database. URL `http://traplabs.dk/patbase/`.

[10] L. Bai, A. Kovach, Q. You, H.-C. Hsu, G. Zhao, and H. Li. Autoinhibition and activation mechanisms of the eukaryotic lipid flippase drs2p-cdc50p. *Nature communications*, 10(1):1–10, 2019.

[11] J. Bell. A simple way to treat PCR products prior to sequencing using ExoSAP-IT. *BioTechniques*, 44, 2008.

[12] C. Berezin, F. Glaser, J. Rosenberg, I. Paz, T. Pupko, P. Fariselli, R. Casadio, and N. Ben-Tal. Conseq: the identification of functionally and structurally important residues in protein sequences. *Bioinformatics*, 20(8): 1322–1324, 2004.

[13] A. L. Berg, J. B. Spitzer, H. M. Towers, C. Bartosiewicz, and B. E. Diamond. Newborn hearing screening in the nicu: profile of failed auditory brainstem response/passed otoacoustic emission. *Pediatrics*, 116(4):933–938, 2005.

[14] A. Berglund and D. K. Ryugo. Hair cell innervation by spiral ganglion neurons in the mouse. *Journal of Comparative Neurology*, 255(4):560–570, 1987.

[15] C. I. Berlin, L. J. Hood, T. Morlet, D. Wilensky, L. Li, K. R. Mattingly, J. Taylor-Jeanfreau, B. J. Keats, P. S. John, E. Montgomery, *et al.* Multi-site diagnosis and management of 260 patients with auditory neuropathy/dys-synchrony (auditory neuropathy spectrum disorder*). *International journal of audiology*, 49(1):30–43, 2010.

[16] J. T. Best, P. Xu, and T. R. Graham. Phospholipid flippases in membrane remodeling and transport carrier biogenesis. *Current opinion in cell biology*, 59:8–15, 2019.

[17] M. Beurg, N. Michalski, S. Safieddine, Y. Bouleau, R. Schneggenburger, E. R. Chapman, C. Petit, and D. Dulon. Control of exocytosis by synaptotagmins and otoferlin in auditory hair cells. *Journal of Neuroscience*, 30(40):13281–13290, 2010.

[18] M. Bitbol, P. Fellmann, A. Zachowski, and P. F. Devaux. Ion regulation of phosphatidylserine and phosphatidylethanolamine outside-inside translocation in human erythrocytes. *Biochimica et Biophysica Acta (BBA)-Biomembranes*, 904(2):268–282, 1987.

[19] N. Blom, T. Sicheritz-Pontén, R. Gupta, S. Gammeltoft, and S. Brunak. Prediction of post-translational glycosylation and phosphorylation of proteins from the amino acid sequence. *Proteomics*, 4(6):1633–1649, 2004.

[20] P. Bonfils and A. Uziel. Clinical applications of evoked acoustic emissions: results in normally hearing and hearing-impaired subjects. *Annals of Otology, Rhinology & Laryngology*, 98(5):326–331, 1989.

[21] F. G. Bowe, B. T. McMahon, T. Chang, and I. Louvi. Workplace discrimination, deafness and hearing impairment: The national eeoc ada research project. *Work*, 25(1):19–25, 2005.

[22] M. C. Brown. Morphology of labeled afferent fibers in the guinea pig cochlea. *Journal of Comparative Neurology*, 260(4):591–604, 1987.

[23] M. Bublitz, J. P. Morth, and P. Nissen. P-type atpases at a glance. *J Cell Sci*, 124(15):2515–2519, 2011.

[24] C. A. Buchman, P. A. Roush, H. F. Teagle, C. J. Brown, C. J. Zdanski, and J. H. Grose. Auditory neuropathy characteristics in children with cochlear nerve deficiency. *Ear and hearing*, 27(4):399–408, 2006.

[25] L. N. Bull, M. J. van Eijk, L. Pawlikowska, J. A. DeYoung, J. A. Juijn, M. Liao, L. W. Klomp, N. Lomri, R. Berger, B. R. Scharschmidt, *et al.* A gene encoding a p-type atpase mutated in two forms of hereditary cholestasis. *Nature genetics*, 18(3):219, 1998.

[26] M. Busslinger. Transcriptional control of early b cell development. *Annu. Rev. Immunol.*, 22:55–79, 2004.

[27] D. Butinar, A. Starr, J. Zidar, P. Koutsou, and K. Christodoulou. Auditory nerve is affected in one of two different point mutations of the neurofilament light gene. *Clinical Neurophysiology*, 119(2):367–375, 2008.

[28] P. Cacciagli, M.-R. Haddad, C. Mignon-Ravix, B. El-Waly, A. Moncla, C. Missirian, B. Chabrol, and L. Villard. Disruption of the atp8a2 gene in a patient with at (10; 13) de novo balanced translocation and a severe neurological phenotype. *European journal of human genetics*, 18 (12):1360–1363, 2010.

[29] S.-Y. Cai, S. Gautam, T. Nguyen, C. J. Soroka, C. Rahner, and J. L. Boyer. Atp8b1 deficiency disrupts the bile canalicular membrane bilayer structure in hepatocytes, but fxr expression and activity are maintained. *Gastroenterology*, 136(3):1060–1069, 2009.

[30] M. Chalat, K. Moleschi, and R. S. Molday. C-terminus of the p4-atpase atp8a2 functions in protein folding and regulation of phospholipid flippase activity. *Molecular Biology of the Cell*, 28(3):452–462, 2017.

[31] C.-Y. Chen, M. F. Ingram, P. H. Rosal, and T. R. Graham. Role for drs2p, a p-type atpase and potential aminophospholipid translocase, in yeast late golgi function. *The Journal of cell biology*, 147(6):1223–1236, 1999.

[32] F. Chen, E. Ellis, S. C. Strom, and B. L. Shneider. Atpase class i type 8b member 1 and protein kinase c ζ induce the expression of the canalicular bile salt export pump in human hepatocytes. *Pediatric research*, 67(2): 183, 2010.

[33] M. A. Chen, P. Webster, E. Yang, and F. H. Linthicum Jr. Presbycusic neuritic degeneration within the osseous spiral lamina. *Otology & Neurotology*, 27(3):316–322, 2006.

[34] T. Y. Ching, J. Day, H. Dillon, K. Gardner-Berry, S. Hou, M. Seeto, A. Wong, and V. Zhang. Impact of the presence of auditory neuropathy spectrum disorder (ansd) on outcomes of children at three years of age. *International journal of audiology*, 52(sup2):S55–S64, 2013.

[35] J. A. Coleman and R. S. Molday. Critical role of the β-subunit cdc50a in the stable expression, assembly, subcellular localization, and lipid transport activity of the p4-atpase atp8a2. *Journal of Biological Chemistry*, 286(19):17205–17216, 2011.

[36] J. A. Coleman, M. C. Kwok, and R. S. Molday. Localization, purification, and functional reconstitution of the p4-atpase atp8a2, a phosphatidylserine flippase in photoreceptor disc membranes. *Journal of Biological Chemistry*, 284(47):32670–32679, 2009.

[37] J. A. Coleman, X. Zhu, H. R. Djajadi, L. L. Molday, R. S. Smith, R. T. Libby, S. W. John, and R. S. Molday. Phospholipid flippase atp8a2 is required for normal visual and auditory function and photoreceptor and spiral ganglion cell survival. *J Cell Sci*, 127(5):1138–1149, 2014.

[38] R. W. Collin, E. Kalay, J. Oostrik, R. Caylan, B. Wollnik, S. Arslan, A. I. Den Hollander, Y. Birinci, P. Lichtner, T. M. Strom, *et al.* Involvement of dfnb59 mutations in autosomal recessive nonsyndromic hearing impairment. *Human mutation*, 28(7):718–723, 2007.

[39] Cologne Center for Genomics. 5 × BigDye BDT sequencing buffer, 2010. URL `http://portal.ccg.uni-koeln.de/ccg/assets/templates/doc/service/BDT_5x_buffer.pdf`.

[40] K. O. De Beeck, G. Van Camp, S. Thys, N. Cools, I. Callebaut, K. Vrijens, L. Van Nassauw, V. F. Van Tendeloo, J. P. Timmermans, and L. Van Laer. The dfna5 gene, responsible for hearing loss and involved in cancer, encodes a novel apoptosis-inducing protein. *European Journal of Human Genetics*, 19(9):965, 2011.

[41] D. R. de Waart, J. Naik, K. S. Utsunomiya, S. Duijst, K. Ho-Mok, A. R. Bolier, J. Hiralall, L. N. Bull, P. J. Bosma, R. P. Oude Elferink, *et al.* Atp11c targets basolateral bile salt transporter proteins in mouse central hepatocytes. *Hepatology*, 64(1):161–174, 2016.

[42] J. Defourny, F. Lallemend, and B. Malgrange. Structure and development of cochlear afferent innervation in mammals. *American Journal of Physiology-Cell Physiology*, 301(4):C750–C761, 2011.

[43] P. Deltenre, A.-L. Mansbach, C. Bozet, F. Christiaens, P. Barthelemy, D. Paulissen, and T. Renglet. Auditory neuropathy with preserved cochlear microphonics and secondary loss of otoacoustic emissions. *Audiology*, 38(4):187–195, 1999.

[44] F.-O. Desmet, D. Hamroun, M. Lalande, G. Collod-Béroud, M. Claustres, and C. Béroud. Human splicing finder: an online bioinformatics tool to predict splicing signals. *Nucleic Acids Research*, 37(9), 2009.

[45] P. F. Devaux, A. Herrmann, N. Ohlwein, and M. M. Kozlov. How lipid flippases can modulate membrane structure. *Biochimica et Biophysica Acta (BBA)-Biomembranes*, 1778(7-8):1591–1600, 2008.

[46] M. S. Dhar, J. S. Yuan, S. B. Elliott, and C. Sommardahl. A type iv p-type atpase affects insulin-mediated glucose uptake in adipose tissue and skeletal muscle in mice. *The Journal of nutritional biochemistry*, 17(12): 811–820, 2006.

[47] P. H. Dixon, M. Sambrotta, J. Chambers, P. Taylor-Harris, A. Syngelaki, K. Nicolaides, A. Knisely, R. J. Thompson, and C. Williamson. An expanded role for heterozygous mutations of abcb4, abcb11, atp8b1, abcc2 and tjp2 in intrahepatic cholestasis of pregnancy. *Scientific Reports*, 7(1): 1–8, 2017.

[48] H. Dodson and M. Charalabapoulou. Pmca2 mutation causes structural changes in the auditory system in deafwaddler mice. *Journal of neurocytology*, 30(4):281–292, 2001.

[49] A. A. Dror and K. B. Avraham. Hearing loss: mechanisms revealed by genetics and cell biology. *Annual review of genetics*, 43:411–437, 2009.

[50] R. A. Dumont, U. Lins, A. G. Filoteo, J. T. Penniston, B. Kachar, and P. G. Gillespie. Plasma membrane ca2+-atpase isoform 2a is the pmca of hair bundles. *Journal of Neuroscience*, 21(14):5066–5078, 2001.

[51] I. Ebermann, M. Walger, H. P. Scholl, P. C. Issa, C. Lüke, G. Nürnberg, R. Lang-Roth, C. Becker, P. Nürnberg, and H. J. Bolz. Truncating mutation of the dfnb59 gene causes cochlear hearing impairment and central vestibular dysfunction. *Human mutation*, 28(6):571–577, 2007.

[52] S. M. Echteler. Developmental segregation in the afferent projections to mammalian auditory hair cells. *Proceedings of the National Academy of Sciences*, 89(14):6324–6327, 1992.

[53] S. M. Echteler, T. Magardino, and M. Rontal. Spatiotemporal patterns of neuronal programmed cell death during postnatal development of the gerbil cochlea. *Developmental brain research*, 157(2):192–200, 2005.

[54] H. Egawa, T. Yorifuji, R. Sumazaki, A. Kimura, M. Hasegawa, and K. Tanaka. Intractable diarrhea after liver transplantation for byler's disease: successful treatment with bile adsorptive resin. *Liver transplantation*, 8(8):714–716, 2002.

[55] O. K. Egilmez and M. T. Kalcioglu. Genetics of nonsyndromic congenital hearing loss. *Scientifica*, 2016, 2016.

[56] C. Elberling and J. Parbo. Reference data for abrs in retrocochlear diagnosis. *Scandinavian Audiology*, 16(1):49–55, 1987.

[57] O. Emanuelsson, H. Nielsen, S. Brunak, G. Von Heijne, *et al.* Predicting subcellular localization of proteins based on their n-terminal amino acid sequence. *Journal of molecular biology*, 300(4):1005–1016, 2000.

[58] O. Emre Onat, S. Gulsuner, K. Bilguvar, A. Nazli Basak, H. Topaloglu, M. Tan, U. Tan, M. Gunel, and T. Ozcelik. Missense mutation in the atpase, aminophospholipid transporter protein atp8a2 is associated with cerebellar atrophy and quadrupedal locomotion. *European Journal of Human Genetics*, 21(3), 2013.

[59] A. Endo, T. Fuchigami, M. Hasegawa, K. Hashimoto, Y. Fujita, Y. Inamo, and H. Mugishima. Posterior reversible encephalopathy syndrome in childhood: report of four cases and review of the literature. *Pediatric emergency care*, 28(2):153–157, 2012.

[60] E. F. Eppens, S. W. van Mil, J. M. L. de Vree, K. S. Mok, J. A. Juijn, R. P. O. Elferink, R. Berger, R. H. Houwen, and L. W. Klomp. Fic1, the protein affected in two forms of hereditary cholestasis, is localized in the cholangiocyte and the canalicular membrane of the hepatocyte. *Journal of hepatology*, 35(4):436–443, 2001.

[61] M. C. B. N. Esteves, A. H. B. Dell'Aringa, G. V. Arruda, A. R. Dell'Aringa, and J. C. Nardi. Brainstem evoked response audiometry in normal hearing subjects. *Brazilian journal of otorhinolaryngology*, 75 (3):420–425, 2009.

[62] G. D. Fairn, M. Hermansson, P. Somerharju, and S. Grinstein. Phosphatidylserine is polarized and required for proper cdc42 localization and for development of cell polarity. *Nature cell biology*, 13(12):1424–1430, 2011.

[63] E. Farge, D. M. Ojcius, A. Subtil, and A. Dautry-Varsat. Enhancement of endocytosis due to aminophospholipid transport across the plasma membrane of living cells. *American Journal of Physiology-Cell Physiology*, 276 (3):C725–C733, 1999.

[64] M. J. Fath and R. Kolter. Abc transporters: bacterial exporters. *Microbiology and Molecular Biology Reviews*, 57(4):995–1017, 1993.

[65] R. E. Feirn, G. Sutton, G. Parker, T. Sirimanna, G. Lightfoot, and S. Wood. Newborn hearing screening and assessment: Guidelines for the assessment and management of auditory neuropathy spectrum disorder in young infants. version 2.2. *NHSP Clinical Group*, 2013.

[66] C. V. Finkielstein, M. Overduin, and D. G. Capelluto. Cell migration and signaling specificity is determined by the phosphatidylserine recognition motif of rac1. *Journal of Biological Chemistry*, 281(37):27317–27326, 2006.

[67] S. Flamant, P. Pescher, B. Lemercier, M. Clement-Ziza, F. Képès, M. Fellous, G. Milon, G. Marchal, and C. Besmond. Characterization of a putative type iv aminophospholipid transporter p-type atpase. *Mammalian genome*, 14(1):21–30, 2003.

[68] A. Florentin and E. Arama. Caspase levels and execution efficiencies determine the apoptotic potential of the cell. *Journal of Cell Biology*, 196 (4):513–527, 2012.

[69] D. E. Folmer, V. A. van der Mark, K. S. Ho-Mok, R. P. Oude Elferink, and C. C. Paulusma. Differential effects of progressive familial intrahepatic cholestasis type 1 and benign recurrent intrahepatic cholestasis type 1 mutations on canalicular localization of atp8b1. *Hepatology*, 50(5):1597–1605, 2009.

[70] D. A. Fruman and L. C. Cantley. Phosphoinositide 3-kinase in immunological systems. In *Seminars in immunology*, volume 14, pages 7–18. Elsevier, 2002.

[71] R. D. Ginzberg and D. K. Morest. Fine structure of cochlear innervation in the cat. *Hearing research*, 14(2):109–127, 1984.

[72] E. Glowatzki, N. Cheng, H. Hiel, E. Yi, K. Tanaka, G. C. Ellis-Davies, J. D. Rothstein, and D. E. Bergles. The glutamate–aspartate transporter glast mediates glutamate uptake at inner hair cell afferent synapses in the mammalian cochlea. *Journal of Neuroscience*, 26(29):7659–7664, 2006.

[73] E. M. Z. Golumbic, D. Poeppel, and C. E. Schroeder. Temporal context in speech processing and attentional stream selection: a behavioral and neural perspective. *Brain and language*, 122(3):151–161, 2012.

[74] R. Goodyear, P. Legan, M. Wright, W. Marcotti, A. Oganesian, S. Coats, C. Booth, C. Kros, R. Seifert, D. Bowen-Pope, *et al.* A receptor-like inositol lipid phosphatase is required for the maturation of developing cochlear hair bundles. *Journal of Neuroscience*, 23(27):9208–9219, 2003.

[75] A. Goossens, N. de la Fuente, J. Forment, R. Serrano, and F. Portillo. Regulation of yeast h+-atpase by protein kinases belonging to a family dedicated to activation of plasma membrane transporters. *Molecular and cellular biology*, 20(20):7654–7661, 2000.

[76] R. J. Gorlin, R. J. Gorlin, H. V. Toriello, and M. M. Cohen. *Hereditary hearing loss and its syndromes*. Number 28. Oxford University Press, USA, 1995.

[77] D. K. Graham, D. DeRyckere, K. D. Davies, and H. S. Earp. The tam family: phosphatidylserine-sensing receptor tyrosine kinases gone awry in cancer. *Nature reviews Cancer*, 14(12):769–785, 2014.

[78] T. R. Graham. Flippases and vesicle-mediated protein transport. *Trends in cell biology*, 14(12):670–677, 2004.

[79] M. Grati, M. E. Schneider, K. Lipkow, E. E. Strehler, R. J. Wenthold, and B. Kachar. Rapid turnover of stereocilia membrane proteins: evidence from the trafficking and mobility of plasma membrane ca2+-atpase 2. *Journal of Neuroscience*, 26(23):6386–6395, 2006.

[80] C. Griesinger, C. Richards, and J. Ashmore. Apical endocytosis in outer hair cells of the mammalian cochlea. *European Journal of Neuroscience*, 20(1):41–50, 2004.

[81] C. B. Griesinger, C. D. Richards, and J. F. Ashmore. Fm1-43 reveals membrane recycling in adult inner hair cells of the mammalian cochlea. *Journal of Neuroscience*, 22(10):3939–3952, 2002.

[82] J. Gromada and P. Rorsman. New insights into the regulation of glucagon secretion by glucagon-like peptide-1. *Hormone and metabolic research*, 36 (11/12):822–829, 2004.

[83] J. W. Gu, B. S. Herrmann, R. A. Levine, and J. R. Melcher. Brainstem auditory evoked potentials suggest a role for the ventral cochlear nucleus in tinnitus. *Journal of the Association for Research in Otolaryngology*, 13 (6):819–833, 2012.

[84] J. Hall. Application of abr in objective assessment of infant hearing. *Audiology Online [internet]*, 2013.

[85] J. W. Hall, S. D. Smith, and G. R. Popelka. Newborn hearing screening with combined otoacoustic emissions and auditory brainstem responses. *Journal of the American Academy of Audiology*, 15(6):414–425, 2004.

[86] Hamburg University. Homepage of Hamburg University, 2016. URL `www.uni-hamburg.de`.

[87] N. Hams, M. Padmanarayana, W. Qiu, and C. P. Johnson. Otoferlin is a multivalent calcium-sensitive scaffold linking snares and calcium channels. *Proceedings of the National Academy of Sciences*, page 201703240, 2017.

[88] R. Hanayama, M. Tanaka, K. Miwa, A. Shinohara, A. Iwamatsu, and S. Nagata. Identification of a factor that links apoptotic cells to phagocytes. *Nature*, 417(6885):182–187, 2002.

[89] H. M. Hankins, R. D. Baldridge, P. Xu, and T. R. Graham. Role of flippases, scramblases and transfer proteins in phosphatidylserine subcellular distribution. *Traffic*, 16(1):35–47, 2015.

[90] J. Hans. The auditory system. In *Clinical Neuroanatomy*, pages 305–329. Springer, 2011.

[91] V. Haucke and G. Di Paolo. Lipids and lipid modifications in the regulation of membrane traffic. *Current opinion in cell biology*, 19(4):426–435, 2007.

[92] R. Hawkins, H. Jansen, and S. Sanyal. Development and degeneration of retina in rds mutant mice: photoreceptor abnormalities in the heterozygotes. *Experimental eye research*, 41(6):701–720, 1985.

[93] D. Hayes, Y. Sininger, and J. Northern. Guidelines for identification and management of infants and young children with auditory neuropathy spectrum disorder. *The Children's Hospital, Colorado, USA, Bill Daniels Center for Children's Hearing*, 2008.

[94] E. Hessel, A. Herrmann, P. Müller, P. P. Schnetkamp, and K.-P. Hofmann. The transbilayer distribution of phospholipids in disc membranes is a dynamic equilibrium: evidence for rapid flip and flop movement. *European Journal of Biochemistry*, 267(5):1473–1483, 2000.

[95] A. E. Hickox and M. C. Liberman. Is noise-induced cochlear neuropathy key to the generation of hyperacusis or tinnitus? *Journal of neurophysiology*, 111(3):552–564, 2013.

[96] H. N. Higgs. Formin proteins: a domain-based approach. *Trends in biochemical sciences*, 30(6):342–353, 2005.

[97] M. Hiraizumi, K. Yamashita, T. Nishizawa, and O. Nureki. Cryo-em structures capture the transport cycle of the p4-atpase flippase. *Science*, 365(6458):1149–1155, 2019.

[98] M. Hirono, C. S. Denis, G. P. Richardson, and P. G. Gillespie. Hair cells require phosphatidylinositol 4, 5-bisphosphate for mechanical transduction and adaptation. *Neuron*, 44(2):309–320, 2004.

[99] N. Hisamoto, A. Tsuge, S. I. Pastuhov, T. Shimizu, H. Hanafusa, and K. Matsumoto. Phosphatidylserine exposure mediated by abc transporter activates the integrin signaling pathway promoting axon regeneration. *Nature communications*, 9(1):1–11, 2018.

[100] L.-C. Huang, P. R. Thorne, G. D. Housley, and J. M. Montgomery. Spatiotemporal definition of neurite outgrowth, refinement and retraction in the developing mouse cochlea. *Development*, 134(16):2925–2933, 2007.

[101] M. M. Humphries, D. Rancourt, G. J. Farrar, P. Kenna, M. Hazel, R. A. Bush, P. A. Sieving, D. M. Sheils, P. Creighton, A. Erven, *et al.* Retinopathy induced in mice by targeted disruption of the rhodopsin gene. *Nature genetics*, 15(2):216–219, 1997.

[102] H. Izzedine, F. Tankere, V. Launay-Vacher, and G. Deray. Ear and kidney syndromes: molecular versus clinical approach. *Kidney international*, 65 (2):369–385, 2004.

[103] E. Jacquemin, V. Malan, M. Rio, A. Davit-Spraul, J. Cohen, P. Landrieu, and O. Bernard. Heterozygous fic1 deficiency: a new genetic predisposition to transient neonatal cholestasis. *Journal of pediatric gastroenterology and nutrition*, 50(4):447–449, 2010.

[104] T. Janssen. A review of the effectiveness of otoacoustic emissions for evaluating hearing status after newborn screening. *Otology & Neurotology*, 34(6):1058–1063, 2013.

[105] O. Jardetzky. Simple allosteric model for membrane pumps. *Nature*, 211 (5052):969–970, 1966.

[106] P. L. Jørgensen and J. Petersen. Purification and characterization of (na+, k+)-atpase. v. conformational changes in the enzyme. transitions between the na-form and the k-form studied with tryptic digestion as a tool. *Biochimica et Biophysica Acta (BBA)-Biomembranes*, 401(3):399–415, 1975.

[107] J. M. Juraska and J. Willing. Pubertal onset as a critical transition for neural development and cognition. *Brain Research*, 1654:87–94, 2017.

[108] K. J. Karczewski, L. C. Francioli, G. Tiao, B. B. Cummings, J. Alföldi, Q. Wang, R. L. Collins, K. M. Laricchia, A. Ganna, D. P. Birnbaum, *et al.* The mutational constraint spectrum quantified from variation in 141,456 humans. *bioRxiv*, page 531210, 2020.

[109] M. Kazmierczak, P. Kazmierczak, A. W. Peng, S. L. Harris, P. Shah, J.-L. Puel, M. Lenoir, S. J. Franco, and M. Schwander. Pejvakin, a candidate stereociliary rootlet protein, regulates hair cell function in a cell-autonomous manner. *Journal of Neuroscience*, 37(13):3447–3464, 2017.

[110] D. T. Kemp. Otoacoustic emissions, their origin in cochlear function, and use. *British medical bulletin*, 63(1):223–241, 2002.

[111] C. R. Kennedy. Neonatal screening for hearing impairment. *Archives of disease in childhood*, 83(5):377–383, 2000.

[112] W. J. Kent, C. W. Sugnet, T. S. Furey, K. M. Roskin, T. H. Pringle, A. M. Zahler, and D. Haussler. The human genome browser at ucsc. *Genome research*, 12(6):996–1006, 2002.

[113] Kent, WJ and others. UCSC Genome Browser. URL `https://genome.ucsc.edu/`.

[114] T. B. Kim, B. Isaacson, T. A. Sivakumaran, A. Starr, B. J. Keats, and M. M. Lesperance. A gene responsible for autosomal dominant auditory neuropathy (auna1) maps to 13q14–21. *Journal of medical genetics*, 41 (11):872–876, 2004.

[115] L. W. Klomp, J. C. Vargas, S. W. van Mil, L. Pawlikowska, S. S. Strautnieks, M. J. van Eijk, J. A. Juijn, C. Pabón-Peña, L. B. Smith, J. A. DeYoung, *et al.* Characterization of mutations in atp8b1 associated with hereditary cholestasis. *Hepatology*, 40(1):27–38, 2004.

[116] A. Konings, L. Van Laer, A. Wiktorek-Smagur, E. Rajkowska, M. Pawelczyk, P. Carlsson, M.-L. Bondeson, A. Dudarewicz, A. Vandevelde, E. Fransen, *et al.* Candidate gene association study for noise-induced hearing loss in two independent noise-exposed populations. *Annals of human genetics*, 73(2):215–224, 2009.

[117] P. J. Kozel, R. A. Friedman, L. C. Erway, E. N. Yamoah, L. H. Liu, T. Riddle, J. J. Duffy, T. Doetschman, M. L. Miller, E. L. Cardell, *et al.* Balance and hearing deficits in mice with a null mutation in the gene encoding plasma membrane ca2+-atpase isoform 2. *Journal of Biological Chemistry*, 273(30):18693–18696, 1998.

[118] N. Kraus and T. Nicol. Auditory evoked potentials. In *Encyclopedia of neuroscience*, pages 214–218. Springer, 2008.

[119] W. Kühlbrandt, J. Zeelen, and J. Dietrich. Structure, mechanism, and regulation of the neurospora plasma membrane h+-atpase. *Science*, 297 (5587):1692–1696, 2002.

[120] S. G. Kujawa and M. C. Liberman. Adding insult to injury: cochlear nerve degeneration after "temporary" noise-induced hearing loss. *Journal of Neuroscience*, 29(45):14077–14085, 2009.

[121] K. Kurima, L. M. Peters, Y. Yang, S. Riazuddin, Z. M. Ahmed, S. Naz, D. Arnaud, S. Drury, J. Mo, T. Makishima, *et al.* Dominant and recessive deafness caused by mutations of a novel gene, tmc1, required for cochlear hair-cell function. *Nature genetics*, 30(3):277–284, 2002.

[122] R. M. La Rovere, G. Roest, G. Bultynck, and J. B. Parys. Intracellular ca2+ signaling and ca2+ microdomains in the control of cell survival, apoptosis and autophagy. *Cell calcium*, 60(2):74–87, 2016.

[123] H. Lage, H. Helmbach, C. Grottke, M. Dietel, and D. Schadendorf. Dfna5 (icere-1) contributes to acquired etoposide resistance in melanoma cells. *FEBS letters*, 494(1-2):54–59, 2001.

[124] R. Lang-Roth, E. Fischer-Krall, C. Kornblum, G. Nürnberg, D. Meschede, I. Goebel, P. Nürnberg, D. Beutner, C. Kubisch, M. Walger, *et al.* Auna2: A novel type of non-syndromic slowly progressive auditory synaptopathy/auditory neuropathy with autosomal-dominant inheritance. *Audiology and Neurotology*, 22(1):30–40, 2017.

[125] J. Lasak, P. Allen, T. McVay, and D. Lewis. Hearing loss: diagnosis and management. *Primary care*, 41(1):19–31, 2014.

[126] M. M. LaVail. Rod outer segment disk shedding in rat retina: relationship to cyclic lighting. *Science*, 194(4269):1071–1074, 1976.

[127] S. Lee, Y. Uchida, J. Wang, T. Matsudaira, T. Nakagawa, T. Kishimoto, K. Mukai, T. Inaba, T. Kobayashi, R. S. Molday, *et al.* Transport through recycling endosomes requires ehd1 recruitment by a phosphatidylserine translocase. *The EMBO journal*, 34(5):669–688, 2015.

[128] G. Lemke. Biology of the tam receptors. *Cold Spring Harbor perspectives in biology*, 5(11):a009076, 2013.

[129] M. A. Lemmon. Membrane recognition by phospholipid-binding domains. *Nature reviews Molecular cell biology*, 9(2):99–111, 2008.

[130] G. Lenoir, P. Williamson, C. F. Puts, and J. C. Holthuis. Cdc50p plays a vital role in the atpase reaction cycle of the putative aminophospholipid transporter drs2p. *Journal of biological chemistry*, 284(27):17956–17967, 2009.

[131] K. Levano, V. Punia, M. Raghunath, P. R. Debata, G. M. Curcio, A. Mogha, S. Purkayastha, D. McCloskey, J. Fata, and P. Banerjee. Atp8a1 deficiency is associated with phosphatidylserine externalization in hippocampus and delayed hippocampus-dependent learning. *Journal of neurochemistry*, 120(2):302–313, 2012.

[132] H. Li, S. Wetten, L. Li, P. L. S. Jean, R. Upmanyu, L. Surh, D. Hosford, M. R. Barnes, J. D. Briley, M. Borrie, *et al.* Candidate single-nucleotide polymorphisms from a genomewide association study of alzheimer disease. *Archives of neurology*, 65(1):45–53, 2008.

[133] M. C. Liberman. The cochlear frequency map for the cat: Labeling auditory-nerve fibers of known characteristic frequency. *The Journal of the Acoustical Society of America*, 72(5):1441–1449, 1982.

[134] Life Technologies Corporation. *NuPAGE Technical Guide*, 2010.

[135] K. Liu, K. Surendhran, S. F. Nothwehr, and T. R. Graham. P4-atpase requirement for ap-1/clathrin function in protein transport from the trans-golgi network and early endosomes. *Molecular biology of the cell*, 19(8): 3526–3535, 2008.

[136] P. Lykavieris, S. van Mil, D. Cresteil, M. Fabre, M. Hadchouel, L. Klomp, O. Bernard, and E. Jacquemin. Progressive familial intrahepatic cholestasis type 1 and extrahepatic features: no catch-up of stature growth, exacerbation of diarrhea, and appearance of liver steatosis after liver transplantation. *Journal of hepatology*, 39(3):447–452, 2003.

[137] C. Madden, L. Hilbert, M. Rutter, J. Greinwald, and D. Choo. Pediatric cochlear implantation in auditory neuropathy. *Otology & Neurotology*, 23 (2):163–168, 2002.

[138] F. Madeira, Y. M. Park, J. Lee, N. Buso, T. Gur, N. Madhusoodanan, P. Basutkar, A. R. Tivey, S. C. Potter, R. D. Finn, *et al.* The embl-ebi search and sequence analysis tools apis in 2019. *Nucleic acids research*, 47(W1):W636–W641, 2019.

[139] G. Manfioletti, C. Brancolini, G. Avanzi, and C. Schneider. The protein encoded by a growth arrest-specific gene (gas6) is a new member of the vitamin k-dependent proteins related to protein s, a negative coregulator in the blood coagulation cascade. *Molecular and cellular biology*, 13(8): 4976–4985, 1993.

[140] S. Manno, Y. Takakuwa, and N. Mohandas. Identification of a functional role for lipid asymmetry in biological membranes: Phosphatidylserine-skeletal protein interactions modulate membrane stability. *Proceedings of the National Academy of Sciences*, 99(4):1943–1948, 2002.

[141] R. Marsault, M. Murgia, T. Pozzan, and R. Rizzuto. Domains of high ca2+ beneath the plasma membrane of living a7r5 cells. *The EMBO journal*, 16(7):1575–1581, 1997.

[142] V. Marshansky, J. L. Rubinstein, and G. Grueber. Eukaryotic v-atpase: novel structural findings and functional insights. *Biochimica et Biophysica Acta (BBA)-Bioenergetics*, 1837(6):857–879, 2014.

[143] J. C. Mason, A. De Michele, C. Stevens, R. A. Ruth, and G. T. Hashisaki. Cochlear implantation in patients with auditory neuropathy of varied etiologies. *The Laryngoscope*, 113(1):45–49, 2003.

[144] Y. Masuda, M. Futamura, H. Kamino, Y. Nakamura, N. Kitamura, S. Ohnishi, Y. Miyamoto, H. Ichikawa, T. Ohta, M. Ohki, *et al.* The potential role of dfna5, a hearing impairment gene, in p53-mediated cellular response to dna damage. *Journal of human genetics*, 51(8):652–664, 2006.

[145] Y. Matsuzaka, H. Hayashi, and H. Kusuhara. Impaired hepatic uptake by organic anion-transporting polypeptides is associated with hyperbilirubinemia and hypercholanemia in atp11c mutant mice. *Molecular pharmacology*, 88(6):1085–1092, 2015.

[146] M. Mazzoli, G. Van Camp, V. Newton, N. Giarbini, F. Declau, and A. Parving. Recommendations for the description of genetic and audiological data for families with nonsyndromic hereditary hearing impairment. *Audiological Medicine*, 1(2):148–150, 2003.

[147] J. G. McCarron, S. Chalmers, M. L. Olson, and J. M. Girkin. Subplasma membrane ca2+ signals. *Iubmb Life*, 64(7):573–585, 2012.

[148] R. W. McCreery, J. Kaminski, K. Beauchaine, N. Lenzen, K. Simms, and M. P. Gorga. The impact of degree of hearing loss on auditory brainstem response predictions of behavioral thresholds. *Ear and hearing*, 36(3):309, 2015.

[149] S. McLaughlin and A. Aderem. The myristoyl-electrostatic switch: a modulator of reversible protein-membrane interactions. *Trends in biochemical sciences*, 20(7):272–276, 1995.

[150] N. Michalski, J. D. Goutman, S. M. Auclair, J. B. de Monvel, M. Tertrais, A. Emptoz, A. Parrin, S. Nouaille, M. Guillon, M. Sachse, *et al.* Otoferlin acts as a ca2+ sensor for vesicle fusion and vesicle pool replenishment at auditory hair cell ribbon synapses. *eLife*, 6, 2017.

[151] R. Mittal, A. Ramesh, S. Panwar, A. Nilkanthan, S. Nair, and P. R. Mehra. Auditory neuropathy spectrum disorder: its prevalence and audiological characteristics in an indian tertiary care hospital. *International journal of pediatric otorhinolaryngology*, 76(9):1351–1354, 2012.

[152] R. Miyano, T. Matsumoto, H. Takatsu, K. Nakayama, and H.-W. Shin. Alteration of transbilayer phospholipid compositions is involved in cell adhesion, cell spreading, and focal adhesion formation. *Febs Letters*, 590 (14):2138–2145, 2016.

[153] N. Miyoshi, H. Ishii, K. Mimori, F. Tanaka, K. Nagai, M. Uemura, M. Sekimoto, Y. Doki, and M. Mori. Atp11a is a novel predictive marker for metachronous metastasis of colorectal cancer. *Oncology reports*, 23(2): 505–510, 2010.

[154] A. R. Møller. *Hearing: anatomy, physiology, and disorders of the auditory system*. Plural Publishing, 2012.

[155] J. Moran, T. Itoh, U. R. Reddy, M. Chen, E. S. Alnemri, and D. Pleasure. Caspase-3 expression by cerebellar granule neurons is regulated by calcium and cyclic amp. *Journal of neurochemistry*, 73(2):568–577, 1999.

[156] J. P. Morth, B. P. Pedersen, M. S. Toustrup-Jensen, T. L.-M. Sørensen, J. Petersen, J. P. Andersen, B. Vilsen, and P. Nissen. Crystal structure of the sodium–potassium pump. *Nature*, 450(7172):1043, 2007.

[157] T. Moser and A. Starr. Auditory neuropathy—neural and synaptic mechanisms. *Nature Reviews Neurology*, 12(3):135, 2016.

[158] T. Moser, N. Strenzke, A. Meyer, A. Lesinski-Schiedat, T. Lenarz, D. Beutner, A. Foerst, R. Lang-Roth, H. von Wedel, M. Walger, *et al.* Diagnostik und therapie der auditorischen synaptopathie/neuropathiediagnosis and therapy of auditory synaptopathy/neuropathy. *Hno*, 54(11):833–841, 2006.

[159] M. Müller. Frequency representation in the rat cochlea. *Hearing research*, 51(2):247–254, 1991.

[160] M. Müller. The cochlear place-frequency map of the adult and developing mongolian gerbil. *Hearing research*, 94(1):148–156, 1996.

[161] S. Nagata. Apoptosis and autoimmune diseases. *Annals of the New York Academy of Sciences*, 1209(1):10–16, 2010.

[162] S. Nagata. Apoptosis and clearance of apoptotic cells. *Annual review of immunology*, 36:489–517, 2018.

[163] T. Naito, H. Takatsu, R. Miyano, N. Takada, K. Nakayama, and H.-W. Shin. Phospholipid flippase atp10a translocates phosphatidylcholine and is involved in plasma membrane dynamics. *Journal of Biological Chemistry*, 290(24):15004–15017, 2015.

[164] H. Nakanishi, K. Irie, K. Segawa, K. Hasegawa, Y. Fujiyoshi, S. Nagata, and K. Abe. Crystal structure of a human plasma membrane phospholipid flippase. *Journal of Biological Chemistry*, pages jbc–RA120, 2020.

[165] T. Nakano, Y. Ishimoto, J. Kishino, M. Umeda, K. Inoue, K. Nagata, K. Ohashi, K. Mizuno, and H. Arita. Cell adhesion to phosphatidylserine mediated by a product of growth arrest-specific gene 6. *Journal of Biological Chemistry*, 272(47):29411–29414, 1997.

[166] S. D. Nash, K. J. Cruickshanks, R. Klein, B. E. Klein, F. J. Nieto, G. H. Huang, J. S. Pankow, and T. S. Tweed. The prevalence of hearing impairment and associated risk factors: the beaver dam offspring study. *Archives of Otolaryngology–Head & Neck Surgery*, 137(5):432–439, 2011.

[167] P. Natarajan, K. Liu, D. V. Patil, V. A. Sciorra, C. L. Jackson, and T. R. Graham. Regulation of a golgi flippase by phosphoinositides and an arfgef. *Nature cell biology*, 11(12):1421–1426, 2009.

[168] S. Negi, S. Pandey, S. M. Srinivasan, A. Mohammed, and C. Guda. Locsigdb: a database of protein localization signals. *Database*, 2015, 2015.

[169] H. D. Nelson, C. Bougatsos, and P. Nygren. Universal newborn hearing screening: systematic review to update the 2001 us preventive services task force recommendation. *Pediatrics*, 122(1):e266–e276, 2008.

[170] B. Neumann, S. Coakley, R. Giordano-Santini, C. Linton, E. S. Lee, A. Nakagawa, D. Xue, and M. A. Hilliard. Eff-1-mediated regenerative axonal fusion requires components of the apoptotic pathway. *Nature*, 517 (7533):219–222, 2015.

[171] New England Biolabs Inc. Tm calculator v1.8.1., 2016. URL `http://tmcalculator.neb.com`.

[172] P. Nikolic, L. E. Järlebark, T. E. Billett, and P. R. Thorne. Apoptosis in the developing rat cochlea and its related structures. *Developmental Brain Research*, 119(1):75–83, 2000.

[173] C. Nishi, S. Toda, K. Segawa, and S. Nagata. Tim4-and mertk-mediated engulfment of apoptotic cells by mouse resident peritoneal macrophages. *Molecular and cellular biology*, 34(8):1512–1520, 2014.

[174] K. Nishizaki, M. Anniko, Y. Orita, Y. Masuda, and T. Yoshino. Programmed cell death in the mouse cochleovestibular ganglion during development. *ORL*, 60(5):267–271, 1998.

[175] S. Okamoto, T. Naito, R. Shigetomi, Y. Kosugi, K. Nakayama, H. Takatsu, and H.-W. Shin. The n- or c-terminal cytoplasmic regions of p4-atpases determine their cellular localization. *Molecular Biology of the Cell, ahead of print*, 7 2020.

[176] N. A. O'Leary, M. W. Wright, J. R. Brister, S. Ciufo, D. Haddad, R. McVeigh, B. Rajput, B. Robbertse, B. Smith-White, D. Ako-Adjei, *et al.* Reference sequence (refseq) database at ncbi: current status, taxonomic expansion, and functional annotation. *Nucleic acids research*, 44 (D1):D733–D745, 2015.

[177] J. C. on Infant Hearing *et al.* Year 2007 position statement: Principles and guidelines for early hearing detection and intervention programs. *Pediatrics*, 120(4):898–921, 2007.

[178] O. E. Onat, S. Gulsuner, K. Bilguvar, A. N. Basak, H. Topaloglu, M. Tan, U. Tan, M. Gunel, and T. Ozcelik. Missense mutation in the atpase, aminophospholipid transporter protein atp8a2 is associated with cerebellar atrophy and quadrupedal locomotion. *European Journal of Human Genetics*, 21(3):281–285, 2013.

[179] K. Op de Beeck, L. Van Laer, and G. Van Camp. Dfna5, a gene involved in hearing loss and cancer: a review. *Annals of Otology, Rhinology & Laryngology*, 121(3):197–207, 2012.

[180] S. Orrenius, B. Zhivotovsky, and P. Nicotera. Regulation of cell death: the calcium–apoptosis link. *Nature reviews Molecular cell biology*, 4(7): 552–565, 2003.

[181] N. Osada, K. Hashimoto, M. Hirai, and J. Kusuda. Aberrant termination of reproduction-related tmem30c transcripts in the hominoids. *Gene*, 392 (1-2):151–156, 2007.

[182] T. Oshima, K. Ikeda, and T. Takasaka. Sensorineural hearing loss associated with byler disease. *The Tohoku journal of experimental medicine*, 187(1):83–88, 1999.

[183] Oxford University Press. Oxford English Dictionary Online. URL `http://www.oed.com/`.

[184] M. Palmgren, M. Sommarin, R. Serrano, and C. Larsson. Identification of an autoinhibitory domain in the c-terminal region of the plant plasma membrane h (+)-atpase. *Journal of Biological Chemistry*, 266(30):20470–20475, 1991.

[185] M. Palmgren, J. T. Østerberg, S. J. Nintemann, L. R. Poulsen, and R. L. López-Marqués. Evolution and a revised nomenclature of p4 atpases, a eukaryotic family of lipid flippases. *Biochimica et Biophysica Acta (BBA)-Biomembranes*, 1861(6):1135–1151, 2019.

[186] M. G. Palmgren. Plant plasma membrane h+-atpases: powerhouses for nutrient uptake. *Annual review of plant biology*, 52(1):817–845, 2001.

[187] M. G. Palmgren and K. B. Axelsen. Evolution of p-type atpases. *Biochimica et Biophysica Acta (BBA)-Bioenergetics*, 1365(1-2):37–45, 1998.

[188] M. G. Palmgren and P. Nissen. P-type atpases. *Annual review of biophysics*, 40:243–266, 2011.

[189] M. G. Palmgren, C. Larsson, and M. Sommarin. Proteolytic activation of the plant plasma membrane h (+)-atpase by removal of a terminal segment. *Journal of Biological Chemistry*, 265(23):13423–13426, 1990.

[190] R. Panatala, H. Hennrich, and J. C. Holthuis. Inner workings and biological impact of phospholipid flippases. *Journal of cell science*, 128(11): 2021–2032, 2015.

[191] T. Pangrsic and C. Vogl. Balancing presynaptic release and endocytic membrane retrieval at hair cell ribbon synapses. *FEBS letters*, 592(21): 3633–3650, 2018.

[192] T. Pangršič, E. Reisinger, and T. Moser. Otoferlin: a multi-c2 domain protein essential for hearing. *Trends in neurosciences*, 35(11):671–680, 2012.

[193] C. C. Paulusma and R. P. O. Elferink. P4 atpases–the physiological relevance of lipid flipping transporters. *FEBS letters*, 584(13):2708–2716, 2010.

[194] C. C. Paulusma, A. Groen, C. Kunne, K. S. Ho-Mok, A. L. Spijkerboer, D. Rudi de Waart, F. J. Hoek, H. Vreeling, K. A. Hoeben, J. van Marle, *et al.* Atp8b1 deficiency in mice reduces resistance of the canalicular membrane to hydrophobic bile salts and impairs bile salt transport. *Hepatology*, 44(1):195–204, 2006.

[195] C. C. Paulusma, D. R. de Waart, C. Kunne, K. S. Mok, and R. P. O. Elferink. Activity of the bile salt export pump (abcb11) is critically dependent on canalicular membrane cholesterol content. *Journal of Biological Chemistry*, 284(15):9947–9954, 2009.

[196] L. Pawlikowska, A. Groen, E. F. Eppens, C. Kunne, R. Ottenhoff, N. Looije, A. Knisely, N. P. Killeen, L. N. Bull, R. P. O. Elferink, *et al.* A mouse genetic model for familial cholestasis caused by atp8b1 mutations reveals perturbed bile salt homeostasis but no impairment in bile secretion. *Human molecular genetics*, 13(8):881–892, 2004.

[197] P. L. Pederse. Transport atpases into the year 2008: a brief overview related to types, structures, functions and roles in health and disease. *Journal of Bioenergetics and Biomembranes*, 39:349–355, 2007.

[198] B. P. Pedersen, M. J. Buch-Pedersen, J. P. Morth, M. G. Palmgren, and P. Nissen. Crystal structure of the plasma membrane proton pump. *Nature*, 450(7172):1111, 2007.

[199] R. Peeters, L. Ng, M. Ma, and D. Forrest. The timecourse of apoptotic cell death during postnatal remodeling of the mouse cochlea and its premature

onset by triiodothyronine (t3). *Molecular and cellular endocrinology*, 407: 1–8, 2015.

[200] J. Penniston and A. Enyedi. Modulation of the plasma membrane ca 2+ pump. *The Journal of membrane biology*, 165(2):101–109, 1998.

[201] V. Perez-Garcia, E. Fineberg, R. Wilson, A. Murray, C. I. Mazzeo, C. Tudor, A. Sienerth, J. K. White, E. Tuck, E. J. Ryder, *et al.* Placentation defects are highly prevalent in embryonic lethal mouse mutants. *Nature*, 555(7697):463–468, 2018.

[202] R. Perkins and D. Morest. A study of cochlear innervation patterns in cats and rats with the golgi method and nomarski optics. *Journal of Comparative Neurology*, 163(2):129–158, 1975.

[203] A. Peterson, J. Shallop, C. Driscoll, A. Breneman, J. Babb, R. Stoeckel, and L. Fabry. Outcomes of cochlear implantation in children with auditory neuropathy. *Journal of the American Academy of Audiology*, 14(4):188–201, 2003.

[204] M. K. Pichora-Fuller and G. Singh. Effects of age on auditory and cognitive processing: implications for hearing aid fitting and audiologic rehabilitation. *Trends in amplification*, 10(1):29–59, 2006.

[205] U. Pirvola, E. Lehtonen, and J. Ylikoski. Spatiotemporal development of cochlear innervation and hair cell differentiation in the rat. *Hearing research*, 52(2):345–355, 1991.

[206] F. Portillo. Regulation of plasma membrane h+-atpase in fungi and plants. *Biochimica Et Biophysica Acta (BBA)-Reviews on Biomembranes*, 1469 (1):31–42, 2000.

[207] F. Portillo, P. Eraso, and R. Serrano. Analysis of the regulatory domain of yeast plasma membrane h+-atpase by directed mutagenesis and intragenic suppression. *FEBS letters*, 287(1-2):71–74, 1991.

[208] I. Psarommatis, M. Riga, K. Douros, P. Koltsidopoulos, D. Douniadakis, I. Kapetanakis, and N. Apostolopoulos. Transient infantile auditory neuropathy and its clinical implications. *International journal of pediatric otorhinolaryngology*, 70(9):1629–1637, 2006.

[209] D. Purves, G. Augustine, D. Fitzpatrick, L. Katz, A. LaMantia, J. McNamara, and S. Williams. Hair cells and the mechanoelectrical transduction of sound waves. *Sinauer Associates Inc.: Sunderland, MA, USA*, 2001.

[210] C. F. Puts and J. C. Holthuis. Mechanism and significance of p4 atpase-catalyzed lipid transport: lessons from a na+/k+-pump. *Biochimica et Biophysica Acta (BBA)-Molecular and Cell Biology of Lipids*, 1791(7): 603–611, 2009.

[211] C. F. Puts, R. Panatala, H. Hennrich, A. Tsareva, P. Williamson, and J. C. Holthuis. Mapping functional interactions in a heterodimeric phospholipid pump. *Journal of Biological Chemistry*, 287(36):30529–30540, 2012.

[212] N. A. Ramakrishnan, M. J. Drescher, and D. G. Drescher. Direct interaction of otoferlin with syntaxin 1a, snap-25, and the l-type voltage-gated calcium channel cav1. 3. *Journal of Biological Chemistry*, 284(3):1364–1372, 2009.

[213] G. Rance. Auditory neuropathy/dys-synchrony and its perceptual consequences. *Trends in Amplification*, 9(1):1–43, 2005.

[214] G. Rance and A. Starr. Pathophysiological mechanisms and functional hearing consequences of auditory neuropathy. *Brain*, 138(11):3141–3158, 2015.

[215] G. Rance, B. Cone-Wesson, J. Wunderlich, and R. Dowell. Speech perception and cortical event related potentials in children with auditory neuropathy. *Ear and hearing*, 23(3):239–253, 2002.

[216] G. Rance, C. McKay, and D. Grayden. Perceptual characterization of children with auditory neuropathy. *Ear and hearing*, 25(1):34–46, 2004.

[217] G. Rance, R. Fava, H. Baldock, A. Chong, E. Barker, L. Corben, and M. B. Delatycki. Speech perception ability in individuals with friedreich ataxia. *Brain*, 131(8):2002–2012, 2008.

[218] G. Rance, L. Corben, E. Barker, P. Carew, D. Chisari, M. Rogers, R. Dowell, S. Jamaluddin, R. Bryson, and M. B. Delatycki. Auditory perception in individuals with friedreich's ataxia. *Audiology and Neurotology*, 15(4): 229–240, 2010.

[219] G. Rance, M. Ryan, P. Carew, L. Corben, E. Yiu, J. Tan, and M. Delatycki. Binaural speech processing in individuals with auditory neuropathy. *Neuroscience*, 226:227–235, 2012.

[220] G. Rance, M. M. Ryan, K. Bayliss, K. Gill, C. O'Sullivan, and M. Whitechurch. Auditory function in children with charcot–marie–tooth disease. *Brain*, 135(5):1412–1422, 2012.

[221] N. B. Ray, L. Durairaj, B. B. Chen, B. J. McVerry, A. J. Ryan, M. Donahoe, A. K. Waltenbaugh, C. P. O'donnell, F. C. Henderson, C. A. Etscheidt, *et al.* Dynamic regulation of cardiolipin by the lipid pump atp8b1 determines the severity of lung injury in experimental pneumonia. *Nature medicine*, 16(10):1120, 2010.

[222] P. Rice, I. Longden, and A. Bleasby. Emboss: the european molecular biology open software suite, 2000.

[223] R. Rizzuto, M. Brini, M. Murgia, and T. Pozzan. Microdomains with high ca2+ close to ip3-sensitive channels that are sensed by neighboring mitochondria. *Science*, 262(5134):744–747, 1993.

[224] J. T. Roland. PEI Transfection Protocol, 2012. URL `http://josephroland.com/lab/PEItransfect.html`.

[225] G. Rosman and D. und Miller. Improved method for plasmid shipment. *BioTechniques*, 8(5):509, 1990.

[226] C. V. Rothlin, E. A. Carrera-Silva, L. Bosurgi, and S. Ghosh. Tam receptor signaling in immune homeostasis. *Annual review of immunology*, 33: 355–391, 2015.

[227] P. Roush, T. Frymark, R. Venediktov, and B. Wang. Audiologic management of auditory neuropathy spectrum disorder in children: a systematic review of the literature. *American journal of audiology*, 20(2):159–170, 2011.

[228] I. Roux, S. Safieddine, R. Nouvian, M. Grati, M.-C. Simmler, A. Bahloul, I. Perfettini, M. Le Gall, P. Rostaing, G. Hamard, *et al.* Otoferlin, defective in a human deafness form, is essential for exocytosis at the auditory ribbon synapse. *Cell*, 127(2):277–289, 2006.

[229] J. Rueda, C. De La Sen, J. M. Juiz, and J. A. Merchan. Neuronal loss in the spiral ganglion of young rats. *Acta oto-laryngologica*, 104(5-6): 417–421, 1987.

[230] C. Sage, M. Huang, M. A. Vollrath, M. C. Brown, P. W. Hinds, D. P. Corey, D. E. Vetter, and Z.-Y. Chen. Essential role of retinoblastoma protein in mammalian hair cell development and hearing. *Proceedings of the National Academy of Sciences*, 103(19):7345–7350, 2006.

[231] M. W. Salter and B. Stevens. Microglia emerge as central players in brain disease. *Nature medicine*, 23(9):1018, 2017.

[232] R. Santarelli. Information from cochlear potentials and genetic mutations helps localize the lesion site in auditory neuropathy. *Genome medicine*, 2 (12):91, 2010.

[233] R. Santarelli, A. Starr, H. J. Michalewski, and E. Arslan. Neural and receptor cochlear potentials obtained by transtympanic electrocochleography in auditory neuropathy. *Clinical Neurophysiology*, 119(5):1028–1041, 2008.

[234] R. Santarelli, I. del Castillo, E. Cama, P. Scimemi, and A. Starr. Audibility, speech perception and processing of temporal cues in ribbon synaptic disorders due to otof mutations. *Hearing research*, 330:200–212, 2015.

[235] M. L. Sapar, H. Ji, B. Wang, A. R. Poe, K. Dubey, X. Ren, J.-Q. Ni, and C. Han. Phosphatidylserine externalization results from and causes neurite degeneration in drosophila. *Cell reports*, 24(9):2273–2286, 2018.

[236] S. Saroussi and N. Nelson. The little we know on the structure and machinery of v-atpase. *Journal of Experimental Biology*, 212(11):1604–1610, 2009.

[237] R. Schaette and D. McAlpine. Tinnitus with a normal audiogram: physiological evidence for hidden hearing loss and computational model. *Journal of Neuroscience*, 31(38):13452–13457, 2011.

[238] C. J. Schoen, S. B. Emery, M. C. Thorne, H. R. Ammana, E. Śliwerska, J. Arnett, M. Hortsch, F. Hannan, M. Burmeister, and M. M. Lesperance. Increased activity of diaphanous homolog 3 (diaph3)/diaphanous causes hearing defects in humans with auditory neuropathy and in drosophila. *Proceedings of the National Academy of Sciences*, 107(30):13396–13401, 2010.

[239] C. J. Schoen, M. Burmeister, and M. M. Lesperance. Diaphanous homolog 3 (diap3) overexpression causes progressive hearing loss and inner hair cell defects in a transgenic mouse model of human deafness. *PloS one*, 8(2): e56520, 2013.

[240] O. Schuldiner and A. Yaron. Mechanisms of developmental neurite pruning. *Cellular and Molecular Life Sciences*, 72(1):101–119, 2015.

[241] T. T. Sebastian, R. D. Baldridge, P. Xu, and T. R. Graham. Phospholipid flippases: building asymmetric membranes and transport vesicles. *Biochimica et Biophysica Acta (BBA)-Molecular and Cell Biology of Lipids*, 1821(8):1068–1077, 2012.

[242] K. Segawa, S. Kurata, Y. Yanagihashi, T. R. Brummelkamp, F. Matsuda, and S. Nagata. Caspase-mediated cleavage of phospholipid flippase for apoptotic phosphatidylserine exposure. *Science*, 344(6188):1164–1168, 2014.

[243] K. Segawa, S. Kurata, and S. Nagata. Human type iv p-type atpases that work as plasma membrane phospholipid flippases and their regulation by caspase and calcium. *Journal of Biological Chemistry*, 291(2):762–772, 2016.

[244] K. Segawa, Y. Yanagihashi, K. Yamada, C. Suzuki, Y. Uchiyama, and S. Nagata. Phospholipid flippases enable precursor b cells to flee engulfment by macrophages. *Proceedings of the National Academy of Sciences*, 115(48):12212–12217, 2018.

[245] M. Seigneuret and P. F. Devaux. Atp-dependent asymmetric distribution of spin-labeled phospholipids in the erythrocyte membrane: relation to shape changes. *Proceedings of the National Academy of Sciences*, 81(12): 3751–3755, 1984.

[246] C. Seiler and T. Nicolson. Defective calmodulin-dependent rapid apical endocytosis in zebrafish sensory hair cell mutants. *Journal of neurobiology*, 41(3):424–434, 1999.

[247] R. Serrano, F. Portillo, B. Monk, and M. Palmgren. The regulatory domain of fungal and plant plasma membrane h (+)-atpase. *Acta physiologica scandinavica. Supplementum*, 607:131–136, 1992.

[248] M. P. Sheetz and S. Singer. Biological membranes as bilayer couples. a molecular mechanism of drug-erythrocyte interactions. *Proceedings of the National Academy of Sciences*, 71(11):4457–4461, 1974.

[249] J. Shi, W. Gao, and F. Shao. Pyroptosis: gasdermin-mediated programmed necrotic cell death. *Trends in biochemical sciences*, 42(4):245–254, 2017.

[250] X. Shi, P. G. Gillespie, and A. L. Nuttall. Na+ influx triggers bleb formation on inner hair cells. *American Journal of Physiology-Cell Physiology*, 288(6):C1332–C1341, 2005.

[251] X. Shi, P. G. Gillespie, and A. L. Nuttall. Apical phosphatidylserine externalization in auditory hair cells. *Molecular membrane biology*, 24(1): 16–27, 2007.

[252] H.-W. Shin and H. Takatsu. Substrates of p4-atpases: beyond aminophospholipids (phosphatidylserine and phosphatidylethanolamine). *The FASEB Journal*, 33(3):3087–3096, 2018.

[253] H.-W. Shin and H. Takatsu. Phosphatidylserine exposure in living cells. *Critical Reviews in Biochemistry and Molecular Biology*, pages 1–13, 2020.

[254] T. Shinoda, H. Ogawa, F. Cornelius, and C. Toyoshima. Crystal structure of the sodium–potassium pump at 2.4 å resolution. *Nature*, 459(7245):446, 2009.

[255] O. M. Siggs, C. N. Arnold, C. Huber, E. Pirie, Y. Xia, P. Lin, D. Nemazee, and B. Beutler. The p4-type atpase atp11c is essential for b lymphopoiesis in adult bone marrow. *Nature immunology*, 12(5):434–440, 2011.

[256] O. M. Siggs, B. Schnabl, B. Webb, and B. Beutler. X-linked cholestasis in mouse due to mutations of the p4-atpase atp11c. *Proceedings of the National Academy of Sciences*, 108(19):7890–7895, 2011.

[257] D. Simmons, L. Manson-Gieseke, T. Hendrix, K. Morris, and S. Williams. Postnatal maturation of spiral ganglion neurons: a horseradish peroxidase study. *Hearing research*, 55(1):81–91, 1991.

[258] D. D. Simmons. A transient afferent innervation of outer hair cells in the postnatal cochlea. *Neuroreport*, 5(11):1309–1312, 1994.

[259] E. Skoe and N. Kraus. Auditory brainstem response to complex sounds: a tutorial. *Ear and hearing*, 31(3):302, 2010.

[260] J. Smit, A. H. Schinkel, R. O. Elferink, A. Groen, E. Wagenaar, L. Van Deemter, C. Mol, R. Ottenhoff, N. Van der Lugt, M. Van Roon, *et al.* Homozygous disruption of the murine mdr2 p-glycoprotein gene leads to a complete absence of phospholipid from bile and to liver disease. *Cell*, 75(3):451–462, 1993.

[261] R. J. Smith, J. F. Bale Jr, and K. R. White. Sensorineural hearing loss in children. *The Lancet*, 365(9462):879–890, 2005.

[262] I. d. A. Soares, P. d. L. Menezes, A. T. L. Carnaúba, K. C. L. de Andrade, and O. G. Lins. Study of cochlear microphonic potentials in auditory neuropathy. *Brazilian journal of otorhinolaryngology*, 82(6):722–736, 2016.

[263] S. Somersan and N. Bhardwaj. Tethering and tickling: a new role for the phosphatidylserine receptor. *The Journal of cell biology*, 155(4):501, 2001.

[264] C. L. Stace and N. T. Ktistakis. Phosphatidic acid-and phosphatidylserine-binding proteins. *Biochimica et Biophysica Acta (BBA)-Molecular and Cell Biology of Lipids*, 1761(8):913–926, 2006.

[265] J. M. Stapelbroek, T. A. Peters, D. H. van Beurden, J. H. Curfs, A. Joosten, A. J. Beynon, B. M. van Leeuwen, L. M. van der Velden, L. Bull, R. P. O. Elferink, *et al.* Atp8b1 is essential for maintaining normal hearing. *Proceedings of the National Academy of Sciences*, 106(24): 9709–9714, 2009.

[266] A. Starr and G. Rance. Auditory neuropathy. In *Handbook of clinical neurology*, volume 129, pages 495–508. Elsevier, 2015.

[267] A. Starr, B. Isaacson, H. J. Michalewski, F.-G. Zeng, Y.-Y. Kong, P. Beale, G. W. Paulson, B. J. Keats, and M. M. Lesperance. A dominantly inherited progressive deafness affecting distal auditory nerve and hair cells. *Journal of the Association for Research in Otolaryngology*, 5(4):411–426, 2004.

[268] F. Stelma and M. Bhutta. Non-syndromic hereditary sensorineural hearing loss: review of the genes involved. *The Journal of Laryngology & Otology*, 128(1):13–21, 2014.

[269] T. N. Stitt, G. Conn, M. Goret, C. Lai, J. Bruno, C. Radzlejewski, K. Mattsson, J. Fisher, D. R. Gies, P. F. Jones, *et al.* The anticoagulation factor protein s and its relative, gas6, are ligands for the tyro 3/axl family of receptor tyrosine kinases. *Cell*, 80(4):661–670, 1995.

[270] V. A. Street, J. W. McKee-Johnson, R. C. Fonseca, B. L. Tempel, and K. Noben-Trauth. Mutations in a plasma membrane ca 2+-atpase gene cause deafness in deafwaddler mice. *Nature genetics*, 19(4):390–394, 1998.

[271] K. Sun, W. Tian, X. Li, W. Liu, Y. Yang, and X. Zhu. Disease mutation study identifies critical residues for phosphatidylserine flippase atp11a. *BioMed Research International*, 2020, 2020.

[272] X. L. Sun, D. Li, J. Fang, I. Noyes, B. Casto, K. Theil, C. Shuler, and G. E. Milo. Changes in levels of normal ml-1 gene transcripts associated with the conversion of human nontumorigenic to tumorigenic phenotypes. *Gene Expression, The Journal of Liver Research*, 8(2):129–139, 1999.

[273] C.-H. Sung and J.-Z. Chuang. The cell biology of vision. *Journal of Cell Biology*, 190(6):953–963, 2010.

[274] R. B. Sutton and S. R. Sprang. Structure of the protein kinase cβ phospholipid-binding c2 domain complexed with ca2+. *Structure*, 6(11): 1395–1405, 1998.

[275] R. B. Sutton, B. A. Davletov, A. M. Berghuis, T. C. Sudhof, and S. R. Sprang. Structure of the first c2 domain of synaptotagmin i: a novel ca2+/phospholipid-binding fold. *Cell*, 80(6):929–938, 1995.

[276] J. Suzuki, T. Fujii, T. Imao, K. Ishihara, H. Kuba, and S. Nagata. Calcium-dependent phospholipid scramblase activity of tmem16 protein family members. *Journal of Biological Chemistry*, 288(19):13305–13316, 2013.

[277] J. Suzuki, E. Imanishi, and S. Nagata. Xkr8 phospholipid scrambling complex in apoptotic phosphatidylserine exposure. *Proceedings of the National Academy of Sciences*, 113(34):9509–9514, 2016.

[278] N. Takada, T. Naito, T. Inoue, K. Nakayama, H. Takatsu, and H.-W. Shin. Phospholipid-flipping activity of p4-atp ase drives membrane curvature. *The EMBO journal*, 37(9):e97705, 2018.

[279] K. Takahashi, K. Kamiya, K. Urase, M. Suga, T. Takizawa, H. Mori, Y. Yoshikawa, K. Ichimura, K. Kuida, and T. Momoi. Caspase-3-deficiency induces hyperplasia of supporting cells and degeneration of sensory cells resulting in the hearing loss. *Brain research*, 894(2):359–367, 2001.

[280] H. Takatsu, K. Baba, T. Shima, H. Umino, U. Kato, M. Umeda, K. Nakayama, and H.-W. Shin. Atp9b, a p4-atpase (a putative aminophospholipid translocase), localizes to the trans-golgi network in a

cdc50 protein-independent manner. *The Journal of Biological Chemistry*, 2011.

[281] H. Takatsu, G. Tanaka, K. Segawa, J. Suzuki, S. Nagata, K. Nakayama, and H.-W. Shin. Phospholipid Flippase Activities and Substrate Specificities of Human Type IV P-type ATPases Localized to the Plasma Membrane. *Journal of Biological Chemistry*, 289(48):33543–33556, 2014.

[282] H. Takatsu, M. Takayama, T. Naito, N. Takada, K. Tsumagari, Y. Ishihama, K. Nakayama, and H.-W. Shin. Phospholipid flippase atp11c is endocytosed and downregulated following ca 2+-mediated protein kinase c activation. *Nature communications*, 8(1):1–15, 2017.

[283] M. Takayama, H. Takatsu, A. Hamamoto, H. Inoue, T. Naito, K. Nakayama, and H.-W. Shin. The cytoplasmic c-terminal region of the atp11c variant determines its localization at the polarized plasma membrane. *Journal of cell science*, 132(17):jcs231720, 2019.

[284] M. Takeda, K. Yamagami, and K. Tanaka. Role of phosphatidylserine in phospholipid flippase-mediated vesicle transport in saccharomyces cerevisiae. *Eukaryotic cell*, 13(3):363–375, 2014.

[285] D. Tang, W. L. Dean, D. Borchman, and C. A. Paterson. The influence of membrane lipid structure on plasma membrane ca2+-atpase activity. *Cell calcium*, 39(3):209–216, 2006.

[286] A. Tessa, A. Giannotti, L. Tieri, L. Vilarinho, G. Marotta, and F. M. Santorelli. Maternally inherited deafness associated with a t1095c mutation in the mdna. *European Journal of Human Genetics*, 9(2):147, 2001.

[287] A. Thomas and K. G. Herbst. Social and psychological implications of acquired deafness for adults of employment age. *British journal of audiology*, 14(3):76–85, 1980.

[288] T. B. Thornley, Z. Fang, S. Balasubramanian, R. A. Larocca, W. Gong, S. Gupta, E. Csizmadia, N. Degauque, B. S. Kim, M. Koulmanda, *et al.* Fragile tim-4–expressing tissue resident macrophages are migratory and immunoregulatory. *The Journal of clinical investigation*, 124(8):3443–3454, 2014.

[289] D. Thyagarajan, S. Bressman, C. Bruno, S. Przedborski, S. Shanske, T. Lynch, S. Fahn, and S. DiMauro. A novel mitochondrial 12srrna point

mutation in parkinsonism, deafness, and neuropathy. *Annals of neurology*, 48(5):730–736, 2000.

[290] M. Timcenko, J. A. Lyons, D. Januliene, J. J. Ulstrup, T. Dieudonne, C. Montigny, M.-R. Ash, J. L. Karlsen, T. Boesen, W. Kühlbrandt, *et al.* Structure and autoregulation of a p4-atpase lipid flippase. *Nature*, 571 (7765):366–370, 2019.

[291] J. B. Tomblin, M. Harrison, S. E. Ambrose, E. A. Walker, J. J. Oleson, and M. P. Moeller. Language outcomes in young children with mild to severe hearing loss. *Ear and Hearing*, 36(0 1):76S, 2015.

[292] T. Tone, K. Nakayama, H. Takatsu, and H.-W. Shin. Atpase reaction cycle of p4-atpases affects their transport from the endoplasmic reticulum. *FEBS letters*, 594(3):412–423, 2020.

[293] E. Torban and P. Goodyer. The kidney and ear: emerging parallel functions. *Annual review of medicine*, 60:339–353, 2009.

[294] C. Toyoshima, M. Nakasako, H. Nomura, and H. Ogawa. Crystal structure of the calcium pump of sarcoplasmic reticulum at 2.6 å resolution. *Nature*, 405(6787):647, 2000.

[295] M. Tsuchiya, Y. Hara, M. Okuda, K. Itoh, R. Nishioka, A. Shiomi, K. Nagao, M. Mori, Y. Mori, J. Ikenouchi, *et al.* Cell surface flip-flop of phosphatidylserine is critical for piezo1-mediated myotube formation. *Nature communications*, 9(1):1–15, 2018.

[296] N. Tygstrup, B. Á. Steig, J. A. Juijn, L. N. Bull, and R. H. Houwen. Recurrent familial intrahepatic cholestasis in the faeroe islands. phenotypic heterogeneity but genetic homogeneity. *Hepatology*, 29(2):506–508, 1999.

[297] Y. Uchida, J. Hasegawa, D. Chinnapen, T. Inoue, S. Okazaki, R. Kato, S. Wakatsuki, R. Misaki, M. Koike, Y. Uchiyama, *et al.* Intracellular phosphatidylserine is essential for retrograde membrane traffic through endosomes. *Proceedings of the National Academy of Sciences*, 108(38): 15846–15851, 2011.

[298] M. Uhlén, L. Fagerberg, B. M. Hallström, C. Lindskog, P. Oksvold, A. Mardinoglu, Å. Sivertsson, C. Kampf, E. Sjöstedt, A. Asplund, *et al.* Tissue-based map of the human proteome. *Science*, 347(6220):1260419, 2015.

[299] Uhlen, M and others. Human Protein Atlas. URL `www.proteinatlas.org`.

[300] University Medical Center Hamburg-Eppendorf. Homepage of University Medical Center Hamburg-Eppendorf, 2016. URL `www.uke.de`.

[301] S. R. Van Camp G. Hereditary hearing loss homepage. URL `https://hereditaryhearingloss.org`.

[302] Van Camp G, Smith RJH. Hereditary Hearing Loss Homepage. URL `http://hereditaryhearingloss.org`.

[303] V. A. van der Mark, D. R. de Waart, K. S. Ho-Mok, M. M. Tabbers, H. W. Voogt, R. P. O. Elferink, A. S. Knisely, and C. C. Paulusma. The lipid flippase heterodimer atp8b1–cdc50a is essential for surface expression of the apical sodium-dependent bile acid transporter (slc10a2/asbt) in intestinal caco-2 cells. *Biochimica et Biophysica Acta (BBA)-Molecular Basis of Disease*, 1842(12):2378–2386, 2014.

[304] V. A. Van Der Mark, H. R. de Jonge, J.-C. Chang, K. S. Ho-Mok, S. Duijst, D. Vidović, M. S. Carlon, R. P. O. Elferink, and C. C. Paulusma. The phospholipid flippase atp8b1 mediates apical localization of the cystic fibrosis transmembrane regulator. *Biochimica et Biophysica Acta (BBA)-Molecular Cell Research*, 1863(9):2280–2288, 2016.

[305] L. M. van der Velden, C. G. Wichers, A. E. van Breevoort, J. A. Coleman, R. S. Molday, R. Berger, L. W. Klomp, and S. F. van De Graaf. Heteromeric interactions required for abundance and subcellular localization of human cdc50 proteins and class 1 p4-atpases. *Journal of Biological Chemistry*, 285(51):40088–40096, 2010.

[306] L. Van Laer, K. Vrijens, S. Thys, V. Van Tendeloo, R. Smith, D. Van Bockstaele, J. Timmermans, and G. Van Camp. Dfna5: hearing impairment exon instead of hearing impairment gene? *Journal of medical genetics*, 41 (6):401–406, 2004.

[307] S. W. van Mil, L. W. Klomp, L. N. Bull, and R. H. Houwen. Fic1 disease: a spectrum of intrahepatic cholestatic disorders. In *Seminars in liver disease*, volume 21, pages 535–544. Copyright© 2001 by Thieme Medical Publishers, Inc., 333 Seventh Avenue, New . . . , 2001.

[308] L. J. Van Winkle. *Biomembrane transport*. Elsevier, 1999.

[309] B. C. Varnum, C. Young, G. Elliott, A. Garcia, T. D. Bartley, Y.-W. Fridell, R. W. Hunt, G. Trail, C. Clogston, R. J. Toso, *et al.* Axl receptor tyrosine kinase stimulated by the vitamin k-dependent protein encoded by growth-arrest-specific gene 6. *Nature*, 373(6515):623–626, 1995.

[310] N. Verdaguer, S. Corbalan-Garcia, W. F. Ochoa, I. Fita, and J. C. Gómez-Fernández. Ca2+ bridges the c2 membrane-binding domain of protein kinase cα directly to phosphatidylserine. *The EMBO journal*, 18(22): 6329–6338, 1999.

[311] A. K. Verma, A. Enyedi, A. G. Filoteo, and J. T. Penniston. Regulatory region of plasma membrane ca2+ pump. 28 residues suffice to bind calmodulin but more are needed for full auto-inhibition of the activity. *Journal of Biological Chemistry*, 269(3):1687–1691, 1994.

[312] A. L. Vestergaard, J. A. Coleman, T. Lemmin, S. A. Mikkelsen, L. L. Molday, B. Vilsen, R. S. Molday, M. Dal Peraro, and J. P. Andersen. Critical roles of isoleucine-364 and adjacent residues in a hydrophobic gate control of phospholipid transport by the mammalian p4-atpase atp8a2. *Proceedings of the National Academy of Sciences*, 111(14):E1334–E1343, 2014.

[313] L. Villard, P. Cacciagli, M.-R. Haddad, C. Mignon-Ravix, B. El-Waly, A. Moncla, C. Missirian, and B. Chabrol. Disruption of the atp8a2 gene in a patient with a t (10; 13) de novo balanced translocation and a severe neurological phenotype. *European Journal of Human Genetics*, 2010.

[314] Vinay and B. C. Moore. Ten (hl)-test results and psychophysical tuning curves for subjects with auditory neuropathy: Resultados de la prueba ten (hl) y de las curvas psicofísicas de entonación en sujetos con neuropatía auditiva. *International journal of audiology*, 46(1):39–46, 2007.

[315] M. A. Vollrath, K. Y. Kwan, and D. P. Corey. The micromachinery of mechanotransduction in hair cells. *Annu. Rev. Neurosci.*, 30:339–365, 2007.

[316] S. Wakatsuki and T. Araki. Specific phospholipid scramblases are involved in exposure of phosphatidylserine, an "eat-me" signal for phagocytes, on degenerating axons. *Communicative & integrative biology*, 10(2):e1296615, 2017.

[317] J. Wang, L. L. Molday, T. Hii, J. A. Coleman, T. Wen, J. P. Andersen, and R. S. Molday. Proteomic analysis and functional characterization of p4-atpase phospholipid flippases from murine tissues. *Scientific reports*, 8 (1):1–14, 2018.

[318] L. Wang, C. Beserra, and D. L. Garbers. A novel aminophospholipid transporter exclusively expressed in spermatozoa is required for membrane lipid asymmetry and normal fertilization. *Developmental biology*, 267(1): 203–215, 2004.

[319] Q. Wang, R. Li, H. Zhao, J. L. Peters, Q. Liu, L. Yang, D. Han, J. H. Greinwald, W.-Y. Young, and M.-X. Guan. Clinical and molecular characterization of a chinese patient with auditory neuropathy associated with mitochondrial 12s rrna t1095c mutation. *American Journal of Medical Genetics Part A*, 133(1):27–30, 2005.

[320] R. Wang, P. Lam, L. Liu, D. Forrest, I. M. Yousef, D. Mignault, M. J. Phillips, and V. Ling. Severe cholestasis induced by cholic acid feeding in knockout mice of sister of p-glycoprotein. *Hepatology*, 38(6):1489–1499, 2003.

[321] Y. Wang, W. Gao, X. Shi, J. Ding, W. Liu, H. He, K. Wang, and F. Shao. Chemotherapy drugs induce pyroptosis through caspase-3 cleavage of a gasdermin. *Nature*, 547(7661):99–103, 2017.

[322] B. Wiechers, G. Gestwa, A. Mack, P. Carroll, H.-P. Zenner, and M. Knipper. A changing pattern of brain-derived neurotrophic factor expression correlates with the rearrangement of fibers during cochlear development of rats and mice. *Journal of Neuroscience*, 19(8):3033–3042, 1999.

[323] P. J. Willems. Genetic causes of hearing loss. *New England Journal of Medicine*, 342(15):1101–1109, 2000.

[324] J. A. Winer and C. E. Schreiner. The central auditory system: a functional analysis. In *The inferior colliculus*, pages 1–68. Springer, 2005.

[325] Z. Wu, N. Grillet, B. Zhao, C. Cunningham, S. Harkins-Perry, B. Coste, S. Ranade, N. Zebarjadi, M. Beurg, R. Fettiplace, *et al.* Mechanosensory hair cells express two molecularly distinct mechanotransduction channels. *Nature neuroscience*, 20(1):24–33, 2017.

[326] D. P. Wynne, F.-G. Zeng, S. Bhatt, H. J. Michalewski, A. Dimitrijevic, and A. Starr. Loudness adaptation accompanying ribbon synapse and auditory nerve disorders. *Brain*, 136(5):1626–1638, 2013.

[327] P. Xu, R. D. Baldridge, R. J. Chi, C. G. Burd, and T. R. Graham. Phosphatidylserine flipping enhances membrane curvature and negative charge required for vesicular transport. *J Cell Biol*, 202(6):875–886, 2013.

[328] Q. Xu, G.-Y. Yang, N. Liu, P. Xu, Y.-L. Chen, Z. Zhou, Z.-G. Luo, and X. Ding. P4-atpase atp8a2 acts in synergy with cdc50a to enhance neurite outgrowth. *FEBS letters*, 586(13):1803–1812, 2012.

[329] M. Yabas, C. E. Teh, S. Frankenreiter, D. Lal, C. M. Roots, B. Whittle, D. T. Andrews, Y. Zhang, N. C. Teoh, J. Sprent, *et al.* Atp11c is critical for the internalization of phosphatidylserine and differentiation of b lymphocytes. *Nature immunology*, 12(5):441–449, 2011.

[330] M. Yabas, L. A. Coupland, D. Cromer, M. Winterberg, N. C. Teoh, J. D'Rozario, K. Kirk, S. Bröer, C. R. Parish, and A. Enders. Mice deficient in the putative phospholipid flippase atp11c exhibit altered erythrocyte shape, anemia, and reduced erythrocyte life span. *Journal of Biological Chemistry*, 289(28):19531–19537, 2014.

[331] Y. Yanagihashi, K. Segawa, R. Maeda, Y.-i. Nabeshima, and S. Nagata. Mouse macrophages show different requirements for phosphatidylserine receptor tim4 in efferocytosis. *Proceedings of the National Academy of Sciences*, 114(33):8800–8805, 2017.

[332] T. Yeung, G. E. Gilbert, J. Shi, J. Silvius, A. Kapus, and S. Grinstein. Membrane phosphatidylserine regulates surface charge and protein localization. *Science*, 319(5860):210–213, 2008.

[333] A. Zachowski. Phospholipids in animal eukaryotic membranes: transverse asymmetry and movement. *Biochemical Journal*, 294(Pt 1):1, 1993.

[334] A. Zachowski, J.-P. Henry, and P. F. Devaux. Control of transmembrane lipid asymmetry in chromaffin granules by an atp-dependent protein. *Nature*, 340(6228):75–76, 1989.

[335] F.-G. Zeng, Y.-Y. Kong, H. J. Michalewski, and A. Starr. Perceptual consequences of disrupted auditory nerve activity. *Journal of Neurophysiology*, 93(6):3050–3063, 2005.

[336] D. R. Zerbino, P. Achuthan, W. Akanni, M. R. Amode, D. Barrell, J. Bhai, K. Billis, C. Cummins, A. Gall, C. G. Girón, *et al.* Ensembl 2018. *Nucleic acids research*, 46(D1):D754–D761, 2018.

[337] X. Zhang, J. Rizo, and T. C. Südhof. Mechanism of phospholipid binding by the c2a-domain of synaptotagmin i. *Biochemistry*, 37(36):12395–12403, 1998.

[338] Y. Zhang, J. Zhou, and Y. Chen. Posterior reversible encephalopathy syndrome in a child with steroid-resistant nephrotic syndrome: a case report and review of literature. *International journal of clinical and experimental pathology*, 7(7):4433, 2014.

[339] X. Zhou, T. T. Sebastian, and T. R. Graham. Auto-inhibition of drs2p, a yeast phospholipid flippase, by its carboxyl-terminal tail. *Journal of Biological Chemistry*, 288(44):31807–31815, 2013.

[340] X. Zhu, R. T. Libby, W. N. De Vries, R. S. Smith, D. L. Wright, R. T. Bronson, K. L. Seburn, and S. W. John. Mutations in a p-type atpase gene cause axonal degeneration. *PLoS genetics*, 8(8):e1002853, 2012.

[341] S. H. Zigmond. Formin-induced nucleation of actin filaments. *Current opinion in cell biology*, 16(1):99–105, 2004.

List of Tables

List of Figures

List of Abbreviations

Acronyms used in this thesis are itemised in alphabetical order. Acronyms listed in the Oxford English Dictionary Online [183], as well as chemicals, reagents, gene and protein names are omitted. The full name of shortened cell lines can be found in section 3.6.

AS/AN	auditory synaptopathy / auditory neuropathy
ABR	auditory brainstem response
CAEP	cortical auditory evoked potentials
cDNA	complementary DNA
CM	cochlear microphonics
ddH_2O	double distilled water
dest.	distilled
DPOAE	distortion product evoked OAE
EE	early endosome
ER	endoplasmic reticulum
ICC	immunocytochemistry
LE	late endosome
mRNA	messenger RNA
OAE	otoacoustic emissions
p.a.	pro analysi
PC	phosphatidylcholine
PCR	polymerase chain reaction
PE	phosphatidylethanolamine
PM	plasma membrane
PS	phosphatidylserine
RE	recycling endosome
RT-PCR	reverse transcription PCR
SM	sphingomyelin
SNP	single nucleotide polymorphism
TEOAE	transient evoked OAE
TGN	trans-Golgi network
T_m	melting temperature
UTR	untranslated region
WB	western blot
WT	wild type

List of Units

Units are additionally provided with their correspondent definition in the International System of Units if necessary.

°C	degree Celsius ($0\,°C \equiv$ -273,15 K)
sec	second
min	minute
h	hour
rpm	revolutions per minute ($1/\,\mathrm{min}$)
×g	times gravity
µl	microliter (mm^3)
ml	milliliter (cm^3)
l	liter (dm^3)
nm	nanometer
µm	micrometer
mm	millimeter
cm	centimeter
(w/v)	percentage by mass ($g\,dm^{-3}$)
pM	picomolar ($pmol\,dm^{-1}$)
µM	millimolar ($µmol\,dm^{-1}$)
mM	millimolar ($mmol\,dm^{-1}$)
M	molar ($mol\,dm^{-1}$)
µg	microgram
mg	milligram
g	gram
V	volt($m^2\,kg\,s^{-3}\,A^{-1}$)
mA	milli ampere
Da	Dalton ($1\,Da \approx 1.66{*}10^{-27}$ kg)
kDa	kilo Dalton
U	enzyme unit ($1\,U \equiv \frac{1}{60}\,µmol\,s^{-1}$)
dB	decibel
bp	base pairs
kb	kilo bases

Appendix

A. Sequences for hATP11A deletion variant

A.1. DNA sequence of hATP11A exon 29^{mut}

GAAAGCACCACCAACGCTGGAGGAGGAGCCGGCCCTCACGCCCGCCCCGCGCCACGCTGT
GGAACGGGGCTCCGGCAAGTGAAACCCAGAGGGTGTTTCCGAGGTGCTCGACAGTAG

A.2. Amino acid sequence of hATP11A deletion variant

MDCSLVRTLVHRYCAGEENWVDSRTIYVGHREPPPGAEAYIPQRYPDNRIVSSKYTFWNF
IPKNLFEQFRRVANFYFLIIFLVQLIIDTPTSPVTSGLPLFFVITVTAIKQGYEDWLRHK
ADNAMNQCPVHFIQHGKLVRKQSRKLRVGDIVMVKEDETFPCDLIFLSSNRGDGTCHVTT
ASLDGESSHKTHYAVQDTKGFHTEEDIGGLHATIECEQPQPDLYKFVGRINVYSDLNDPV
VRPLGSENLLLRGATLKNTEKIFGVAIYTGMETKMALNYQSKSQKRSAVEKSMNAFLIVY
LCILISKALINTVLKYVWQSEPFRDEPWYNQKTESERQRNLFLKAFTDFLAFMVLFNYII
PVSMYVTVEMQKFLGSYFITWDEDMFDEETGEGPLVNTSDLNEELGQVEYIFTNKTGTLT
ENNMEFKECCIEGHVYVPHVICNGQVLPESSGIDMIDSSPSVNGREREELFFRALCLCHT
VQVKDDDSVDGPRKSPDGGKSCVYISSSPDEVALVEGVQRLGFTYLRLKDNYMEILNREN
HIERFELLEILSFDSVRRRMSVIVKSATGEIYLFCKGADSSIFPRVIEGKVDQIRARVER
NAVEGLRTLCVAYKRLIQEEYEGICKLLQAAKVALQDREKKLAEAYEQIEKDLTLLGATA
VEDRLQEKAADTIEALQKAGIKVWVLTGDKMETAAATCYACKLFRRNTQLLELTTKRIEE
QSLHDVLFELSKTVLRHSGSLTRDNLSGLSADMQDYGLIIDGAALSLIMKPREDGSSGNY
RELFLEICRSCSAVLCCRMAPLQKAQIVKLIKFSKEHPITLAIGDGANDVSMILEAHVGI
GVIGKEGRQAARNSDYAIPKFKHLKKMLLVHGHFYYIRISELVQYFFYKNVCFIFPQFLY
QFFCGFSQQTLYDTAYLTLYNISFTSLPILLYSLMEQHVGIDVLKRDPTLYRDVAKNALL
RWRVFIYWTLLGLFDALVFFFGAYFVFENTTVTSNGQIFGNWTFGTLVFTVMVFTVTLKL
ALDTHYWTWINHFVIWGSLLFYVVFSLLWGGVIWPFLNYQRMYYVFIQMLSSGPAWLAIV
LLVTISLLPDVLKKVLCRQLWPTATERVQESTTNAGGGAGPHARPAPRCGTGLRQVKPRG
CFRGARQ

B. gBlock Gene Fragments for cloning

B.1. gBlock Gene Fragment for hATP11A isoform 2

AAGATGGAGACGGCCGCGGCCACGTGCTACGCCTGCAAGCTCTTCCGCAGGAACACGCAG
CTGCTGGAGCTGACCACCAAGAGGATCGAGGAGCAGAGCCTGCACGACGTCCTGTTCGAG
CTGAGCAAGACGGTCCTGCGCCACAGCGGGAGCCTGACCAGAGACAACCTGTCCGGACTT
TCAGCAGATATGCAGGACTACGGTTTAATTATCGACGGAGCTGCACTGTCTCTGATAATG
AAGCCTCGAGAAGACGGGAGTTCCGGCAACTACAGGGAGCTCTTCCTGGAAATCTGCCGG
AGCTGCAGCGCGGTGCTCTGCTGCCGCATGGCGCCCTTGCAGAAGGCTCAGATTGTTAAA
TTAATCAAATTTTCAAAAGAGCACCCAATCACGTTAGCAATTGGCGATGGTGCAAATGAT
GTCAGCATGATTCTGGAAGCGCACGTGGGCATAGGTGTCATCGGCAAGGAAGGCCGCCAG
GCTGCCAGGAACAGCGACTATGCAATCCCAAAGTTTAAGCATTTGAAGAAGATGCTGCTT
GTTCACGGGCATTTTTATTACATTAGGATCTCTGAGCTCGTGCAGTACTTCTTCTATAAG
AACGTCTGCTTCATCTTCCCTCAGTTTTTATACCAGTTCTTCTGTGGGTTTTCACAACAG
ACTTTGTACGACACCGCGTATCTGACCCTCTACAACATCAGCTTCACCTCCCTCCCCATC
CTCCTGTACAGCCTCATGGAGCAGCATGTTGGCATTGACGTGCTCAAGAGAGACCCGACC
CTGTACAGGGACGTCGCCAAGAATGCCCTGCTGCGCTGGCGCGTGTTCATCTACTGGACG
CTCCTGGGACTGTTTGACGCACTGGTGTTCTTCTTTGGTGCTTATTTCGTGTTTGAAAAT
ACAACTGTGACAAGCAACGGGCAGATATTTGGAAACTGGACGTTTGGAACGCTGGTATTC
ACCGTGATGGTGTTCACAGTTACACTAAAGCTTGCATTGGACACACACTACTGGACTTGG
ATCAACCATTTTGTCATCTGGGGGTCGCTGCTGTTCTACGTTGTCTTTTCGCTTCTCTGG
GGAGGAGTGATCTGGCCGTTCCTCAACTACCAGAGGATGTACTACGTGTTCATCCAGATG
CTGTCCAGCGGGCCCGCCTGGCTGGCCATCGTGCTGCTGGTGACCATCAGCCTCCTTCCC
GACGTCCTCAAGAAAGTCCTGTGCCGGCAGCTGTGGCCAACAGCAACAGAGAGAGTCCAG
AATGGGTGCGCACAGCCTCGGGACCGCGACTCAGAATTCACCCCTCTTGCCTCTCTGCAG
AGCCCAGGCTACCAGAGCACCTGTCCCTCGGCCGCCTGGTACAGCTCCCACTCTCAGCAG
GTGACACTCGCGGCCTGGAAGGAGAAGGTGTCCACGGAGCCCCCACCCATCCTCGGCGGT
TCCCATCACCACTGCAGTTCCATCCCAAGTCACAGCTGCCCTAGGTCCCGTGTGGGAATG
CTCGTGCCGCGGTTCGAACTCGAGTATCCATACGATGTACCAGACTACGCAGAG

B.2. gBlock Gene Fragment for hATP11A deletion variant

AAGATGGAGACGGCCGCGGCCACGTGCTACGCCTGCAAGCTCTTCCGCAGGAACACGCAG
CTGCTGGAGCTGACCACCAAGAGGATCGAGGAGCAGAGCCTGCACGACGTCCTGTTCGAG
CTGAGCAAGACGGTCCTGCGCCACAGCGGGAGCCTGACCAGAGACAACCTGTCCGGACTT
TCAGCAGATATGCAGGACTACGGTTTAATTATCGACGGAGCTGCACTGTCTCTGATAATG
AAGCCTCGAGAAGACGGGAGTTCCGGCAACTACAGGGAGCTCTTCCTGGAAATCTGCCGG
AGCTGCAGCGCGGTGCTCTGCTGCCGCATGGCGCCCTTGCAGAAGGCTCAGATTGTTAAA
TTAATCAAATTTTCAAAAGAGCACCCAATCACGTTAGCAATTGGCGATGGTGCAAATGAT
GTCAGCATGATTCTGGAAGCGCACGTGGGCATAGGTGTCATCGGCAAGGAAGGCCGCCAG
GCTGCCAGGAACAGCGACTATGCAATCCCAAAGTTTAAGCATTTGAAGAAGATGCTGCTT
GTTCACGGGCATTTTTATTACATTAGGATCTCTGAGCTCGTGCAGTACTTCTTCTATAAG
AACGTCTGCTTCATCTTCCCTCAGTTTTTATACCAGTTCTTCTGTGGGTTTTCACAACAG
ACTTTGTACGACACCGCGTATCTGACCCTCTACAACATCAGCTTCACCTCCCTCCCCATC
CTCCTGTACAGCCTCATGGAGCAGCATGTTGGCATTGACGTGCTCAAGAGAGACCCGACC
CTGTACAGGGACGTCGCCAAGAATGCCCTGCTGCGCTGGCGCGTGTTCATCTACTGGACG
CTCCTGGGACTGTTTGACGCACTGGTGTTCTTCTTTGGTGCTTATTTCGTGTTTGAAAAT
ACAACTGTGACAAGCAACGGGCAGATATTTGGAAACTGGACGTTTGGAACGCTGGTATTC
ACCGTGATGGTGTTCACAGTTACACTAAAGCTTGCATTGGACACACACTACTGGACTTGG
ATCAACCATTTTGTCATCTGGGGGTCGCTGCTGTTCTACGTTGTCTTTTCGCTTCTCTGG
GGAGGAGTGATCTGGCCGTTCCTCAACTACCAGAGGATGTACTACGTGTTCATCCAGATG
CTGTCCAGCGGGCCCGCCTGGCTGGCCATCGTGCTGCTGGTGACCATCAGCCTCCTTCCC
GACGTCCTCAAGAAAGTCCTGTGCCGGCAGCTGTGGCCAACAGCAACAGAGAGAGTCCAG
GAAAGCACCACCAACGCTGGAGGAGGAGCCGGCCCTCACGCCCGCCCCGCGCCACGCTGT
GGAACGGGGCTCCGGCAAGTGAAACCCAGAGGGTGTTTCCGAGGTGCTCGACAGCCGCGG
TTCGAACTCGAGTATCCATACGATGTACCAGACTACGCAGAG

B.3. gBlock Gene Fragment for multiple cloning site

AATTTGCTAGCGAGCTCTGCGGCCGCAGATCTCTAGTTAAGCTATCAACAAGTTTGTACA
AAAAAGCAGGCTCTTTAAAGGAACCAATTCAGTCGACTGGATCCACCGACTATAGGGAGA
CCCAAGCTGGCTAGCGTTTAAACGGGCCCTCTAGACTCGAGCGGCCGCCACTGTGCTGGA
TATCTGCAGAATTCCACCACACTGGACTAGTGGATCCGAGCTCGGTACCAAGCTTAAGTT
TAAACCGCTGATCAGAATTCGTACCCATACGACGTCCCA

C. Vector maps

C.1. HFN-hCDC50A pcDNA3

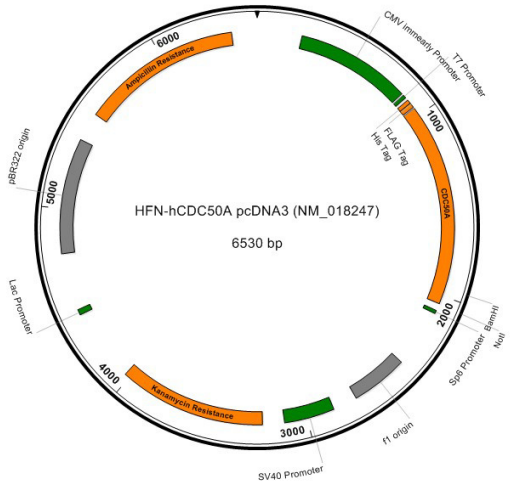

C.2. hATP11A-HA Isoform 1 pCAG

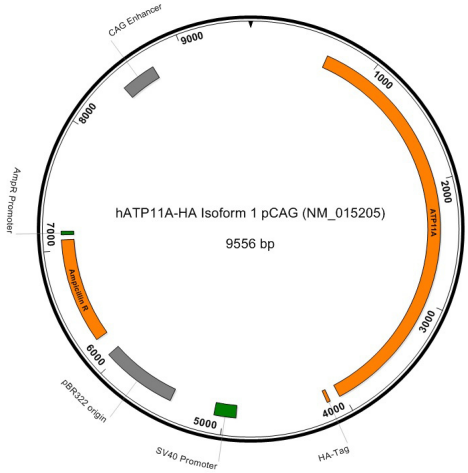

C.3. hATP11A-HA Isoform 1 E186Q pCAG

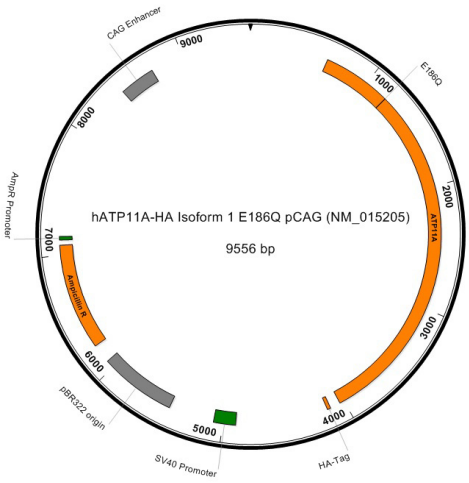

C.4. hATP11A-HA Isoform 1 D414N pCAG

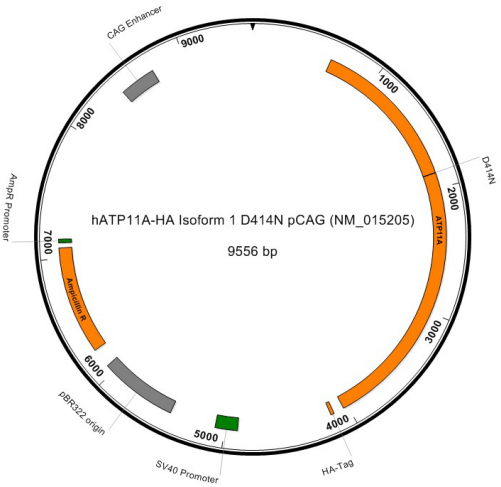

C.5. hATP11A-HA Isoform 2 pCAG

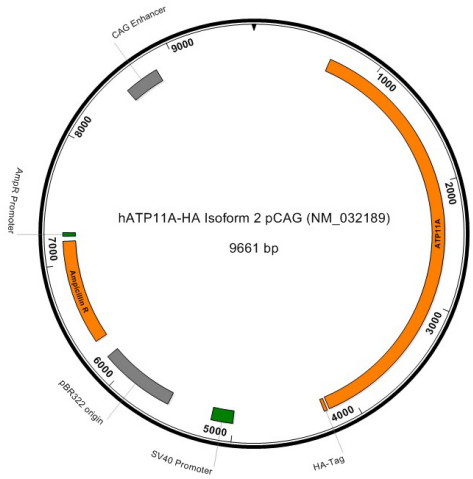

C.6. hATP11A-HA Deletion variant pCAG

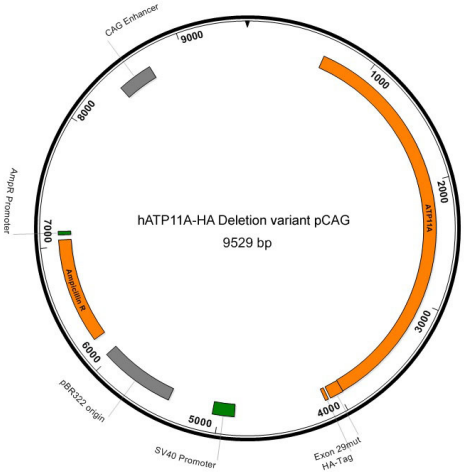

C.7. hATP11A-Myc/His Isoform 1 pCAG

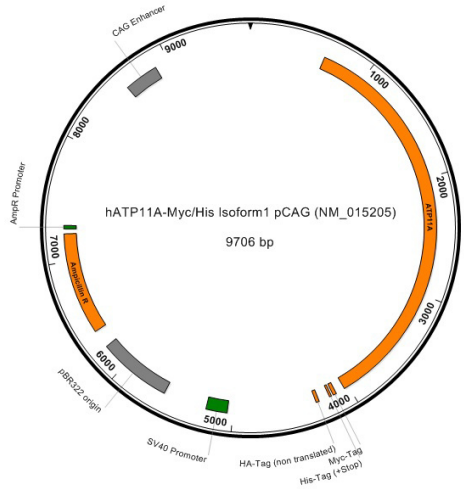

C.8. hATP11A-HA until ex28 pCAG

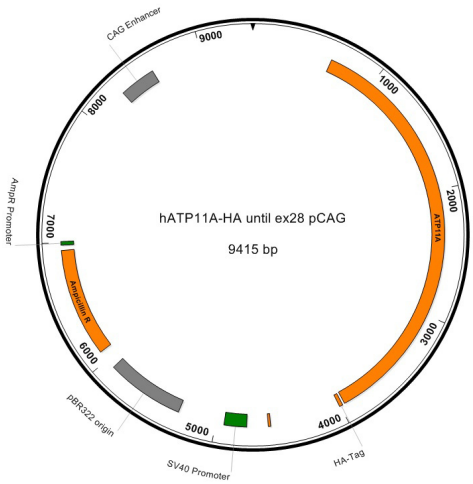

C.9. MCS-HA pCAG

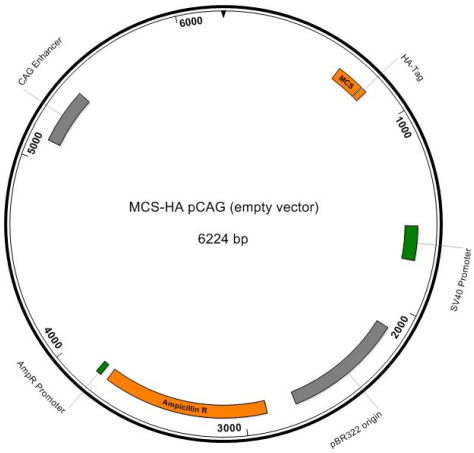

C.10. tdTomato-ER-3

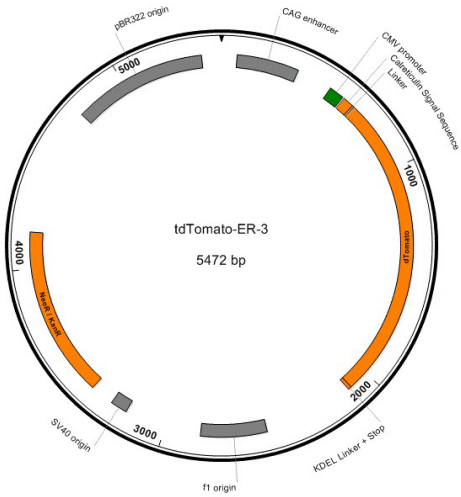

C.11. pDonr211 CDC50A

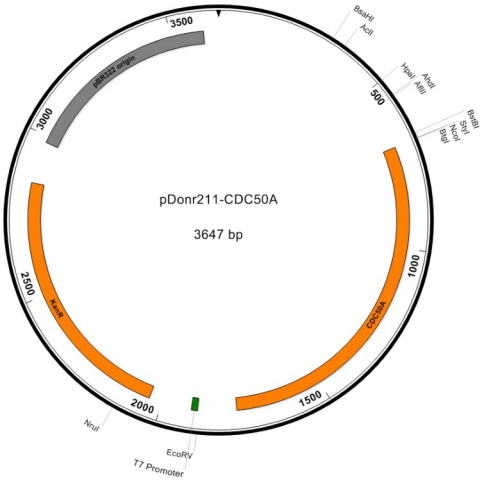

C.12. pEF5/FRT hCDC50A-V5

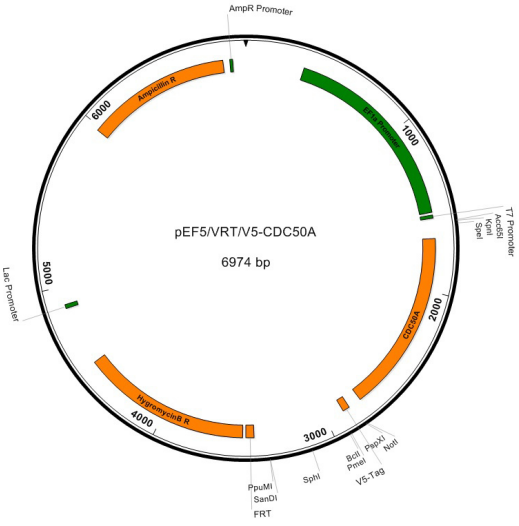

Solemn declaration

I hereby declare upon oath that this thesis with the title:

ATP11A causes autosomal-dominant progressive, non-syndromic auditory synaptopathy / auditory neuropathy

has been written independently and that I have used no other material than that I have specified. Those passages taken from other works, either verbatim or in spirit, I have identified in each individual case by indicating the source.

I further declare that all my academic work has been written in line with the principles of proper academic research according to the guidelines for safeguarding good scientific practice of the University of Hamburg.

Bielefeld, _____

_____

Sarah Maria von Loh